UNIVERSITY OF BIRMINGHAM

A methodology for the Lower Limb Robotic Rehabilitation system

By

Alireza Rastegarpanah

A thesis submitted to

The University of Birmingham

for the degree of

DOCTOR OF PHILOSOPHY

School of Mechanical Engineering
University of Birmingham
Birmingham, United Kingdom

March 2016

Abstract

The overall goal of this thesis is to develop a new functional lower limb robot-assisted rehabilitation system for people with a paretic lower limb. A unilateral rehabilitation method is investigated, where the robot acts as an assistive device to provide the impaired leg therapeutic training through simulating the kinematics and dynamics of the ankle and lower leg movements. Foot trajectories of healthy subjects and post-stroke patients were recorded by a dedicated optical motion tracking system in a clinical gait measurement laboratory. A prototype 6 degrees of freedom parallel robot was initially built in order to verify capability of achieving singularity-free foot trajectories of healthy subjects in various exercises. This was then followed by building and testing another larger parallel robot to investigate the real-sized foot trajectories of patients. The overall results verify the designed robot's capability in successfully tracking foot trajectories during different exercises. The thesis finally proposes a system of bilateral rehabilitation based on the concept of self-learning, where a passive parallel mechanism follows and records motion signatures of the patient's healthy leg, and an active parallel mechanism provides motion for the impaired leg based on the kinematic mapping of the motion produced by the passive mechanism.

I dedicate this thesis to my

Mother; Shahrzad Goli,

Father; Hassan Rastegarpanah,

Brother; Mohammad Rastegarpanah,

and my best friend; Bakhtiar Khazaei

for their constant support and unconditional love. I love you all dearly.

Acknowledgments

"East, West, South, or North makes little difference. No matter what your destination, just be sure to make every journey a journey within. If you travel within, you'll travel the whole wide world and beyond"

Shams-e Tabriz

The completion of my dissertation and subsequent Ph.D. has been a long journey which I enjoyed every moments and I knew that "This too shall pass". Much as happened and changed during this journey, however I could not have succeeded without the invaluable support of a several. Without these supporters, I may not have gotten to where I am today.

I would like to express my special appreciation and thanks to my supervisor Dr. Mozafar Saadat. He was a excellent mentor who helped me to make this research sweet with his enthusiasm, his inspiration, and his amiable character. I would have been lost without him throughout my research period, but he provided encouragement, advice, good company and lots of good ideas in order to accomplish my research. I would like to thank him for encouraging my research and for allowing me to grow as a research scientist. Your advice on both research as well as on my career have been irreplaceable.

A special thanks to my family. Words cannot reveal how grateful I am to my mother, father and brother for all of the sacrifices that you have made on my behalf. Your prayer for me was what kept me thus far. My hard-working parents have sacrificed their lives for my brother and myself and provided unconditional love and care. I love them so much and I would not have made it this far without them. Both have infused many admirable qualities in me and given me a good foundation with which to meet life. They have taught me about hard work and self-respect and also about diligence and about how to be independent. Both have always expressed how proud they are of me and how much they love me. I am so proud of them and love them very much. Thank you Mum and Dad for being a constant source of inspiration (even in the darkest times).

The best outcome of these past five years is finding my spiritual master, best friend, and brother. I cannot begin to express my gratitude and feelings for this beloved angel. It cannot be argued with that the most influential person in my life has been my spiritual master, Bakhtiar Khazaei. He is a

genuine friend who helped me to appreciate and admire my inner self. Shams states: “True mentors are as transparent as glass. They let the light of God pass through them”. The encounter with Bakhtiar triggered the completion of a paradigm shift in my attitude and mentality to the world. He and his family have been a true and great supporter and have unconditionally loved and helped me during my good and bad times.

I would like to express my sincere appreciation and gratitude to Dr Rustam Stolkin who supported, advised and accompanied me during last couple of years. I will never forget his kind and outstanding supports. I believe that his actions provided me with the unique opportunity to gain a wider breadth of experience in robotics. He involved me in various research projects and I am very glad that he gave me the opportunity to work with him as a postdoctoral researcher in one of the largest EU funded projects.

I would also like to thank all of my friends who supported me in writing and helped me to strive towards my goal. In addition, there are other names that I have to thank them, Amir Mohammad Hajiyavand, Guivani Jules, Pooria Ghavam, Salman Saeedloo, Hamid Rakhodaei, Yongjing Wang, Yuya Takeuchi and other researcher in the Robotic Laboratory of School of Mechanical Engineering, University of Birmingham.

I would like to thank the West Midlands Rehabilitation Centre (WMRC), part of Birmingham Community Healthcare NHS Trust for providing gait measurement laboratory support and special thanks to Professor Clive Thursfield, Professor David Pratt, Dr David Fish and Mr Ralph Palmer.

I would like to thank the Applied Computing and Engineering Ltd (AC&E) and Mr Yash Khandhia, as manager of the company, for their sponsorship of this project.

Table of Contents

List of Figures

List of Tables

Chapter 1

Introduction

1.1 Global and national importance

In societies where the majority of the members are past middle age, the necessity of health care and rehabilitation becomes more important, especially amongst the aged and disabled people who are not able to perform their daily activities easily or independently [1-3]. Neurological disorders like strokes, traumatic brain and spinal cord injuries are the leading cause of reduced or no muscle activity in the lower limb, especially for the ankle, which is one of the most complex bony structures in the skeleton of a human [4]. Ankle disability is a leading cause of long periods of deterioration in a person's health and restricts the activities of daily life [5]. Stroke is the second most leading cause of death and thirds common cause of death worldwide [6]. Despite many advances in prevention, stroke continues to be a major health problem [7] and many survivors are often unable to carry out normal activities of daily living such as dressing and walking. The costs are a major impact on the nation's economy and account for almost 6% of NHS and Social Services expenditure. Moreover, the costs of stroke care are projected to rise as the proportion of older people in society increases. The role of high quality rehabilitation within comprehensive stroke services is widely acknowledged in the National Stroke Strategy [8]. Combined evidence from a meta-analysis of high quality clinical trials indicates that much more intensive physiotherapy improves functional outcome and that repetitive task practice enhances results [9]. Performing 45 minutes exercise on each weekday by the patients has been recommended by national clinical

guidelines for stroke in the United Kingdom, while based on evidence stroke patients receives only 30.6 minutes practical physical therapy in United Kingdom. The lack of physiotherapy is also evident after discharge from hospital and many survivors and their families complain of being abandoned at this point. Of particular interest is the group of survivors with severe impairments. [10]

Every year, an estimated 100,000 people in the UK have a first stroke. Most people affected are over 65, but nearly 1000 people under 30 have a stroke each year. Around 25% of stroke survivors cannot walk functionally 12 months following stroke, and many of those who can walk are severely limited by the reduced level of their walking [11]. Most patients require assistance to practice and therapy time is very expensive. They have a poor quality of life, experience many unpleasant complications and consume the highest proportion of care resources [12]. Intensive efforts of therapists and patients are required during traditional rehabilitation sessions; furthermore, 44% of patients who are rehabilitated by physiotherapy will have future problems [13]. However, the amount of therapy that the NHS is able to provide to stroke patients can be frustratingly low and patients do not receive the required intensity of exercises that they need. In this research project, a robot-assisted lower limb rehabilitation system for stroke survivors, particularly for those in early stage of recovery, will be developed. Through the use of active/passive parallel robot platforms, the patient will be able to conduct training depending on the level of impairment of the leg. There are three overall aspirations of the research as follows:

(a) To create an environment that will facilitate the provision of the much needed extra weekly hours of rehabilitation.

(b) To concentrate on gait training and other related functional rehabilitation.

(c) To allow the real possibility of developing a rehabilitation system that will be small and cheap enough to be used in local clinics and hospitals and operated by non-specialist staff. The investigation will aim to develop a rehabilitation methodology that can provide safe, measurable, accurate, reliable, and viable exercises primarily for early stage rehabilitation requiring complete assistance, but also capable of providing full range of support including when only a small amount of assistance is required.

1.2 Robotic lower limb rehabilitation

The improvement of motor recovery and motor plasticity of a patient along specific patterns is the aim of rehabilitation exercises and there are three phases to return the ability to the patient through the rehabilitation process: (i) mobilizing the patient into a chair, (ii) reviving of his/her gait, and (iii) enhancing the gait functions [5]. The utilizing of robotic technology in rehabilitation can accelerate the treatment and recovery of the disabled and it actuates the rehabilitation clinics to change their path from labour-intensive operations to technology–assisted operations [4].

Emerging robotic technology in a traditional rehabilitation therapy session would provide high quality treatment at a lower cost and effort. Usually for a typical therapy session, at least three therapists will be required to help the patient to perform the training exercises manually [4]. Robotic systems will be utilized as standard rehabilitation tools in the near future and they can be a suitable replacement for the traditional physical training from a therapist. Based on robotic rehabilitation, the level of motor recovery of patients can be quantified by defining different rehabilitation exercises for the robot [14]. Currently, a patient's recovery of their walking ability is usually quantified by employing clinical measures such as the Barthel index [15]. By using robotic technology, all labour-intensive operations will be performed by robot-assisted rehabilitation

devices and based on the obtained data, diagnosis and customization of therapy will be facilitated [16].

Based on severity of patient`s injury different control strategy have been used for lower limb rehabilitation systems such as assistive, challenge based, haptic simulation and coaching for robotic movement training based [17]. But, allocating the proper control strategy and rehabilitation system for a specific lower limb disability is still under research and it should be investigated more[20].Based on evidences therapists suggest the active assist exercises provide functional benefits for the patients to do the exercises with the minimum level of manual assistance [5,18].Parallel mechanism developed in [19] is a an good example of assistive robots using backdrivable actuators.

Robotic therapy has been developed as a response to this on the basis that it lends itself to repetitive therapeutic tasks and can provide the patient with more opportunity for self-directed practice. The content of robotic therapy in this context is based on the evidence that practising motor skills with the weak limb results in both neuroplastic and functional change, which persists with chronic stroke [20].

1.3 Aim and Objectives

The aim of this project is to develop a robotic rehabilitation system using parallel robot (Stewart platform) in order to follow the foot trajectory of patients with lower limb disability. The system is aimed at providing a step-change capability that will allow patient-directed, repetitive therapeutic exercises with the aim of accelerating the rate of recovery by increasing therapy time at affordable costs. To reach to this goal the following objectives have been addressed in this research:

- Identification and measurement of human leg segmental motion characteristics (signatures) in order to create a unique biomechanical relationship between the left and right legs needs

to be developed, which will be used to relate the human biomechanical motion to the robotic device.

- Designing and building a prototype parallel robot in order to track the foot trajectories of healthy subjects during various rehabilitation exercises. The accuracy of the robot is validated by a Kinect camera.
- Gait analysis of post-stroke patients during normal waking.
- Developing a new parallel robot in real-life scale to provide a control system suitable for human-machine therapeutic interaction. This will be achieved by facilitating assistive exercises for a unilateral mode of operation, where only the impaired leg of the patient is engaged for training.
- Proposing a bilateral system for lower limb rehabilitation based on the concept of self-learning. In this context, term of self-learning states the process of learning of movements from patient`s own signature of motion. The proposed system provides bilateral training using a separate parallel kinematics machine used passively by the healthy leg to facilitate gait training.

1.4 Thesis Layout

Chapter 1 presents the global importance of this research and gives brief introduction about the research and presents the research aim and objectives.

Chapter 2 provides a literature review on available robots and technologies use for lower limb rehabilitation.

Chapter 3 investigates the effect of laterality on symmetry/asymmetry of the lower limb Joints based on mechanical modeling. In this chapter Vicon system is utilized in order to measure the range of motion of lower limb`s joints.

Chapter 4 investigates the effect of Targeting on the symmetry of stride length of healthy subjects during walking. In this chapter ANOVA test is used to compare the results of Targeting test versus Non-Targeting test.

In Chapter 5, the foot trajectories of healthy subjects during various exercises are measured and simulated by Vicon system. Then, the simulated trajectories are used by the built prototype of parallel robot in order to simulate different foot trajectories by the robot.

In Chapter 6, the foot trajectories of post-stroke patients will be tracked by the developed parallel platform (in bigger scale) based on kinematics and dynamics analysis of the robot.

In chapter 7 a novel bilateral rehabilitation system has been proposed based on the concept of self-learning. The proposed rehabilitation system includes an active/assistive platform using by the paretic leg, and a passive platform using by the healthy leg.

Chapter 8 provides a conclusion of this project based on the obtained results. A proposed future direction of this project has been discussed in this chapter.

Chapter 2

Literature review

2.1 Introduction

Neurologic injuries like a stroke, traumatic brain and spinal cord injuries can cause lower limb disabilities [5]. The prevalence of strokes is likely to increase in the future due to the aging population [21]. Robotic therapy has been developed as a response to this on the basis that it lends itself to repetitive therapeutic tasks and can provide the patient with more opportunity for self-directed practice. The content of robotic therapy in this context is based on the evidence that practising motor skills with the weak limb results in both neuroplastic and functional change, which persists with chronic stroke [22, 23].

2.2 Various Robot-Assisted rehabilitation systems

Basically there are two main types of robot-assisted lower limb rehabilitation devices available including wearable devices and platform-based devices. Usually platform-based lower limb rehabilitation devices have parallel configurations with multiple degrees of freedom (DOF) to reduce the size of the robots. First group are designed to improve the lower limb performance during gait, while the second group only concentrates on improvement of lower limb performance [21, 23]. It is hard to understand the correlation between functional improvements in the rehabilitation clinics and daily life`s activities. However, functional recovery of gait can be an indicator of lower limb functional recovery specifically for the ankle joint. Several different robots

have been developed for lower limb rehabilitation such as Rutgers, IT-HPARR, AKROD, GIST and NUVABAT [24].

Based on systematic review on exoskeletons in stroke rehabilitation, it was concluded that combination of these devices and physiotherapy help patients to walk independently [25]. The most famous wearable exoskeletons are ReWalk™, Ekso Bionics™, Indego™, Rex™. Usually platform based lower limb rehabilitation devices have parallel configurations with multiple degrees of freedom (DOF) to reduce the size of robots. These devices have been designed in a way to perform different rehabilitation exercises such as motion therapy and muscle strength training. Motion therapy can be carried out in five different modes including passive, active, active-resistive, active-assistive and bilateral exercises that each one of these modes needs different level of participation from patients. In some studies, resistive force has been provided during exercise and haptic simulation has been interacted with VR simulation [26]. Allocating the proper control strategy and rehabilitation system for a specific lower limb disability is still under research and it should be investigated more [27].

Several robot systems have been developed for assisted gait therapy which are complex, highly expensive and not suitable to non-specialist rehabilitation environments. A considerable number of studies have demonstrated some gains during the experimental phase but there is very little information on the long-term effects, particularly relating to functional activities [22]. Rutgers is one of the pioneer ankle rehabilitation devices which it`s developments have been cited in different studies [28-34].It was found that combination of Rutgers with Virtual Reality (VR) system has better outcomes on the gait of post-stroke patients rather using the robot alone [35]. The second generation of Rutgers in accompany with VR and haptic effects were used for ankle rehabilitation of three participants and results indicated the strength capability of some ankle muscles increased [29]. The next version of Rutgers robot proposed in [27], for ankle rehabilitation of Cerebral Palsy

(CP) patients. In another study, the concept of telerehabilitation was applied and 6 post-stroke patients rehabilitated by Rutgers Ankle based on VR [33]. However, using pneumatic actuators require special air compressor, which has acoustic noises, and it would not be suitable to be used in clinics.

Rutgers system was used in [27, 36] for Cerebral Palsy (CP) patients and based on results they found that patient function and quality of life improved by increasing the ankle strength and motor control. In another study, a six degree of freedom parallel robot named R-2000 used to simulate a gait cycle and ground reaction forces in vitro based on data obtained in vivo gait [37]. In order to create a correct gait cycle for the robot, the Complementary Limb Motion Estimation (CLME) method has been proposed to generate the desire trajectory of affected leg based on movements of healthy leg [38].

In another study, a high performance 2 DOF over-actuated parallel mechanism has been designed and built for ankle rehabilitation based on custom designed backdrivable actuators and impedance control system [39-41]. In another study, the prototype of a 3-RSS/S parallel mechanism has been produced for ankle rehabilitation application [42, 43], while no clinical trials found for this system.

Despite a decade or more of development of therapeutic robotic devices the uptake within health care remains poor and still there is no effective patient evaluation system available [44]. Lack of enough patient trials is one of the most significant factors in advanced robotic rehabilitation systems which should be considered and the robot-assisted rehabilitation needs to comply with neurophysiological therapy principles. There are feasibility issues that the systems remain complex, expensive and have to be situated in specialist clinics. In addition, little is known about their long-term functional outcomes and economic effectiveness.

2.3 Path planning

One of the most important issues for the control system of the robot is path planning, in which the inputs of each motion are the geometric path, kinematics and dynamics' constraints; the output is the trajectory of the joints based on position, velocity and acceleration data. There are different optimization techniques for trajectory selection of the manipulator; such as minimum seeking algorithms, genetic algorithms, multiple objective optimizations, minimum time trajectory, minimum energy trajectory, and collision free trajectory. All of these techniques are based on kinematics and dynamics' constraints of the manipulator during the path motion. The dynamics' results are much more realistic in comparison with the kinematics' results, in terms of fitting in torque constraints and limitation of the joints [45]. In other studies, the path planning of Hybrid parallel robot for ankle rehabilitation have been investigated based on healthy subjects [46, 47].The dynamics' results are much more realistic in comparison with the kinematics' results, in terms of fitting in torque constraints and limitation of the joints [48].

Ankle joint is capable of three different movements named plantar/dorsiflexion, inversion/eversion and adduction/abduction. All three rotations will be used during a gait cycle. In [39], the designed robot was able to perform only two rotations because the first two movements are the dominant actions in ankle rehabilitation. To determine the appropriate trajectory for movement of robot, there are different methods such as modelling the trajectory based on Normative movements, pre-recorded trajectory obtained by gait analysis and pre-recorded trajectory during therapist assistance [49-53].

2.4 Bilateral rehabilitation of lower limb

Different lower limb rehabilitation assisting robots have been developed to revive the functional mobility of damaged limbs, ranging from complex computerized stations to simple structures. NeXOS is another robot which has been developed in England for hip and knee joint exercises [54]. The Active Knee Rehabilitation Orthotic Device (AKROD) is another type of robot which has been built and expanded for the purpose of the rehabilitation of post-stroke and other patients with a neurological disease who are suffering from knee injuries, to speed up their motor recovery [52]. However, using 6 DoF parallel robot can be an applicable method for lower limb rehabilitation due to its simple configuration and high flexibility in performing a different range of motions [53]. Assisted robots for the rehabilitation of lower limbs, like Rutgers, allow patients to perform a wide range of passive-active exercises along different trajectories based on virtual reality [19] with minor supervision of physiotherapists [57]. To develop the robotic devices, first the motor learning and motor adaption of healthy people should be investigated and based on the obtained results, the neurologically injured patients can be rehabilitated [58]. By utilizing the robotic devices, new dynamic and gait exercises for the lower limb can be defined in a repeatable way and the recovery process would be controlled and quantified by this method [59].

Despite a decade or more of the development of therapeutic robotic devices, the uptake within health care remains poor and still there is no effective patient evaluation system available [44]. Lum (2006) stated that combining both unilateral and bilateral robotic upper limb rehabilitation has more advantages in comparison with conventional therapy and robotic therapy creates larger improvements on a motor impairment scale and a measure of abnormal synergies [60]. In another study, it is mentioned that performing repetitive movements by robot might be more effective than non robotic movements, especially for the patients with severe injury [60]. Robotic rehabilitation increases the efficiency of neuoro rehabilitation without increasing the costs of healthcare [61].

There are different research groups who are working on robotic devices for bilateral stroke therapy and some early research has shown that mirror image movements might have advantages rather than similar unilateral movements [62-66]. A bilateral mode may increase the effectiveness of the unilateral mode based on a hypothesis of different potential mechanisms of two different modes and he claimed that a bilateral mode may have unique benefits in decreasing the abnormal synergies [60].

After a stroke, paretic leg motor impairment causes unilateral control deficit. It is worth mentioning that most of the neural circuitry controlling normal leg function is organized bilaterally to produce coordinated, task-specific activity in the two legs. So, the position of the healthy leg may affect on the motor pattern generation of the affected leg during bilateral tasks [67].

Boian introduced a bilateral lower limb rehabilitation system which modelled a walking surface using two Rutgers Mega-Ankle (RMA) robots. In that study, platforms were placed on the floor close to each other with a minimum distance apart to avoid collision during performance of the exercise. Virtual reality (VR) simulation has been used to evaluate the platforms and simulate the normal walking. In a virtual environment, patients are supposed to pass along the street at different speeds based on a dynamic street model. With respect to different defined states of simulation, both force control and position control have been utilized during performance of the exercise [68, 69]. There are feasibility issues that make existing systems complex, expensive and have to be situated in specialist clinics.

2.5 Kinematics and dynamics

Kinematics and dynamics of 6 DoF parallel robot have been addressed in various studies [70-87]. In [78], forward kinematic of Stewart platform has been analysed when six limbs create three concurrent pairs at either the base or the hand member. In [71], soma coordinates has been used in order to analyse forward displacement of Stewart platform. In [72], tensor representation was used in order to derive a dynamic model for a class of Stewart platform. In [74], a stiffness control system of Stewart platform has been designed for milling application. In [75], the inverse dynamic of a Stewart-Gough platform has been analysed based on principle of virtual work and the concept of link Jacobian matrices. In [76], the geometrical conditions for closed-form solutions of forward kinematics of parallel platforms have been addressed. In [77, 81, 84, 86], the Newton-Euler formulation has been used in order to drive the dynamic equations of Stewart platform. In [78], neural networks have been utilized in order to find the forward kinematics solution of Stewart platform. In [80], dynamic of Stewart platform has been analysed based on the theory of screws and principle of virtual work. In [82], each leg has been considered as an independent substructure and dynamic of Stewart platform was analysed based on Kane`s equation. In [83], the implementation of adaptive control system used to control noncompliant motion of a Stewart platform has been addressed. In [85], the accuracy improvement of Stewart platform has been investigated by means of calibration.

2.6 Workspace and singularity of parallel robot

In [88], the workspace, singularity and stiffness of parallel robot has been investigated and it was proved there are six classes of manipulators that exert the same wrenches all over the workspace. In [89], the dexterity of Stewart platform has been improved and a modified 6 DoF parallel robot has been presented. In [90, 93] the singularity loci of Stewart platform have been

addressed based on analytical expressions of determinant of the Jacobian matrix. In [91], an algorithm was developed to construct continuous paths within the workspace of the robot by avoiding singularities. Determination of the maximal singularity free zones and the maximal singularity-free orientation workspace of Stewart platform have been addressed in [92] and [93,95] respectively.

In [96], sliding mode control was used in order to track a high speed 6-6 Stewart platform manipulator when manipulator was assumed to be operated on a low frequency planar motion unit. In [97], global potential energy functions and exponential map were utilized in order to have a compliant control for the Gough-Stewart platform. In [98], a simple robust auto disturbance rejection controller (ADRC) was proposed in order to track a general Stewart platform. In [99], the inverse dynamic controller (IDC) was used to control Stewart platform in real-time. In [100], a controller was proposed based either on Cartesian or and actuator coordinates. This robust controller, with considering the uncertainty, was used for s Stewart platform. In [53], a Stewart platform was used for ankle rehabilitation which the system allows for both position and force control of the platform. In [101], both position control and force control were used for the bilateral rehabilitation system. In [102], the impedance control was utilized in order to control both force and motion of the moving platform of the parallel robot.

2.7 Kinect camera

Kinect camera was used in various clinically-evaluated systems, especially for upper rehabilitation systems [103-105]. Regarding accuracy, Kinect camera is a practicable replacement to red, green, blue, depth (RGB-D) cameras. In [106] Kinect camera was used in a lower limb rehabilitation system. Vicon camera as an expensive and bulky marker-based motion capture system has been compared with Kinect camera; the position errors between the Kinect and Vicon system are all

below 10mm [107]. The successful rate of Kinect varies with respect to various activities, but still there is a good overall relationship between the results of the Kinect and the Vicon system for most movements [108]. In [109], the foot trajectories of elderly people were tracked by the Vicon system to measure the variation of stride velocity. Multiple colour spaces have been suggested for computer vision but the problem with these methods is that they assume that colour is a linear transformation [110] but in reality, it is distorted as the background changes and light adds to the complexity [111]. To avoid complex segmentation algorithms [112], it would be better to create an environment with a neutral background and controllable light.

2.8 Summary of literature review

Based on the literature review, it was found that different technologies have been developed for rehabilitation of lower limb in both unilateral and bilateral modes. However, most of them didn`t address the personalization of signature of motion of patients corresponding to various rehabilitation exercises. In most of researches the predefined trajectories were used as reference trajectories for moving the robot in order to perform an specific exercise, while in this research we are proposing a bilateral robotic rehabilitation system which the reference trajectory will be generated by the patient`s own signature of motion which is personalized and looks more natural. In addition, in unilateral mode, the personalized data obtained by gait analysis will be used to perform the exercise. In this research, we are introducing a system which is able to perform different rehabilitation exercises, and on top of that system would be able to perform bilateral exercises such as normal walking, treadmill walking and stair climbing.

Chapter 3

Effect of Laterality on Symmetry/Asymmetry of the Lower Limb Joints Based on Mechanical Modelling

3.1 Introduction

One of the challenging issues in robotic rehabilitation is mapping the movements of the healthy leg to the affected leg by a robot in bilateral mode. In master-slave mechanism for ankle rehabilitation, in which the master device control the slave device, the patient's motion signature will be taken into account in the mapping of motions from the passive device onto the active device due to the lack of pure left/right symmetry. Thus, the consideration of the symmetry/asymmetry between the two lower limbs has a significant effect on the success of the robot-assistive therapeutic treatment. The purpose of this chapter is to establish the asymmetrical behaviour of the joints between the lower limbs for able-bodied during a gait cycle. The outcome of this study will provide useful information to design a cognitive control system for the proposed robotic rehabilitation system.

Based on literature review, the term of gait symmetry used when there are some statistical differences between the lower extremities on kinematic parameters. Term of asymmetry generally was used by researchers to show side structural and functionality disparity, although asymmetries in the brain`s functional map and cytoarchitecture have been associated with asymmetrical behavioural traits such as handedness and footedness ,that laterality is entirely related to this functional asymmetry. In some studies, asymmetry has been used to show a pathological case, while in most of studies, gait symmetry has been used for simplifying the data analysis. For able-

bodied, asymmetry in spas patio-temporal parameters such as range of motion, speed of the walking, step and stride has been reported without reporting the cause of these differences [113].

In able-bodied gait, strong relation between the limb preference and mobilization tasks in bilateral/ unilateral modes observed [114]. The preference in using one side of the body over the other side called laterality. Different mechanical models for the human lower extremities have been presented so far. In most of studies, joint angles were only computed based on only right or left leg, while in this study the mechanical model presented for both limbs. [115-117]

A unique investigation in laterality and the angular symmetry/asymmetry of the hip, knee and ankle joints of left and right legs has been carried out based on obtained data from gait measurements and mechanical model of lower limb. The work will lead to the identification of rules for the relationships, and will help to generate a map between two legs. This map will be based on kinematic relationships, using both first and second order kinematics. The theoretical model validated using experimental measurements on 28 healthy volunteers selected from both genders.

In this chapter the symmetry/asymmetry between the range of motion of lower limb`s joints have been investigated and results have been utilized in designing the control system of the robot. Concept of Targeting and Normative applies in goal-directed exercises, where if required, they will be simulated in virtual reality environment. In some score-based exercises, patients will be asked to hit specific targets. This is done in order to understand the differences between the natural and the pre-defined movements of the lower limb during exercises, which in turn, helps the design of the motion control system.

3.2 Methodology

3.2.1 Gait analysis

Before starting the experiment, some anthropometric measurements were evaluated and recorded which they are required for running the Vicon software (Plug-in Gait lower body model). Study was started with the identification and measurement of leg segmental motion characteristics (signatures) of 28 healthy participants, 14 male and 14 female. The characteristics of subjects have been shown in Table 3-1:

Table 3-1: The characteristics of the subjects

	Age(years)	Weight(kg)	Height(cm)	BMI(kg/m^2)
Male(n=14)	26.43±4.32	85.1±4.56	176.2±3.41	22.48±3.1
Female(n=14)	25.4±2.17	65±4.58	164±4.85	22.02±5.58

The experiment performed in the gait measurement laboratory of West Midland Rehabilitation Centre, Birmingham, United kingdom .As it can be seen in Figure 3-1, the laboratory was equipped with 12 infrared cameras (six MX T40 cameras and six MX3+ cameras) with a sampling frequency of 100 Hz recorded the 3D spatial location of each marker as the subject walked. Two digital video cameras were utilized, recording the coronal plane and sagittal plane. A Kistler force plate at a sampling rate of 1000Hz was embedded in the middle of walkway. Two different set of retro-reflective markers (Diameter of 9mm) were placed on specific anatomical landmarks; the first one was oxford foot model [118] which was used for the left leg and standard plug in gait was used for the right leg. The 3D gait data were collected with the Vicon system and processed by the Vicon Nexus (version 1.7.1) software.

The experiment was performed in 2 modes; term of Normative was used for the first mode in which Participants were unaware of the existence of the force plate when asked to walk at self-selected speed along a 10-m walkway. Term of Targeting was used in which participants were aware of the existence of the force plate, as a target, when asked to walk along the walkway. Minimum of three firm barefoot strikes with the force plate by the left leg and three barefoot strikes by the right leg were recorded in each mode. For each tester 12 dynamic trials (6 Normative trials and 6 Targeting trials) with at least one full left and right gait cycle each walk recorded.

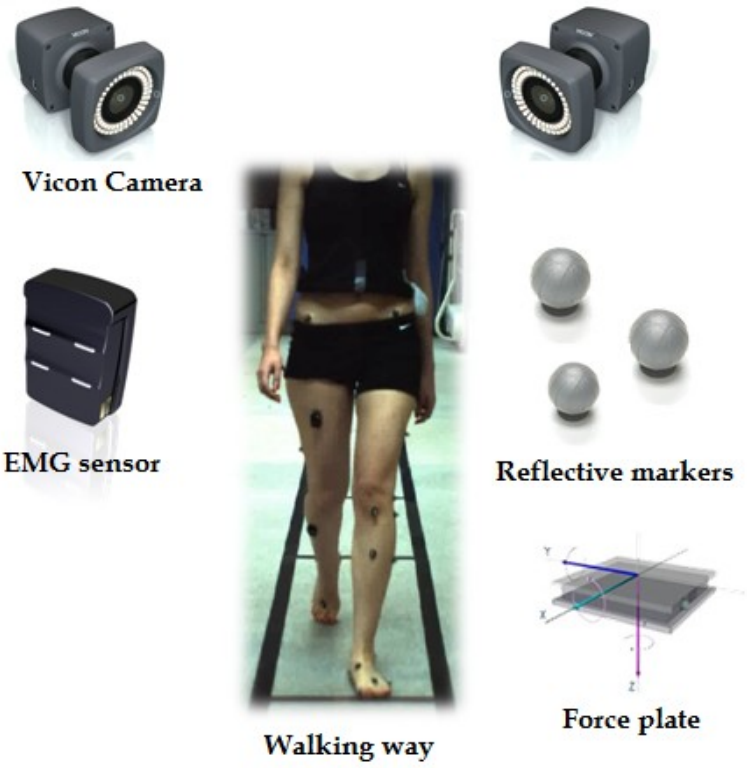

Figure 3-1: Equipment used in gait lab including Vicon cameras, EMG sensors, force plates and reflective markers

3.2.2 Kinematics of lower limb

To imitate the angular motion of joints for human lower limb, each leg was modelled as a serial robot with 10 rigid links connected by nine rotary joints. Each 3 revolute joints representing an specific human joint such as hip, knee and ankle joints, that the order of rotation for each joint is based on kinematics of Vicon and Plug In Gait (PIG) which is flexion/extension, internal/external and abduction/adduction respectively. Based on DH method [119], the 4×4 transformation matrix between two adjacent coordinate frame presented by equation 1.

$$T_n^{n-1} = \begin{bmatrix} \cos\theta_n & -\sin\theta_n \cos\alpha_n & \sin\theta_n \sin\alpha_n & a_n \cos\theta_n \\ \sin\theta_n & \cos\theta_n \cos\alpha_n & -\cos\theta_n \sin\alpha_n & a_n \sin\theta_n \\ 0 & \sin\alpha_n & \cos\alpha_n & d_n \\ 0 & 0 & 0 & 1 \end{bmatrix} \quad (3.1)$$

Where α, a, d and Θ representing link length, link twist, joint distance and joint angle (degree), respectively. The values of the required parameters and definition of angles were respectively defined for the links 1-9 and it is shown in Table 3-2.

Table 3-2: Link parameters

		Right Leg	Right Leg Θ	Right Leg α	Left leg	Left leg Θ	Left leg α
Hip	θ_1	Flexion	Θ+90	-90	Flexion	Θ+90	+90
	θ_2	Abduction	Θ+90	-90	Adduction	Θ-90	+90
	θ_3	External rotation	Θ-90	-90	Internal rotation	Θ+90	+90
Knee	θ_4	Extension	Θ+90	-90	Extension	Θ+90	+90
	θ_5	Valgus	Θ+90	-90	varus	Θ-90	+90
	θ_6	External rotation	Θ-90	-90	Internal rotation	Θ+90	+90
Ankle	θ_7	Dorsi- flexion	Θ+90	-90	Dorsi-flexion	Θ+90	+90
	θ_8	Valgus	Θ+90	-90	varus	Θ-90	+90
	θ_9	External rotation	Θ+180	0	External rotation	Θ+ 180	0

The joint angles were calculated based on comparing the relative rotation of the two segments. With respect to fixed and moving coordinates of the segments, which are shown in Figure 3-2, the transformation matrix was computed followed by calculation of the location of centre of rotation.

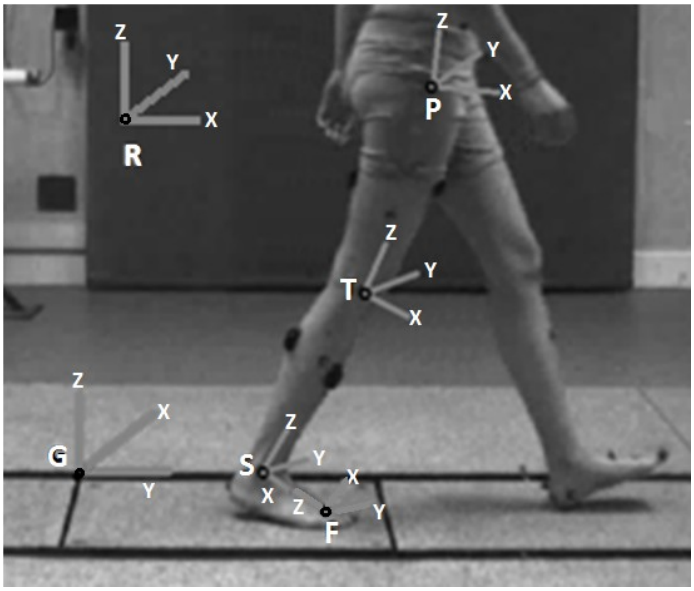

Figure 3-2: Points P, T, S, F, G and R corresponding pelvis, Thigh, Shank, Foot, Global coordinate and rotated coordinate respectively.

To compute the angular rotation of joints with respect to the time, kinematics of the leg`s model and associated transformation matrices were developed in MATLAB, using the linear equation with matrices to find the unknown angles. X, Y and Z axis were defined, based on defined coordinate systems for each segment. As it is shown in Figure 3-3, all of the markers have been labelled and position of markers can be found. In addition, it is shown that the global coordinate reference (G) has been placed on the top right corner of the force plate.

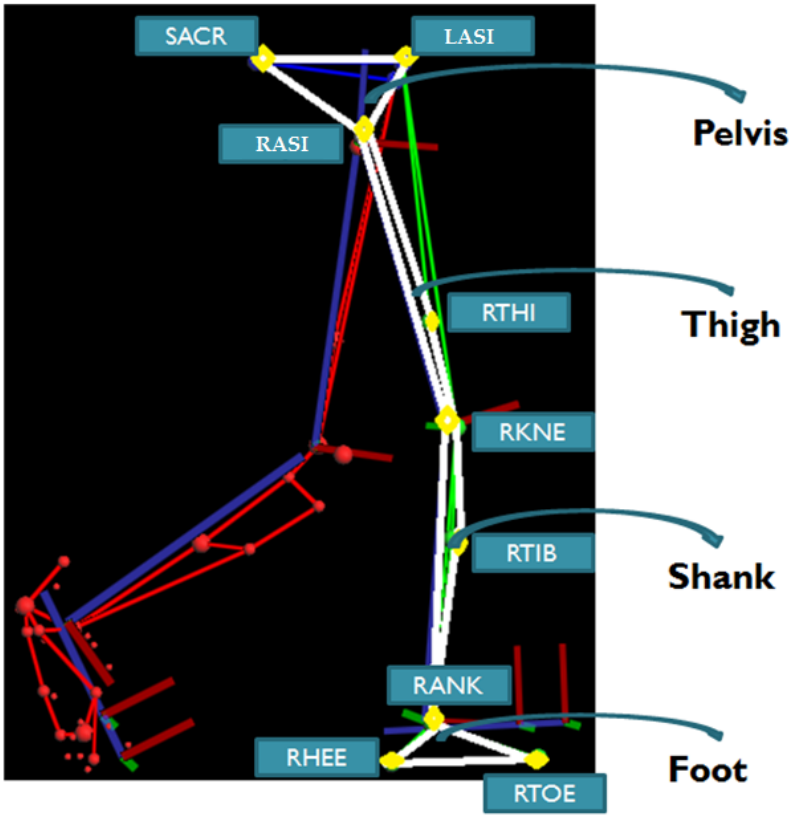

Figure 3-3: Marker labels and lower limb segments

To determine the coordinate system for the Pelvis, the midpoint of RASI and LASI considered as the origin point. RASI marker or Right ASIS marker was placed on the right anterior superior iliac spine, LASI marker or Left ASIS was placed on the left anterior superior iliac spine, SACR or Sacral wand Marker was placed on the skin mid-way between the posterior superior iliac spines.

$$\overrightarrow{J_{Pelvis}} = \frac{LASI-((RASI+LASI)/2)}{\left|LASI-(\frac{RASI+LASI}{2})\right|} \quad (3.2)$$

$$\overrightarrow{I_{Pelvis}} = \frac{SACR-(\frac{RASI+LASI}{2})}{\left|SACR-(\frac{RASI+LASI}{2})\right|} \quad (3.3)$$

$$\overrightarrow{k_{Pelvis}} = \overrightarrow{I_{Pelvis}} \times \overrightarrow{J_{Pelvis}} \quad (3.4)$$

To determine the coordinate system for the thigh segment, the knee joint centre (KJC) was considered as the origin point of coordinate system. RTHI or Right Tight marker was placed on the lower lateral 1/3rd surface of the thigh, RKNE or Right Knee marker was placed on the lateral epicondyle of the left knee and RHJC which representing the Right Hip Joint Centre [4].

$$\overrightarrow{k_{Knee}} = \frac{RKJC - RHJC}{|RKJC - RHJC|} \tag{3.5}$$

$$\overrightarrow{i_{Knee}} = \frac{(RKJC - RTHI) \times (RKJC - RHJC)}{|(RKJC - RTHI) \times (RKJC - RHJC)|} \tag{3.6}$$

$$\overrightarrow{j_{Knee}} = \overrightarrow{i_{Knee}} \times \overrightarrow{k_{Knee}} \tag{3.7}$$

To define a coordinate system for the shank segment, the ankle joint centre was determined and it was considered as the origin of the knee coordinate system. RTIB (right tibia marker) was placed over the lower 1/3rd of the shank.

$$\overrightarrow{k_{Shank}} = \frac{RKJC - RAJC}{|RKJC - RAJC|} \tag{3.8}$$

$$\overrightarrow{i_{Shank}} = \frac{(RAJC - RTIB) \times (RAJC - RKJC)}{|(RAJC - RTIB) \times (RAJC - RKJC)|} \tag{3.9}$$

$$\overrightarrow{j_{Shank}} = \overrightarrow{i_{Shank}} \times \overrightarrow{k_{Shank}} \tag{3.10}$$

Another coordinate system placed on foot segment, using 3 markers of RTOE (which it was placed over the second metatarsal head), RANK and RHEE (which it was placed on the calcaneus) markers. RTOE was considered as the origin.

$$\overrightarrow{k_{Foot}} = \frac{RHEE - RTOE}{|RHEE - RTOE|} \tag{3.11}$$

$$\overrightarrow{i_{Foot}} = \frac{(RTOE - RHEE) \times (RTOE - RAJC)}{|(RTOE - RHEE) \times (RTOE - RAJC)|} \tag{3.12}$$

$$\overrightarrow{j_{Knee}} = \overrightarrow{i_{Knee}} \times \overrightarrow{k_{Knee}} \tag{3.13}$$

With respect to Figure 3-2, to compute the rotation of each segment with respect to the global coordinate reference (G), the intermediate transformation matrices between the segments applied. For instance, based on equation 3.14, the rotation of the shank with respect to thigh has been calculated.

$$R_T^S = R_T^G \times R_G^S \tag{3.14}$$

The MATLAB code developed to calculate the rotation of the knee joint;

$$\text{RShankThigh} = \begin{matrix} [(s4 * s5 * s6) + c4c6 & (s4 * c5) & (s4 * s5 * c6) - (c4 * s6)\ ; \\ (c4 * s5 * s6) + (s4 * c6) & (c4 * c5) & (s5 * c4 * c6) - (s4 * s6)\ ; \\ (c5 * s6) & (s5) & (c5 * c6)]; \end{matrix} \tag{3.15}$$

RShankThigh represents the rotation of the shank with respect to thigh. c and s corresponding Cos(Θ) and Sin(Θ) .

With respect to the time of first foot strike and second foot strike for each leg, data for the heel to heel period of time was extracted for each leg and pure normalization of the time was performed for all of the trials based on equation 3.16 [120]:

$$P_k = \frac{P_k - \text{MinVal}}{\text{MaxVal} - \text{MinVal}} \times 100 \tag{3.16}$$

When P_k is the index of data, MinVal and MaxVal show Minimum and Maximum value respectively.

Based on gait analysis, the simulation of joints trajectories have been simulated in both Normative and Targeting modes by Vicon Nexus and they have been illustrated in Figure 3-4.

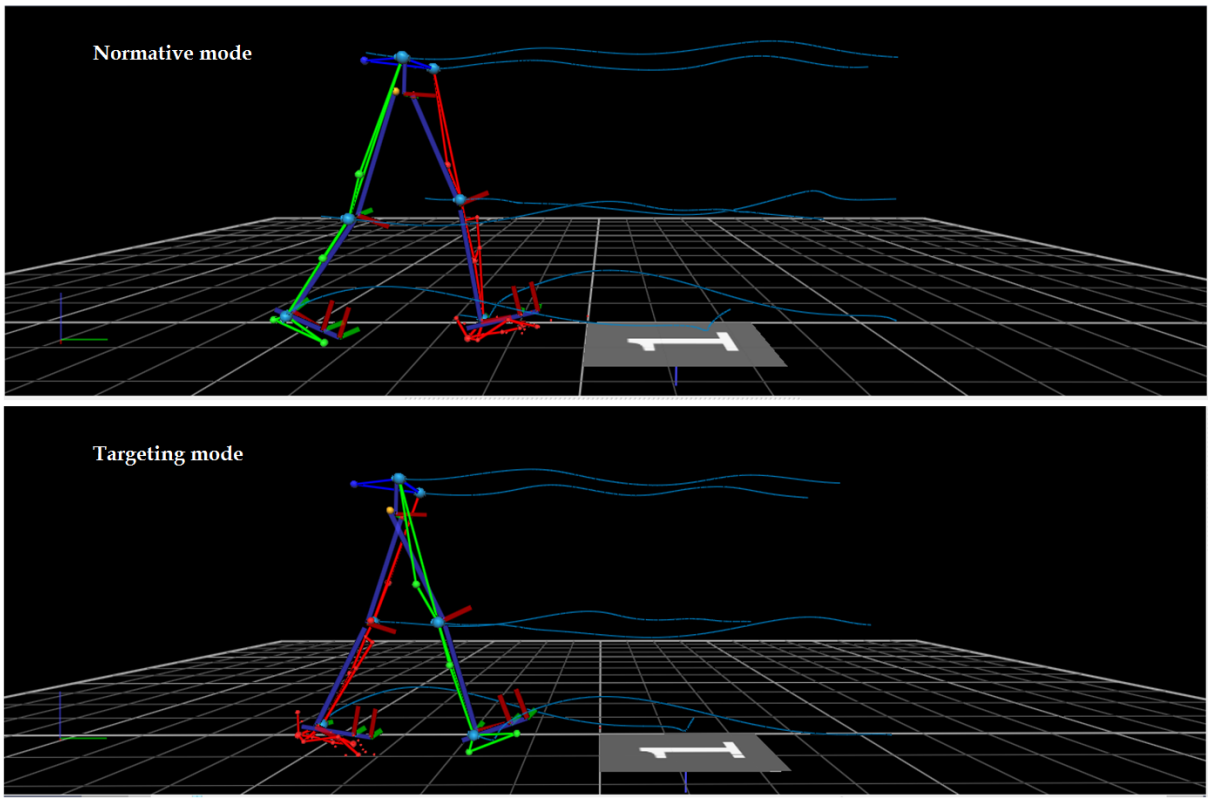

Figure 3-4: Trajectory of lower limb joints during Normative and Targeting mode

3.3 Result and discussion

3.3.1 Validation

By applying t-test using a significance level of a = 0.05, obtained data from MATLAB was validated with obtained data from Vicon using Minitab software and it was shown in Table 3.3. After normalizing the obtained data from both MATLAB and Vicon, the mean value for angular rotation of each joint with respect to normalized time was calculated based on equation 3.16. Then, the values for the right and left in both modes were compared, using t-test.

$$\bar{\theta}_i = \frac{\sum_i X_i}{N} \tag{3.17}$$

Where, N is the number of the participants and Θ is the angular rotation of the joint.

As it can be seen in Table 3-3 ,by applying t-test and comparing the obtained data from MATLAB with Vicon, the P-value for all angular rotations of joints were bigger than alpha level (P>0.05) ,that regarding to null hypothesis , the P value bigger than alpha level representing the similarity between 2 set of data.

Table 3-3: P value based on t-test for Hip, Knee and ankle joints (angle) with 95% CI. MLN correspond to (obtained data by MATLAB for the left leg in Normative mode). In the same way V,R,L,N and T representing Vicon, Right foot, Left foot, Normative mode and Targeting mode respectively .

	θ1	θ2	θ3	θ4	θ5	θ6	θ7	θ8	θ9
MLN-VLN	0.784	0. 409	0.531	0.996	0.984	0.998	0.555	0.992	0.154
MLT-VLT	0.702	0. 431	0.322	0.651	0.459	0.784	0.995	0.847	0.607
MRN-VRN	0.839	0.297	0.798	0.994	0.436	0.271	0.245	0.999	0.569
MRT-VRT	0.225	0.574	0.312	0.886	0.982	0.668	0.745	0.955	0.665

3.3.2 Laterality and motor function

By a glance at Table 3-4, it can be found that in bilateral context, there is high symmetry between the joint movements of right leg in Normative and Targeting modes.

Table 3-4: P-value for rotation of hip, knee and ankle joints. (**) corresponding the P-value<0.001, (*) corresponding the P-value<0.05

Mode	θ1	θ2	θ3	θ4	θ5	θ6	θ7	θ8	θ9
LN-LT	0.4	0.3	0.7	0.6	0.2	0.2	0.5	*	*
LN-RN	0.9	0.7	0.4	0.2	0.2	0.4	0.6	0.5	0.6
LT-RT	0.9	0.7	*	*	0.6	*	*	0.4	**
RN-RT	0.5	0.5	0.1	0.7	0.7	0.1	0.2	0.6	0.4

P-value<0.001 states the significant difference between two sets of data, and P-value<0.05 shows the asymmetry. Where LN (Left Leg in Normative mode), LT (Left Leg in Targeting mode), RN (Right Leg in Normative mode), RT (Right Leg in Targeting mode).

As it can be seen in Figure 3-5, significant asymmetry in angular rotations of hip joint in abduction/adduction movement during a gait cycle have been observed between the right foot and left foot . As it is shown in Figure 3-6, the asymmetry have been observed in knee valgus/varus and external/internal movements between left and right legs in Normative mode which the maximum difference between the legs in these two motions were 2.5˚ and 3.6˚ respectively. In addition, as it is shown in Figure 3-7, asymmetry has been observed in ankle external/internal rotation which the maximum asymmetry was 8.6˚ which was happened one second before foot strike.

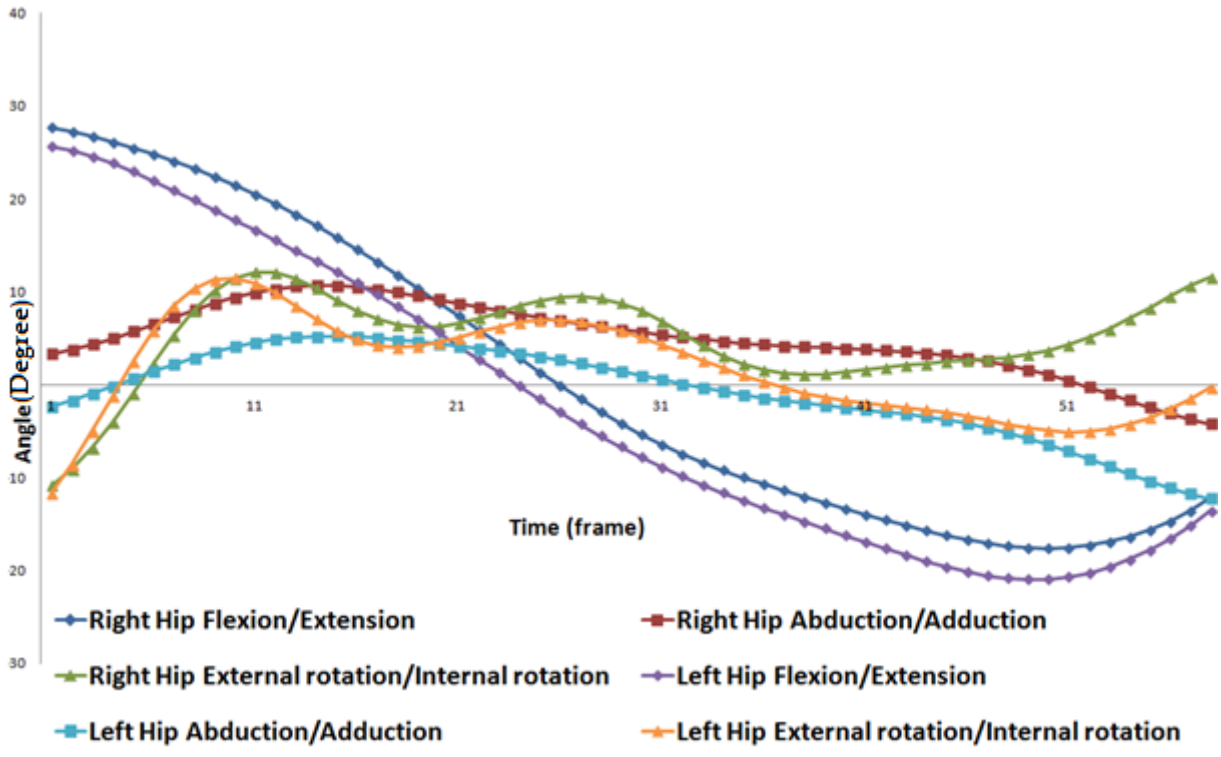

Figure 3-5: Hip rotation of right and left leg during the Normative mode

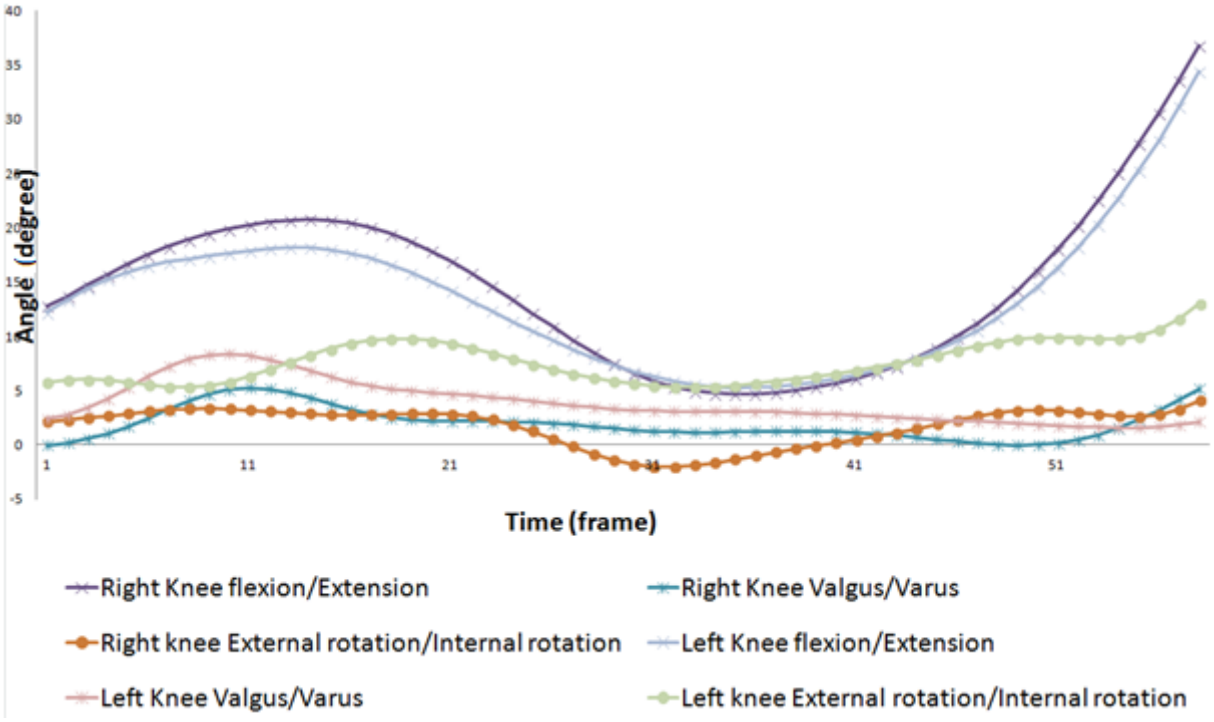

Figure 3-6: Knee rotation of right and left leg during the Normative mode

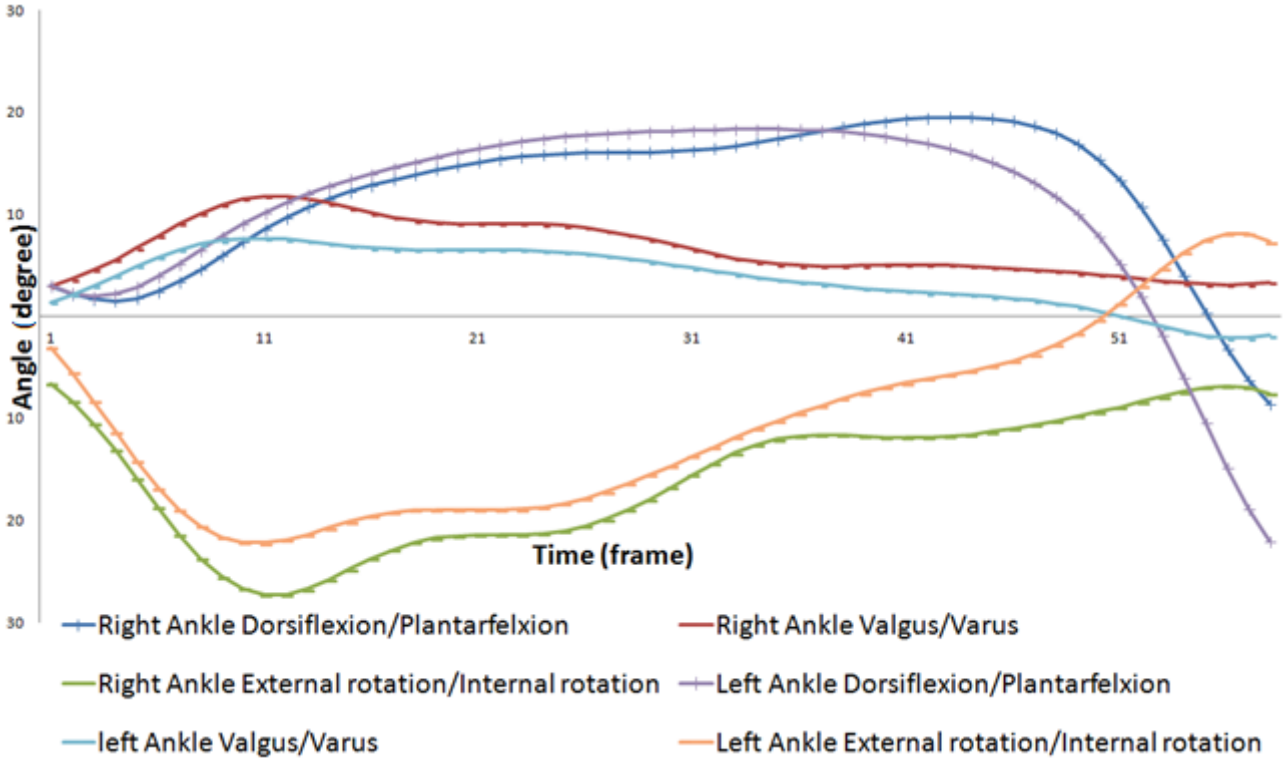

Figure 3-7: Ankle joint`s rotation of right and left leg during the Normative mode

With respect to Figure 3-8, there is asymmetry between rotation of right and left hip joints in external/internal rotation during Targeting mode. The maximum difference between these two trajectories reaches to 6˚, while the trend of these two trajectories was perfectly similar to each other during 9s of start. Based on Figure 3-9, the maximum difference of 7˚ has been observed in knee valgus/varus movement during Targeting mode while their trends are quite similar from time (36s-58s). With respect to Figure 3-10, the significant asymmetry of 16˚ has been observed in ankle external/internal rotation in Targeting mode. Also, 4˚ difference has been observed between trajectories of dorsiflexion/plantarflexion and it has been illustrated in Figure 3-9.

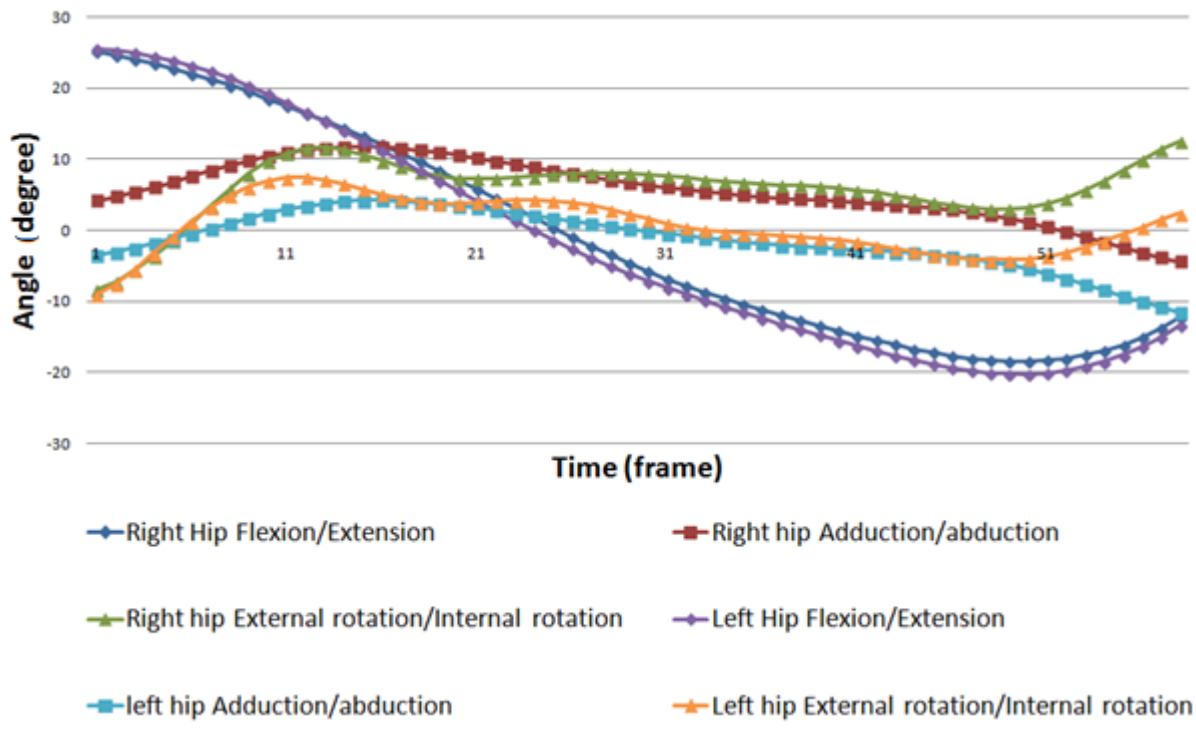

Figure 3-8: Hip rotation of right and left leg during the Targeting mode

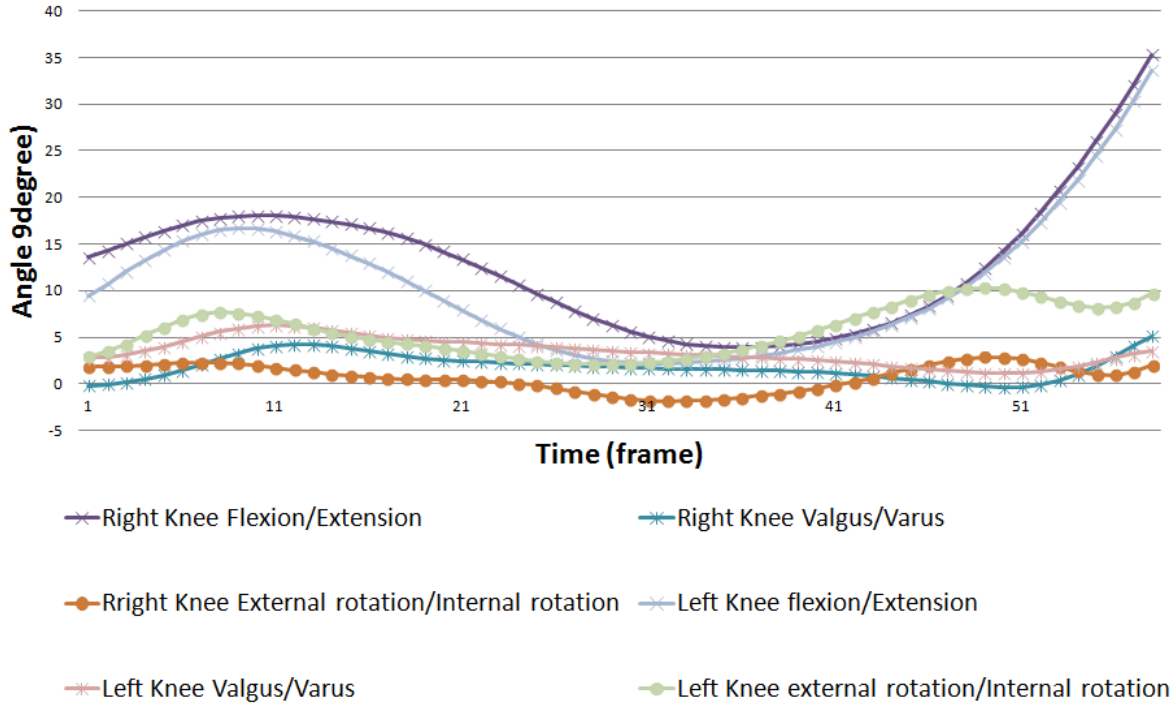

Figure 3-9: Knee rotation of right and left leg during the Targeting mode

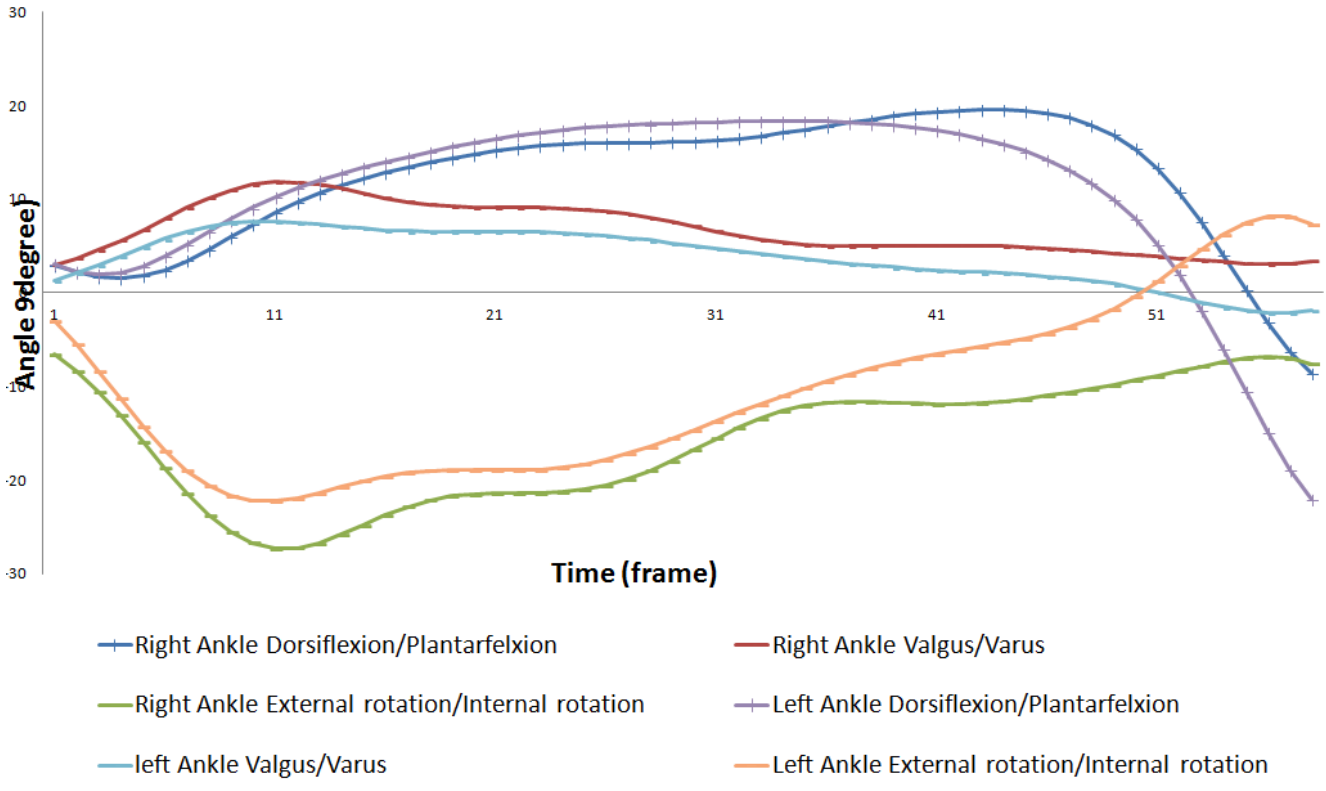

Figure 3-10: Ankle rotation of right and left leg during Targeting mode

Based on Figures 3-5, 3-10 and Table 3-4, it can be found that there is symmetry between the trend of trajectories of hip joints in Normative and Targeting mode. There was symmetry in few seconds of start, between external/internal rotation of hip joint in Normative mode while there is not that similarity in Targeting mode. We can see that there is not significant asymmetry between the rotations of knee joints in Normative and Targeting modes and the trend of lines are very similar to each other. We can see this similarity in Figures 3-6 and 3-10, for the rotations of ankle joint during Normative and Targeting modes.

3.4 Conclusion

In this chapter the symmetrical/asymmetrical behaviour of the joints in the lower limbs of able-bodied during gait cycle using joints' mechanical modelling was investigated. Experimental data from a gait laboratory were used to calculate the joints' angles for the left and right legs of a number of able-bodied participants. In addition, the effect of laterality on symmetry/asymmetry of angular rotation of joints for 28 participants was investigated based on gait measurements and the mechanical model. With respect to obtained data from the mechanical model of the leg, it was found that laterality had no specific relation with angular rotation of the lower limb`s joints before and after hitting the target. Therefore, it can be concluded that there is not significant asymmetry between rehabilitation exercises which will be defined to be done by the patients with their natural movements of the body like normal gait walking and stair climbing, or goal directed exercises like kicking a ball, hitting a target and score-based games. So the hypothesis of existence of asymmetry between the lower limb joint`s motions has been failed. So in this case, the factor of symmetry/asymmetry between the joints can be neglected from our considerations during designing the control system.

Chapter 4

Biomechanical relationships of the lower limbs

4.1 Introduction

In chapter 3, it was found that Normative/Targeting modes don`t affect on symmetry/asymmetry of lower limb`s joints rotations. In this chapter, the step length as another important gait parameter will be studied [121].

Gait is one of the fundamental abilities of a human to walk in a cluttered environment. The anticipation of foot placement mostly occurs during locomotion control; and the most common anticipation is adjusting step length based on received data from the visual system to avoid contacting with obstacles and to have stable foot placement [122].

Generally, gait involves both motor programming (Normative) and visual control (Targeting). Motor programming is like normal walking and visual control is considering a specific area on the floor for foot placement [123]. Differences and asymmetries have been often observed in kinematic and spatio-temporal parameters, such as step and stride length and range of joint motion [124,125]. Inequality in using the lower limbs during walking has been reported in [126, 127].

One of the arguable factors in gait analysis is Targeting. A study of step adjustment during running demonstrates significant step alteration, which occurs on the force plate contact. Here, it is also shown that the majority of step adjustments occur on the last step. Furthermore, subjects often used Targeting during their approach to the force plate. As a result, the variability of step length increases on the target. In addition, studies related to the effect of Targeting on Ground Reaction

Force GRF show that the results are similar whether or not the subject has been informed of the presence of the force plate. In some other studies, it was found that Targeting has no effect on the magnitude, timing and variability of GRF within a specific time domain [123, 128, 129].

In most cases subjects are not aware of the presence of a force plate along the walkway. However, this may decrease the probability of locating the entire foot on the force plate. Consequently, the subjects are directed by the clinicians to initiate their gait cycle in such a way that the force plate is struck [123]. Extension and flexion of step length is one of the most common effects of Targeting on humans' gaits. This means that subjects use visual strategies to adjust their step length and reach the target. In a study involving two step lengths either side of the force plate for two different conditions (i.e. Targeting and Normative), it was shown that there is no statistical difference between the mean step length of each condition [123].

The aim of this chapter is to determine the effect of Targeting on step length during walking. For designing a suitable rehabilitation exercises like normal walking, it is important to know the effect of step length during natural and pre-defined exercises. Any asymmetry will be defined as a constant value in biomechanical equations of lower limbs which will be implemented in to the control system of the robot. A series of experimentations were conducted using eight able-bodied volunteers of both sexes, in a gait laboratory. A statistical two-way ANOVA test was applied to the measured data in order to determine possible appreciable differences amongst them. The methodology for the experiments is presented in section 2 and the results and discussion are presented in section 3.

4.2 Methodology

4.2.1 Gait analysis

Eight able-bodied volunteers (four males and four females) were tested in the Clinical Measurements Laboratory (CML) at the West Midlands Rehabilitation Centre (WMRC), Birmingham, UK. In this study four males with an age of (26.1 years±4.1), height of (176.34 cm±7.92), weight of (79.2 kg±6.03), BMI of (24.42±2.01) and four Females with an age of (25.76 years ±5.39), height of (168.65cm±4.54), weight of (72.63 kg±3.59) and BMI of (23.42±1.69) participated. Prior to the experimentation ethical approval was granted to the WMRC and all subjects completed a data collection consent form and a health declaration form. Their anthropomorphic measurements were also recorded.

The laboratory was equipped with two Basler digital video cameras, twelve Vicon infrared cameras (with a sampling frequency of 100 Hz) together with associated Vicon Nexux software and a KISTLER force plate (at a sampling rate of 1000Hz) with the dimensions of 600×400×100 mm. The Basler video cameras were aligned with the centre line of the force plate and were used for recording along sagittal and coronal planes. The infrared cameras contained six MXT40 and six MX30 placed around the laboratory.

In this chapter, same as previous chapter, two types of experiments were conducted: Normative and Targeting. In the Normative test, the subjects were asked to walk with self speed, while they were not aware of the presence of a force plate along the walkway. In the Targeting test subjects were informed about the presence of the force plate. As can be seen in Figure 4.1, the obtained data was processed and a 3D model of the lower extremities was simulated using the Vicon Nexus software.

As it is shown in Figure 4-1, in order to find the exact differences between the step lengths, the gait cycle of the volunteered subjects was divided into three sections: (i) one step before the force plate; (ii) on the force plate; and (iii) one step after the force plate. The difference between the calculated step lengths is then considered based on statistical ANOVA analysis.

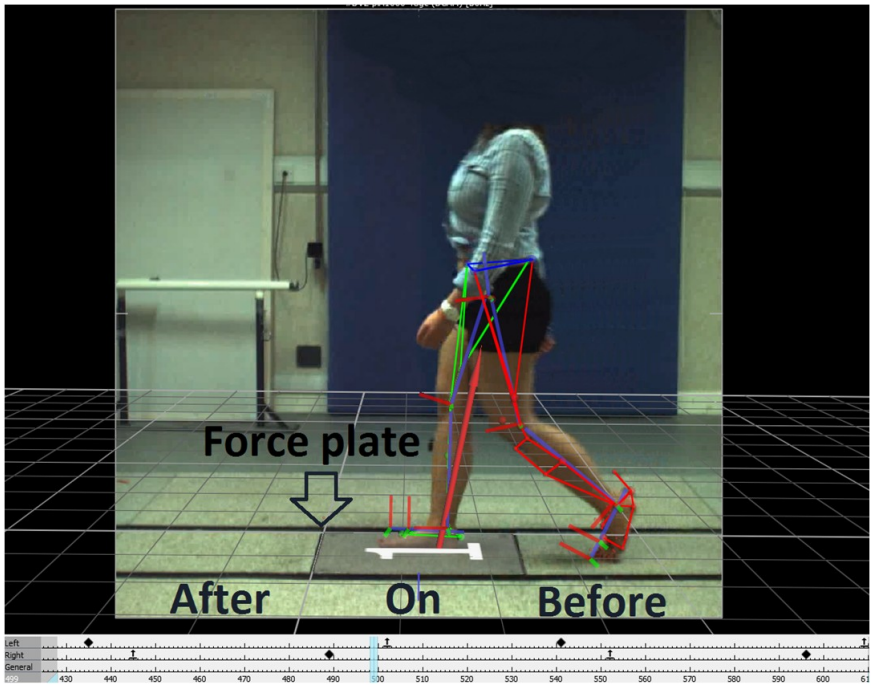

Figure 4-1: Step difference before, on and after the force plate

In the experiments 5 trials for each subject were conducted; resulting in a total of 5 (trials per subject) × 8 (subjects) × 3 (specified sections) × 2 (Targeting and Normative test) = 240 trials. The obtained data were normalized using equation 16. The average and standard deviation values of the left and right step lengths and the difference between them in each section, for both Normative and Targeting tests were then calculated.

4.3 Results and Statistical analysis

Before using the ANOVA test, Levene`s test was used to check the homogeneity of variances of subjects in Targeting and Normative groups and it was found that both groups met the assumption of homogeneity of variance. The ANOVA test was run by IBM SPSS Statistics 22 software to find the effect of sex and foot strike position on step difference between the right and left leg during the Targeting and Normative tests. The confidence level of 0.05 was used in this experiment and based on null hypothesis P value < 0.05 represents difference between two factors, P value < 0.001 shows the significant difference between two factors.

As it can be seen in Table 4-1, there was a significant effect from the position of the foot strike on the maximum step difference of the right leg and left leg in the Targeting test, $F(2,114)=61.011, p<.001$. While a non-significant effect of sex on the maximum step difference of the right and left leg was found during the Targeting test $F(2,114)=0.474$, $p=0.492$. A non-significant interaction between the sex of the participants and the position of the foot strike on step difference between the right and left leg was found $(2,114)=0.177$, $p=0.838$.

As it can be seen from the interaction plot of Figure 4-2, the mean step difference of male and female participants has been decreased sharply on the force plate and this difference declined gradually after the force plate.

Table 4-1: ANOVA Table for the Targeting test

Tests of between-subjects effects(Targeting)

Dependent Variable: step

Source	Type III Sum of Squares	df	Mean Square	F	Sig.
Corrected Model	0.042[a]	5	0.008	24.570	0.000
Intercept	0.113	1	0.113	327.778	0.000
Sex	0.000	1	0.000	0.474	0.492
Position	0.042	2	0.021	61.011	0.000
Sex * Position	0.000	2	6.083E-5	0.177	0.838
Error	0.039	114	0.000		
Total	0.194	120			
Corrected Total	0.082	119			

a. R Squared = .519 (Adjusted R Squared = .498)

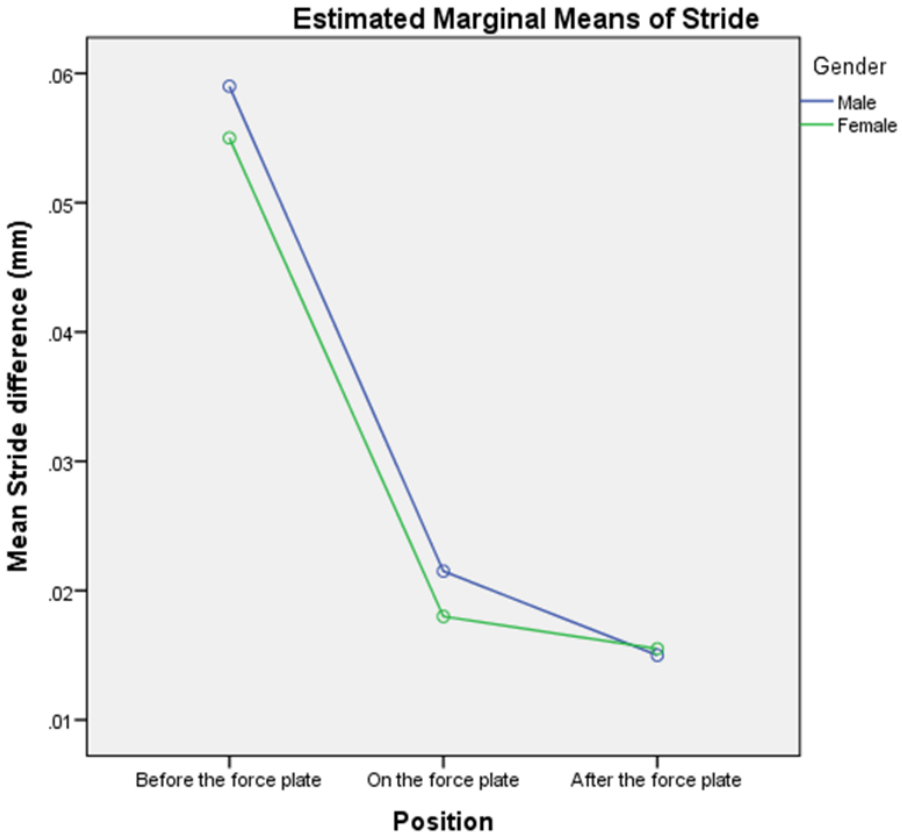

Figure 4-2: Interaction plot (Targeting)

With respect to the interaction plot, the average step difference of male and female participants was very similar. In this particular graph the lines actually cross, which illustrates a fairly small interaction between independent variables. The interaction effect illustrates that sex has no effect on step length during all positions until the foot strikes after the force plate and that the effect of position is very small in male participants where this difference is negligible. On the other hand, the sex of the participants didn`t have a significant effect on step difference of the right and left leg before, on and after the force plate.

Based on post hoc tests, the step difference of participants was similar on the platform and after the platform, $M_{diff} = 0.0045, 95\%\ CI\ [0.0007, 0.0098], p = 0.841$; however it was lower before the force plate compared to after the force plate, $M_{diff} = 0.0418, 95\%\ CI\ [0.0518, 0.0317], \mathrm{p} < .001$

and a little lower before the force plate compared to on the force plate, $M_{diff} = 0.373, 95\%\ CI\ [0.0283, 0.0462], p < .001$. The mean step difference of participants on the force plate (0.0198mm) and after the force plate (0.0153mm) were so similar that the probability of the obtained difference between those means is 0. 841.The R-E-G-W-Q test confirms that the means of the 'on the platform' and' after the platform' positions were equal; where the mean of the 'before the force plate' position was different.

The results given in Figure 4-3 for the Targeting tests clearly demonstrate that visual control does affect the symmetry of left and right step lengths and provides a remarkable difference between them. Here significant differences are particularly exhibited between step lengths at one step before the force plate. Moreover, fluctuations amongst the results of this section are higher than the two other sections. This considerable fluctuation at one step before the force plate is due to the expansion and flexion of steps in order to adjust foot placement and reach the target.

As shown in Figure 4-3, there are significant fluctuations amongst the results of step lengths one step before the force plate. Furthermore, in the majority of the cases there is a remarkable difference between the values of the step lengths' difference one step before the force plate, in contrast with the other two sections. The difference of the step lengths one step before the force plate changes between 0.01 m to 0.13 m. On the force plate the values vary between 0 to 0.05 m and after the force plate the variations are between 0 to 0.04 m. The fluctuation of differences between left and right step lengths on the force plate tends to decrease in comparison with the corresponding values one step before the force plate. However, more variations between left and right step lengths still exist in comparison with the step length after the force plate.

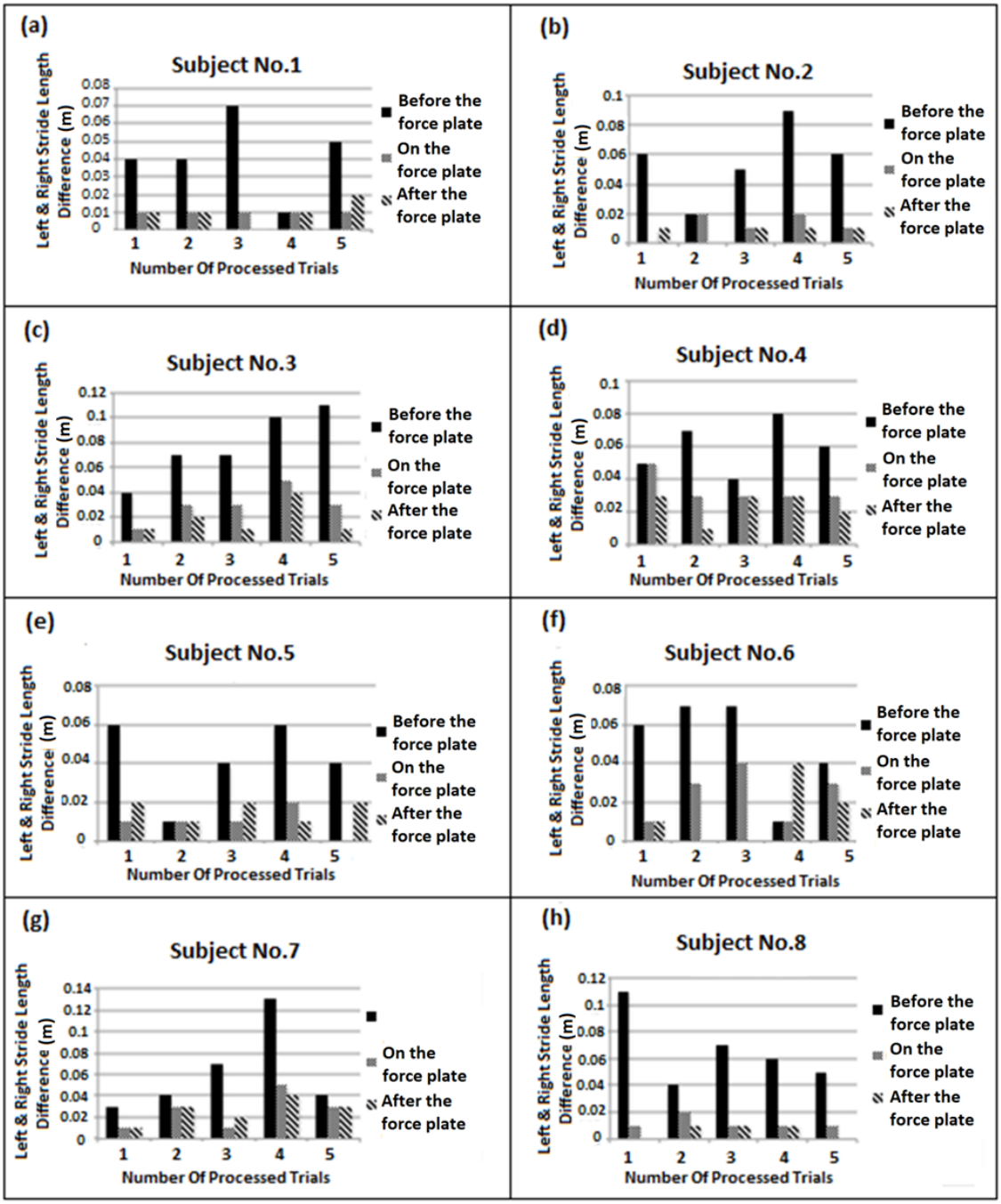

Figure 4-3: **Step length differences before, on and after the force plate in Targeting mode**

As it can be seen in Table 4-2, both sex and position had a non-significant of (F (1,114) =0.395, p=0.531) and (F (2,114) =0.653, p=0.522) on step difference, respectively. A non-significant interaction between sex of participants and position of foot strike, on step difference between the right and left leg was (2,114) =0.153, p=0.858.

Table 4-2: ANOVA Table for the Normative test

Tests of between-subjects effects(Normative)

Dependent Variable: step

Source	Type III Sum of Squares	df	Mean Square	F	Sig.
Corrected Model	0.000[a]	5	4.150E-5	0.401	0.847
Intercept	0.026	1	0.026	252.546	0.000
Sex	4.083E-5	1	4.083E-5	0.395	0.531
Position	0.000	2	6.750E-5	0.653	0.522
Sex * Position	3.167E-5	2	1.583E-5	0.153	0.858
Error	0.012	114	0.000		
Total	0.038	120			
Corrected Total	0.012	119			

a. R Squared = .017 (Adjusted R Squared = -.026)

As it can be seen in the following interaction plot of Figure 4-4, step difference in males gradually decreased on the force plate and then sharply declined after the force plate. Step difference in

females increased on the force plate and then it dropped sharply. It is worth mentioning that the step difference for both males and females declined after the force plate, but this difference was very significant in males. The mean step difference was similar for both males and females before the force plate.

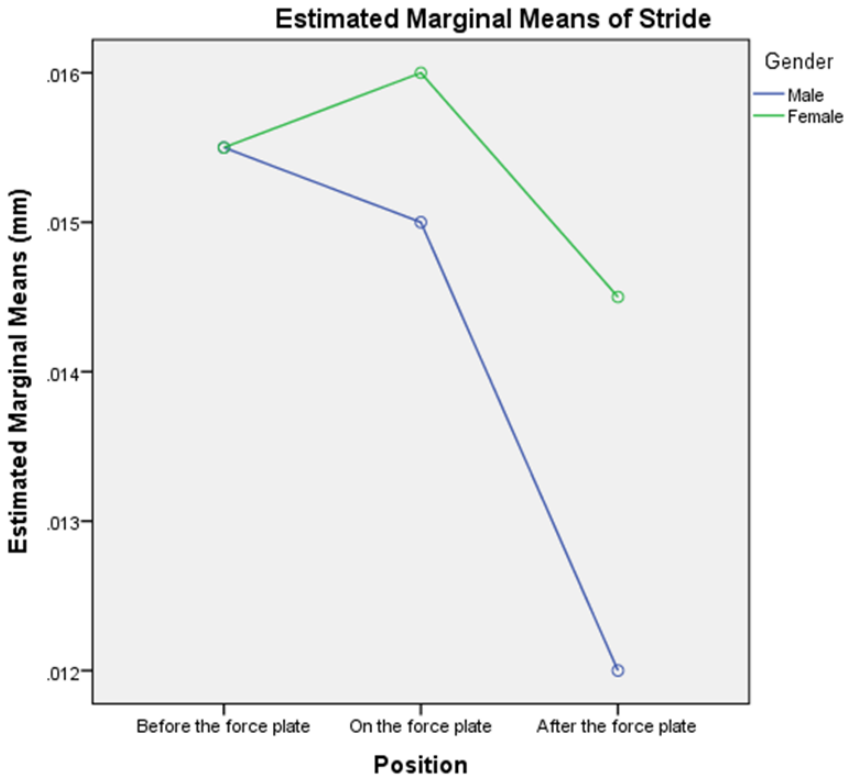

Figure 4-4: **Interaction plot (Normative)**

Based on the post hoc test, the step difference between the right and left leg was very similar before the force plate and on the force plate, $M_{diff} = 0.0000, 95\%\ CI\ [-0.0054, 0.0054], p = 1$, however it was lower before the force plate and after the force plate

$M_{diff} = 0.0023, 95\%\ CI\ [-0.0031, 0.0076]\ , p = 0.585$ and it is same on the force plate and after the force plate, $M_{diff} = 0.0022, 95\%\ CI\ [-0.0031, 0.0076], p = 0.585$.

Figure 4.5 illustrates the differences between left and right step lengths of five processed trials of eight able-bodied subjects. The graphs in the Figure show that no specific pattern could be found in each step length.

The results given in Figure 4.5 show that when the subjects are not considering visual control to reach a specific area on the floor, the difference between step lengths varies within a narrow range of between 0 to 0.04 m. However, in the majority of the trials the corresponding value is 0.02 m, or less. This small difference between step lengths could be due to the provision of motor control during walking, experimental error, inaccurate positioning of markers, or defining gait events at an inappropriate time within a cycle.

After a comparison of step difference within each experiment (Targeting/Normative), the effect of target and position on step difference between the right and left leg has been investigated .With respect to the results of Table 4-3, there were significant effects from Targeting/Normative ($F(1,234)=0.015$, $p < .001$) and the position of the leg ($F(2,234)=0.011$, $p < .001$) on the step difference. Also, it is found that there is a significant effect from interaction between Targeting/Normative and position on step difference between the left and right leg ($F(2,234)=0.010$, $p < .001$).

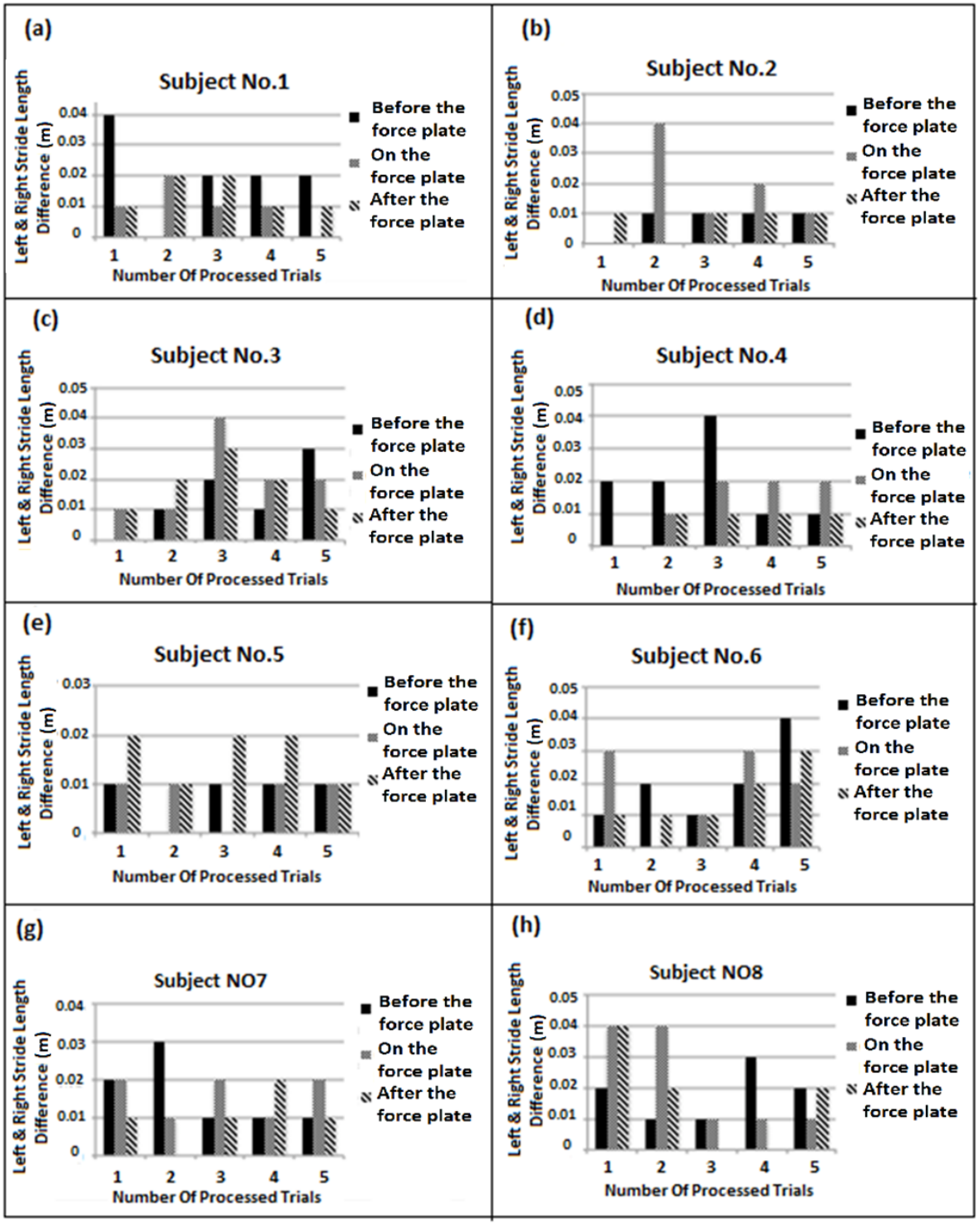

Figure 4-5: **Step length differences before, on and after the force plate in Normative test**

Table 4-3: ANOVA Table for the Targeting/Normative test

Tests of between-subjects effects(Targeting/Normative)

Dependent Variable: step

Source	Type III Sum of Squares	df	Mean Square	F	Sig.
Corrected Model	0.057[a]	5	0.011	52.222	0.000
Intercept	0.124	1	0.124	563.505	0.000
Target	0.015	1	0.015	69.210	0.000
Position	0.022	2	0.011	51.134	0.000
Target * Position	0.020	2	0.010	44.817	0.000
Error	0.051	234	0.000		
Total	0.232	240			
Corrected Total	0.109	239			

a. R Squared = .527 (Adjusted R Squared = .517)

With respect to the interaction plot of Figure 4-6, it can be seen that the mean step is hugely different between Targeting and Normative before the force plate, but this difference gradually decreased on the force plate and after the force plate. Planning and adjusting the foot to hit the force plate is the main reason for the sharp decline of step difference in the Targeting test in position one.

Figure 4-6: **Interaction plot (Targeting/Normative)**

Figures 4-7(a) and Figure 4-7(d) present average values of left step length, right step length, and differences between left and right step lengths of eight healthy subjects in the three cycle sections. It can be seen from the results that the average of the differences between left and right step lengths in the Normative test is approximately zero; while the corresponding average in the Targeting test increased and varied around 0.01 *m*. In addition, the average of the left and right step lengths increased in Figure 4-7(d).

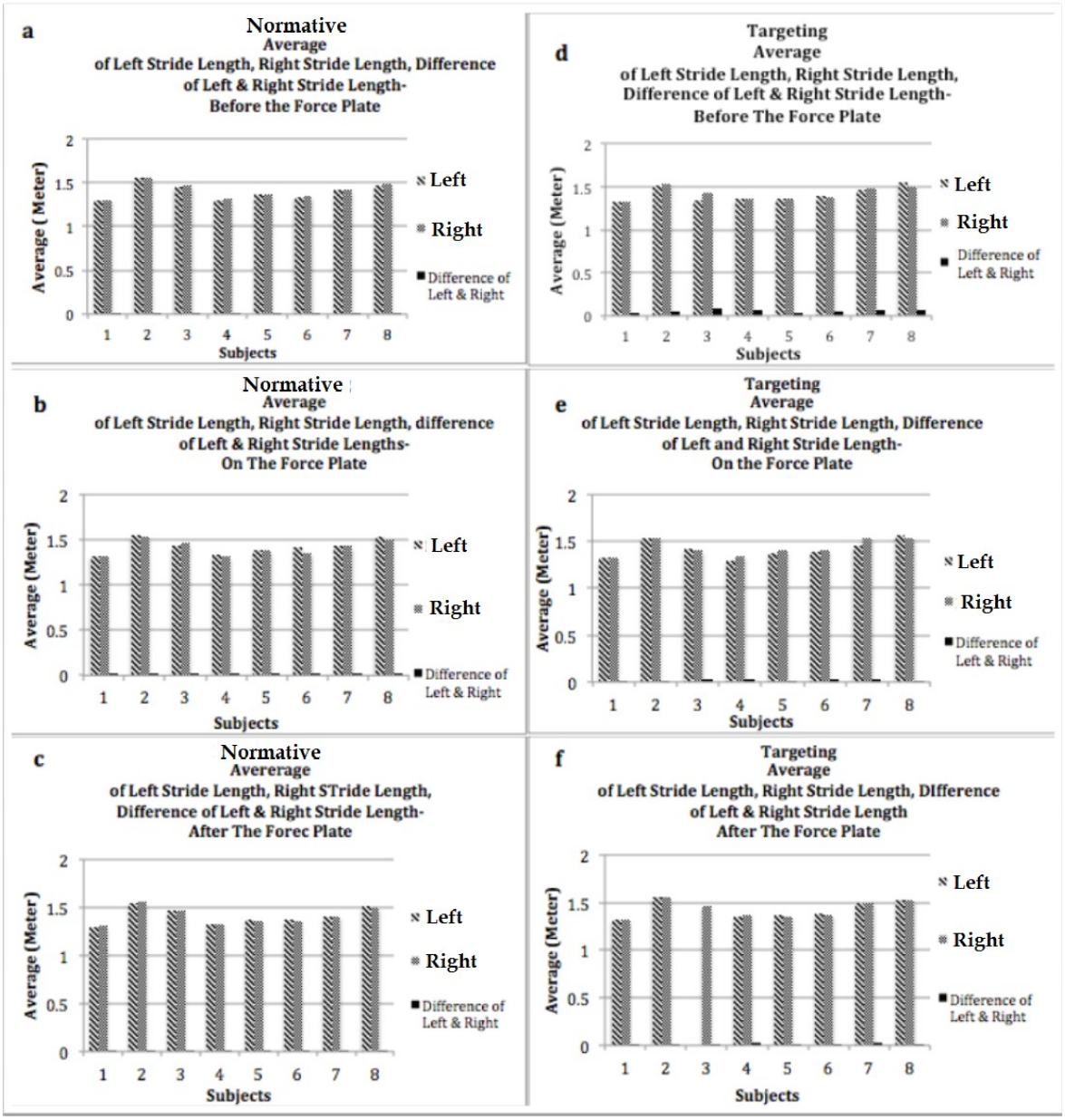

Figure 4-7: **Average values of left step length**

Figures 4-7(b), 4-7(c), 4-7(e) and 4-7(f) display very small differences between the average of the left and right step lengths on the force plate and after the force plate. Consequently, the average of the difference between the left and right step lengths is about zero, in the last two cycle sections.

Figure 4-8 presents the standard deviations (SD) that correspond to the values given in Figure 8. It can be seen that the SDs of the difference between the left and right step lengths given in Figure 4-

8(d) tend to increase in comparison with that of Figure 4-8(a). In the Normative test, the SDs are less than 0.01; while in the Targeting test the corresponding values range from 0.013and 0.04. It is also noted that although fluctuations between SD values in the Targeting and Normative test on the force plate are reduced in comparison with the step length before the force plate, the variation is higher than that in the step length section after the force plate.

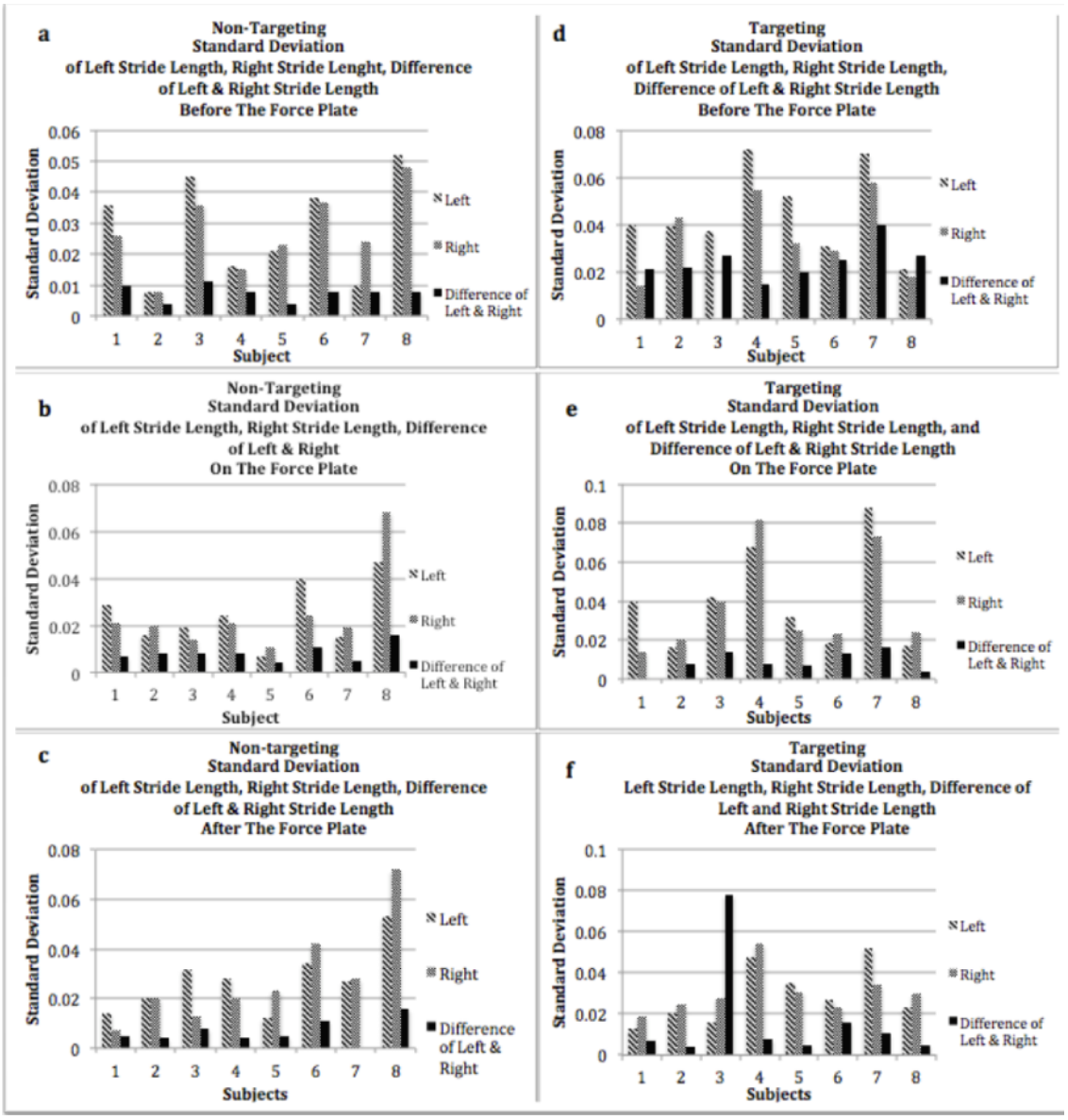

Figure 4-8: **Standard deviation of differences of step length**

4.4 Biomechanical relationship of right and left leg

As shown in Figure 4-9, the skeleton model and muscles of healthy subject have been modelled in OpenSim using UpperLower Body model [130] in order to have a better understanding about symmetries/asymmetries between the right and left legs during a gait cycle. It was linked to Vicon Nexus using Lee-Son's Toolbox in order to visualize the range of rotation of lower body`s joints.Then, it was linked to Vicon Nexus using Lee-Son's Toolbox in order to visualize the range of rotation of lower body`s joints.

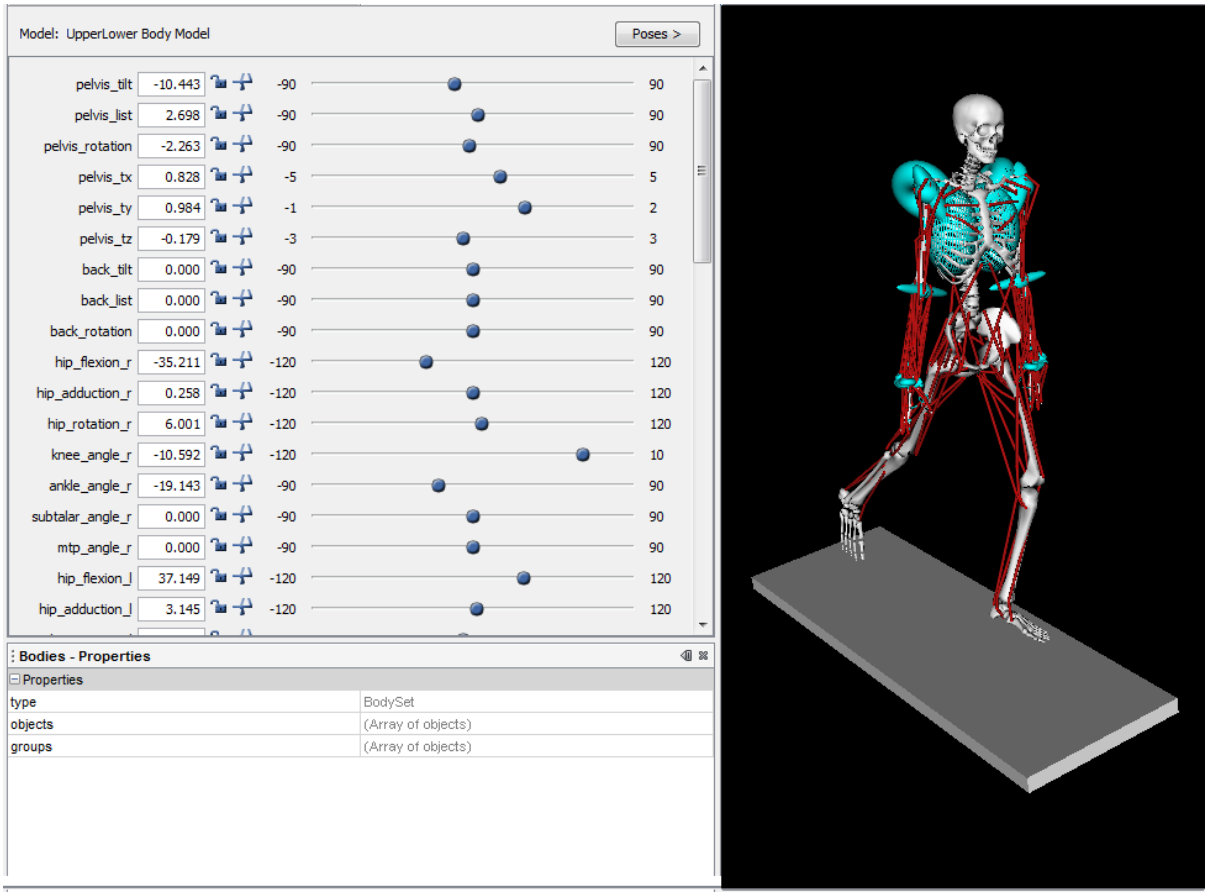

Figure 4-9: Skeleton model of lower modeled in OpenSim using LowerUpper Body model

Based on foot step analysis and lower limb joint rotations, the trajectory of left foot and right foot have been modelled ,during a gait cycle in Normative mode, in Matlab using curve fitting. A

constant value will be defined based on step length differences, for calculation of biomechanical relationship of the legs, and then it will be implemented into the control system of the robot. It is very important to implement the differences between the right and left legs in order to rehabilitate the patients based on their own natural lower limb signatures. In the same way, the trajectory of right and left legs have been modelled and analyzed during Targeting mode.

As shown in Figure 4-10, In order to personalize the relationship between right and left leg for each subject, the trajectory of foot segment has been analyzed and modeled during a gait cycle. The time delay between start point of right foot trajectory and left foot trajectory was 0.48s.

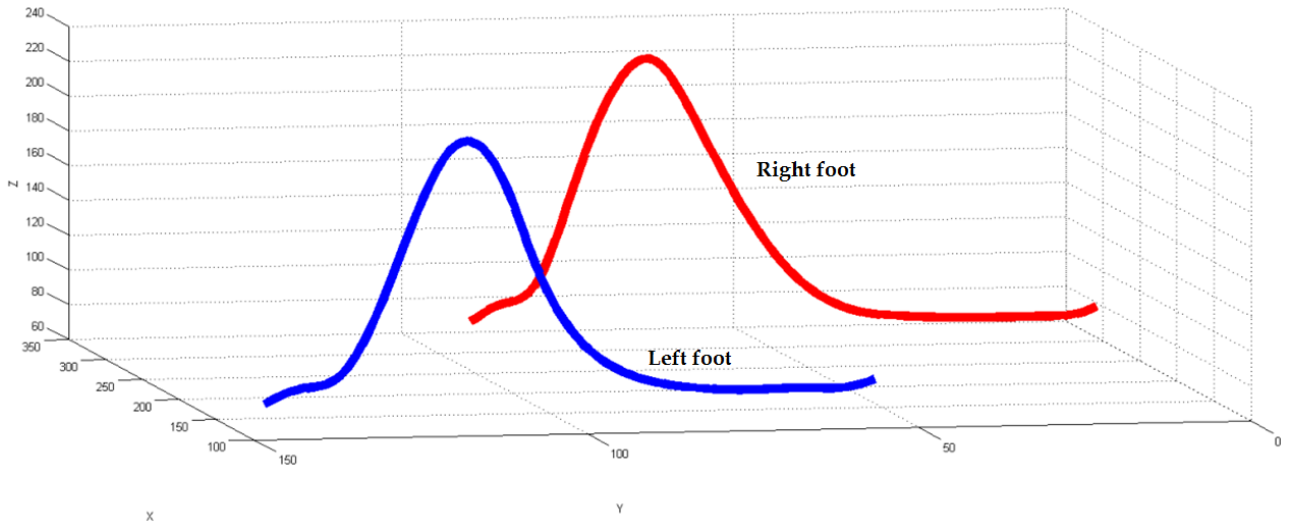

Figure 4-10: Right and left foot trajectory of healthy subject during a gait cycle in Normative mode. Red line shows the trajectory of right foot and the blue line shows the trajectory of left leg

Matlab has been used to fit the surface representing the trajectory of each leg. In order to find the proper model for representing the trajectory, the position of points have been imported to the Surface Fitting toolbox, then a fifth degree Polynomial with LAR robustness has been selected. The following linear model Poly55 represents the fitted surface for the right foot (Figure 4-11):

$f(x,y)_{Right}$ = p00 + p10*x + p01*y + p20*x^2 + p11*x*y + p02*y^2 + p30*x^3 + p21*x^2*y + p12*x*y^2 + p03*y^3 + p40*x^4 + p31*x^3*y + p22*x^2*y^2 + p13*x*y^3 + p04*y^4 + p50*x^5 + p41*x^4*y + p32*x^3*y^2 + p23*x^2*y^3 + p14*x*y^4 + p05*y^5 (4. 1)

Where x is normalized by mean 313.1 and standard deviation (SD) 11.21, and where y is normalized by mean 48 and SD 28.15. Constant values have been calculated and shown in Table 4-4:

Table 4-4: Constant values used in equation 4.1

p00 =112.3	p10 = 6.35	p01 =108.1	p20 =-19.18	p11 =120.9	p02 = -19.23	p30 = -4.57
p21 =65.51	p12 = -48.48	p03 = -74.38	p40 = 3.581	p31 = -2.1	p22 = -24.91	p13 = -60.93
p04 =0.2699	p50 = -1.506	p41 = -2.855	p32 =-2.014	p23 =-20.86	p14 =11.99	p05 = 9.556

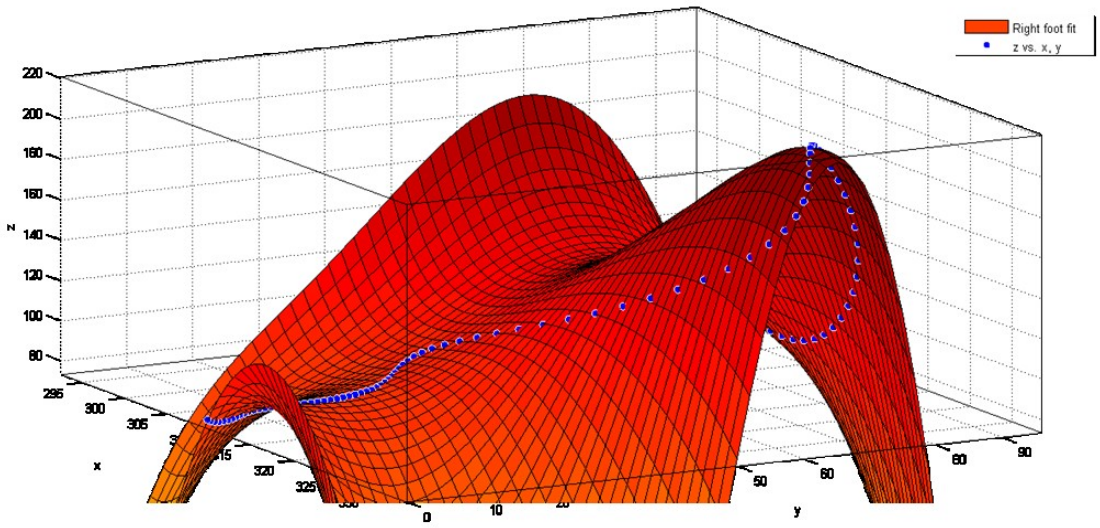

Figure 4-11: Surface fitting of the right foot trajectory

The summed square of residuals (SSE) has been calculated in order to measure the total deviation of the response values from the fit to the response value (Figure 4-12). The SSE of 1.0552 indicates that the model has a smaller random error component. R-square shows how successful the fit is in

explaining the variation of data and the R-Square of 0.9999 indicates that the fit explains 0.99% of the total variation in the data about average. The residual degree of freedom was 76 and the adjusted R-square of 0.998 indicates that the surface has been fitted properly. Root Mean Squared Error (RMSE) or fit standard error has been calculated to estimate the standard deviation of the random component in the data. The RMSE of 0.2494 shows that fit is useful for prediction.

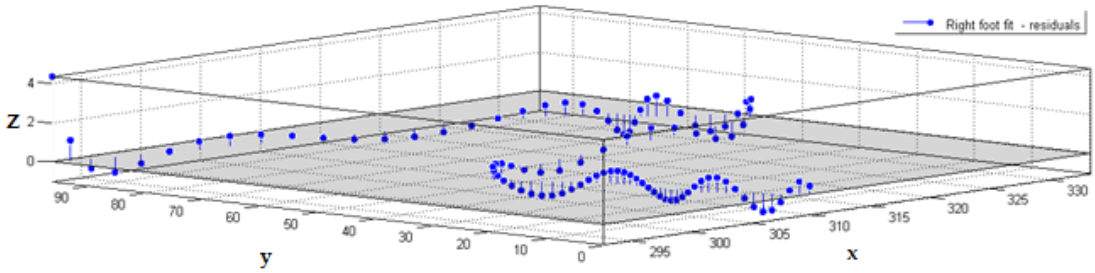

Figure 4-12: Residual plot of the right foot trajectory

The following contour plot (Figure 4-13) displays isolines of matrix z where z is interpreted as heights with respect to the x-y plane for the right trajectory:

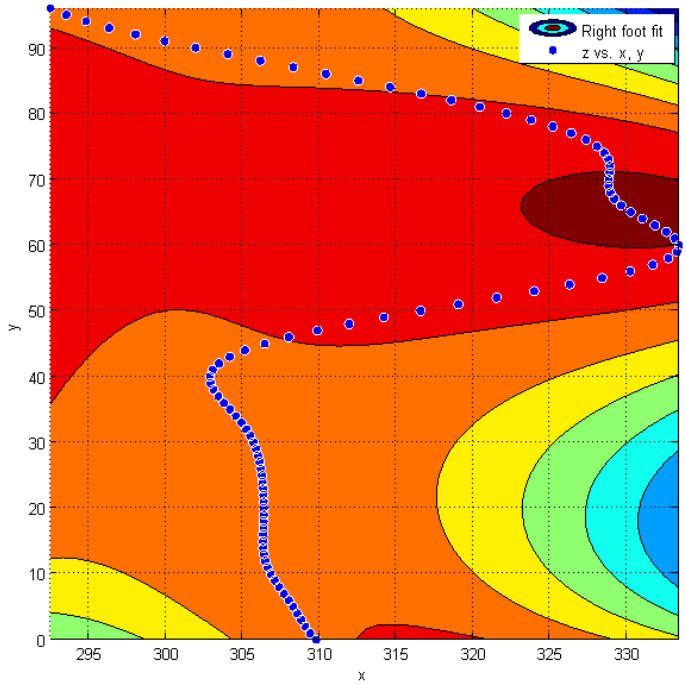

Figure 4-13: **Contour plot of the right foot trajectory**

The following linear model Poly55 represents the fitted surface for the right foot (Figure 4.14):

$f(x,y)_{Left}$ = p00 + p10*x + p01*y + p20*x^2 + p11*x*y + p02*y^2 + p30*x^3 + …. + p05*y^5

(4.2)

Where x is normalized by mean 161 and SD 23.2 and where y is normalized by mean 96 and SD 28.15. Constant values with 95% confidence bounds have been calculated and shown in Table 4-5:

Table 4-5: Constant values used in equation 4.2

p00 =148.9	p10 = -67.2	p01 =-30.14	p20 =-28.9	p11 =48.1	p02 = -61.3	p30 = 87.3
p21 =402.8	p12 = 337.3	p03 = 52.28	p40 = -39.88	p31 = -303.4	p22 = -331.4	p13 = -172.6
p04 =-17.45	p50 = 38.27	p41 = 283	p32 =847.8	p23 =801.5	p14 =286.7	p05 = 40.92

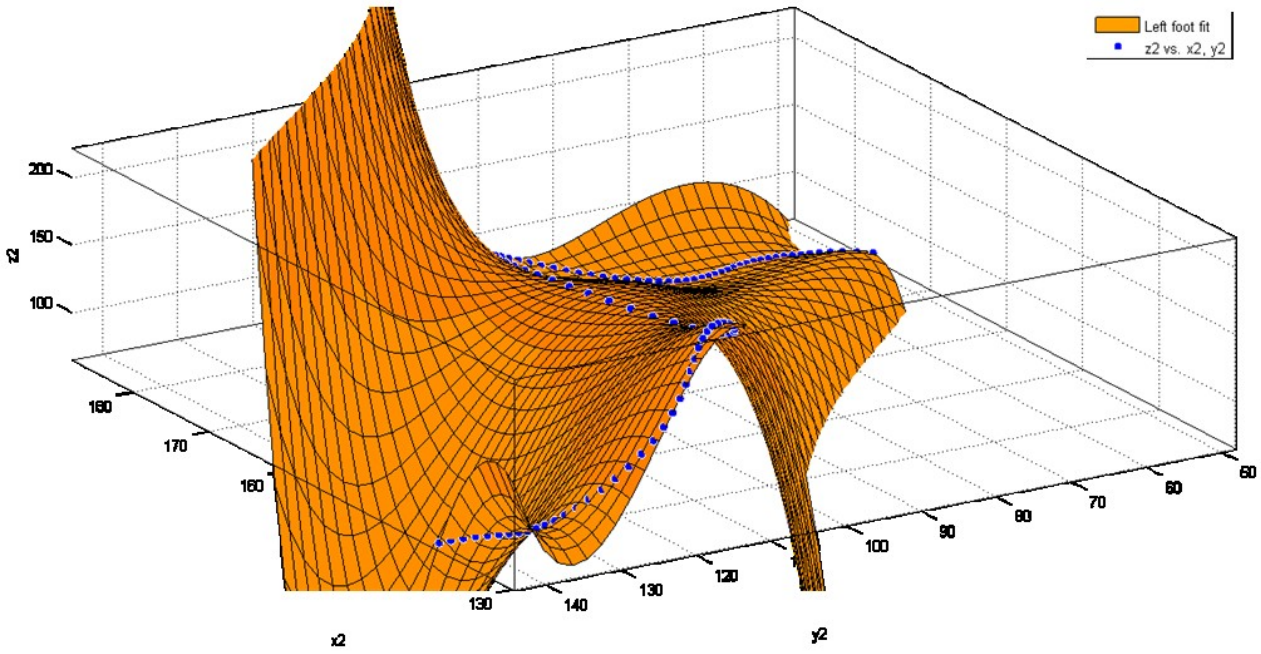

Figure 4-14: Surface fitting of the left foot trajectory

For the left leg, the total deviation of the response values from the fit to the response value (SSE) was 0.9396 which indicates that the model has a smaller random error component than the trajectory of right leg (Figure 4-15). The R-square for the left foot was 0.99 which it indicates that the fit explains 0.99% of the total variation in the data about average. The residual degree of freedom was 76 and the adjusted R-square of 0.999 indicates that the surface has been fitted properly. Fit standard error of 0.1858 shows that fit is more useful for prediction than right RMSE.

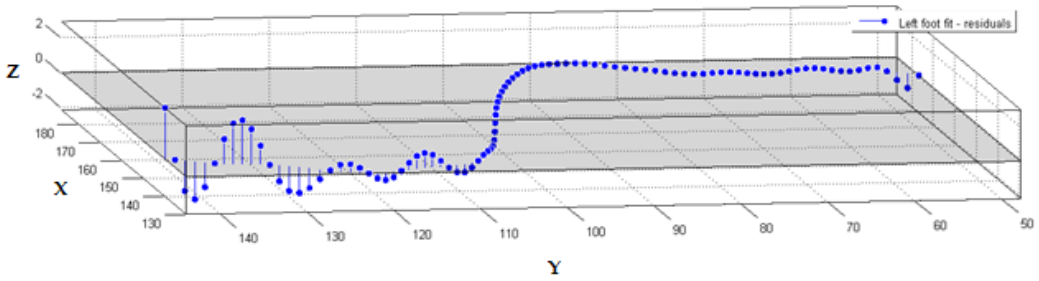

Figure 4-15: Residual plot of the left foot trajectory

The following contour plot (Figure 4-16) displays isolines of matrix z where z is interpreted as heights with respect to the x-y plane for the right trajectory:

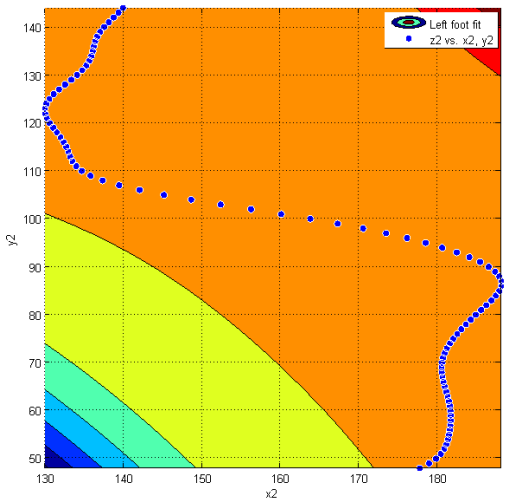

Figure 4-16: Contour plot of the left foot trajectory

With respect to the constant value for representing the step differences and the functions found for trajectories of right and left leg, the following equation represents the relation between right and left legs:

$$\zeta(\text{right, left}) = \alpha \times (f(x,y)_{\text{Right}} - f(x,y)_{\text{Left}}) \quad (4.3)$$

Where ζ(right, left) represents the biomechanical relation between right and left leg and α represents the constant value of step differences between the right and left legs.

4.5 Discussion and conclusion

This chapter presented the results of a series of experimental tests to determine the step length differences of gait cycles of eight able-bodied subjects in a gait laboratory. The experimentation produced 240 trials of Targeting and Normative tests for three different gait cycle sections including before, on and after a force plate along a gait walkway. A statistical ANOVA test was used to evaluate the results. The results suggest that sex has no significant effect on step difference between the left and right leg; while the position of the foot strike has a significant effect on step difference during the Targeting test. The tests show that, in the Targeting test when participants had a foot strike on the force plate and after the force plate, they had similar step differences =0.841; while the step difference before the force plate was significantly different than on the force plate ($p<.001$) and after the force plate ($p<.001$). In the Normative test the difference between the left and right step lengths varies in a narrow range. Both sex and positions were non-significant effects on step difference. In the Normative test, the step difference between the right and left leg was very similar before the force plate and on the force plate($p = 1$); however it was lower before the force plate and after the force plate ($p = 0.585$) and it was the same on the force plate and after the force plate ($p = 0.585$). Generally, it was found that both the presence/lack of target and position of the foot strike have significant effects on step difference. Results of this test

provide suitable information for the therapists during gait analysis. Based on the obtained results, the mathematical model for the right and left leg has been calculated by curve fitting toolbox in Matlab. With respect to the similarities and differences between the legs and calculated functions for the trajectories, the biomechanical relationship between the legs has been established for healthy subjects. Based on established database, a particular model can be generated by the control system for rehabilitation of hemiplegic patients. Based on that control system, the movements of patients will be corrected with respect to the healthy database.

Chapter 5

Lower Limb Rehabilitation Exercises Using a Parallel Robot

5.1 Introduction

The aim of this study is to investigate the behaviour of a 6 DoF parallel robot during the performance of various rehabilitation exercises. The foot trajectories of twenty healthy participants have been measured by a Vicon system during the performing of four different exercises. Based on the kinematics and dynamics of a parallel robot, a MATLAB program was developed in order to calculate the length of the actuators, the actuators' forces, workspace and singularity locus of the robot during the performing of the exercises. The calculated length of the actuators and the actuators' forces were used by motion analysis in SolidWorks in order to simulate different foot trajectories by the CAD model of the robot. AS A physical parallel robot prototype was built in order to simulate and execute the foot trajectories. A Kinect camera was used to track the motion of the leg`s model placed on the robot. The results demonstrate the robot's capability to perform various rehabilitation exercises [131].

5.2 Methodology

5.2.1 Gait analysis

Twenty healthy people participated in this study; ten males with average age of 35.23±3.02 years, height of 175.2±4.34 cm, weight of 82.764±4.89kg and ten females with an average age of 33.75±2.34 years, height of 168.23±3.43 cm, weight of 59.453±5.563 kg. The participants have

been selected based on the following criteria: (1) able-bodied with no disabilities like drop foot, stroke; (2) weight less than 100kg; (3) ability to perform functional movements like stair climbing and normal walking. The protocol was approved by the West Midlands Rehabilitation Centre (WMRC), Birmingham, UK. The experiment was advertised at the University of Birmingham and prior to the experimentation the ethical approval was granted to the WMRC and all participants completed a data collection consent form and a health declaration form.

As shown in Figure 5-1, based on consulting with physiotherapists at the WMRC, four different exercises were designed to be performed by the participants in barefoot mode:

(1) hip flexion/extension, (2) ankle dorsiflexion/plantarflexion, (3) stair climbing, (4) marching. For each exercise, each participant had six good trials with their right leg and six good trials with their left leg. Before starting each exercise, each participant had a warm up trial. The gait laboratory was equipped with 12 Vicon cameras (six MX 3+ and six MX T40), two force plates (one Kistler FP1 with a frequency of 1000Hz and one Ampti optima with a frequency of 1000Hz), two digital cameras (sagittal plane and coronal plane), reflective markers and Vicon Nexus software 1.8.5 and Vicon Polygon 3.5.1 software. After anthropometric measurements, 16 reflective markers were placed on anatomical landmarks with the assistance of therapists at the WMRC.

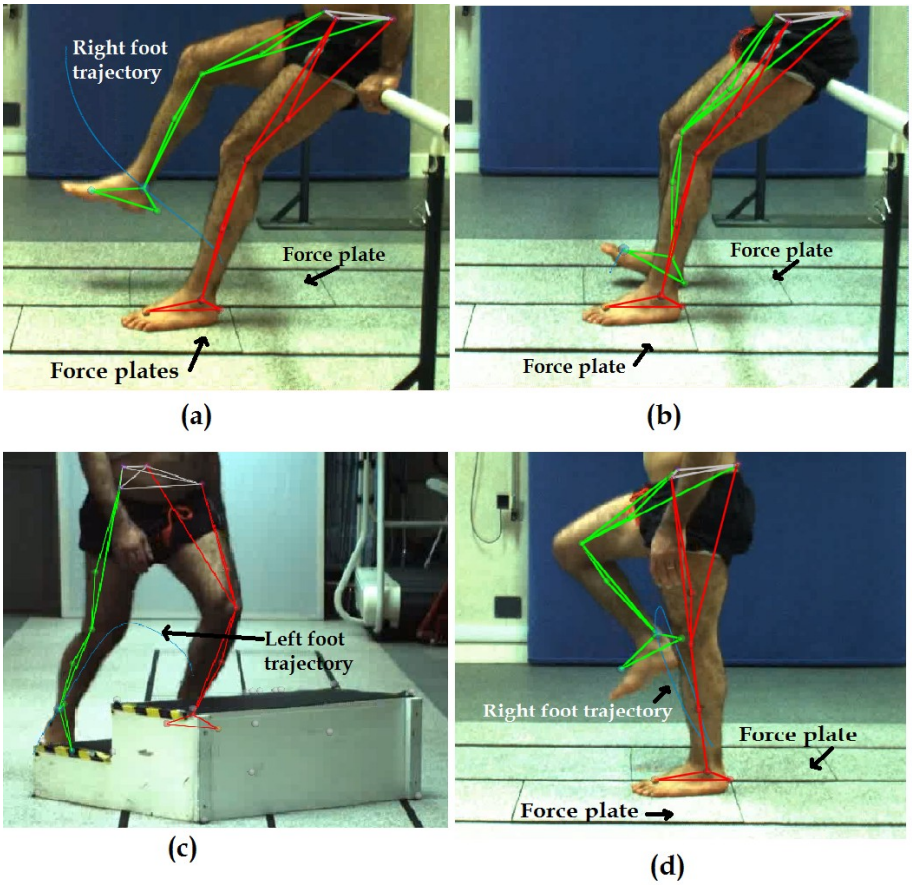

Figure 5-1: Four rehabilitation exercises performed by healthy subjects in the gait laboratory and the foot trajectories were simulated using the Vicon system: (a) hip flexion/extension; (b) ankle dorsiflexion/plantar flexion; (c) stair climbing; (d) marching.

In the first exercise shown in Figure 5-1(a), participants were asked to sit on a bar and while they grasped the support bar both their feet were placed on the force plates. Then, the participants were asked to perform hip flexion/extension with one leg while the other leg remained on the force plate. In the second exercise shown in Figure 5-1(b), participants were asked to sit on the support bar to perform the exercise of ankle dorsiflexion; while both their feet were placed on the force plates and both their hands were free. For the third exercise, a two-step platform was placed in the middle of the gait laboratory`s walkway. Stair climbing was started with the participant`s right foot for the first six trials and their left foot was used to start the next trials. The height of each step was 209.739mm and the reflective markers were placed on the edges of the step platform to define the location of the stairs. This exercise was created by three sub-movements; the starting foot moves

from the floor to the first step; then the other leg starts its movement from the floor to the second step and finally the starting leg moves from the first step to the second step. In this study only the first movement of the foot segment from the floor to the first step will be investigated. For instance, the left leg was the starting leg in Figure 5-1(c). In the last exercise shown in Figure 5-1(d), participants were asked to stand on the force plate with one foot on each of the right and left force plates. Then participants were asked to bend their knees to the point that their femur was parallel to the ground. This exercise was called marching due to its similarity to military marching. In each exercise the maximum applied force by the leg was measured by the force plate and this was used as an external force which was applied on top of the parallel robot. As it is shown in Figure 5-2, the profile of the ground reaction force was created by the force plate and the peak force was measured from this profile. With respect to the different weights of the subjects, the mean value of the maximum forces was calculated for each exercise. After processing the data, it was extracted and normalized by the Equation 3.16.

As it is shown in Figure 5-2, the foot trajectory has been calculated by the normal vector of the plane created by the heel marker, ankle marker and toe marker and it is given by:

$$\vec{\boldsymbol{n}} = \overrightarrow{P_{ankle}P_{heel}} \times \overrightarrow{P_{ankle}P_{toe}} \tag{5.1}$$

Where $P_{ankle} = (\mathrm{x_{ankle}}, \mathrm{y_{ankle}}, \mathrm{z_{ankle}})$; $P_{toe} = (\mathrm{x_{toe}}, \mathrm{y_{toe}}, \mathrm{z_{toe}})$; $P_{heel} = (\mathrm{x_{heel}}, \mathrm{y_{heel}}, \mathrm{z_{heel}})$ and they represent the position of the ankle marker, toe marker and heel markers based on the laboratory`s coordinate reference. The end-effector of the hexapod will follow the trajectory of the normal vector of the foot plane and the angular rotation of the ankle during all exercises.

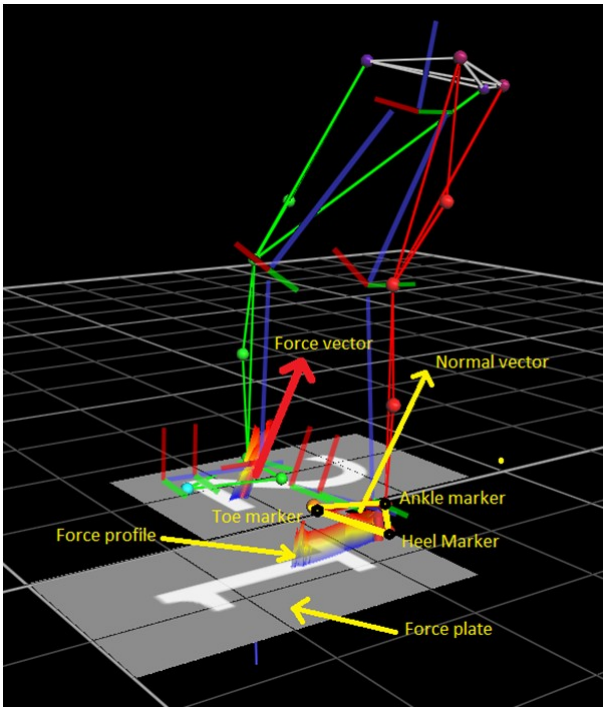

Figure 5-2: 3D model of lower limb during performance of ankle dorsiflexion/plantarflexion

5.2.2 Inverse kinematics

The coordinate system (*X, Y, Z*) was placed on the centre of the fixed platform with the *Z* axis pointing vertically upwards, called the base frame. The end-effector's coordinate system (*x, y, z*) was attached to the centre of the moving platform (top) with the z axis perpendicular to the end-effector, pointing upwards; [*L1, L2,..., L6*] represent the lengths of the actuators; $t = [Px, Py, Pz]^{\mathrm{T}}$ representing the location of the moving platform (top) with respect to the base and $\Re = (\alpha, \beta, \gamma)$ representing the rotation angles of the top frame, first around the X axis to α degrees, then around the Y axis to β degrees and lastly around the Z axis to γ degrees. It is worth mentioning that all of the angles have been calculated based on the right hand sided rule. Therefore the position and orientation of the moving platform has been expressed by $\boldsymbol{Xp} = [px, py, pz, \alpha, \beta, \gamma]^T$ according to Screw theory. It is known that one end of each leg is connected to one of the six vertices of the base. The coordinates of these points have been calculated with respect to the base. The coordinates

of these Points with respect to the Base frame are known and fixed, as can be seen in Table 5.1 and Table 5-2.

Table 5-1 : Coordinates of Base joints with respect to the side`s dimensions

Base Joints	X	Y	Z
$\mathbf{B_1}$	$\frac{\sqrt{3}}{6}(2M+N)$	$\frac{N}{2}$	0
$\mathbf{B_2}$	$-\frac{\sqrt{3}}{6}(M-N)$	$\frac{M+N}{2}$	0
$\mathbf{B_3}$	$-\frac{\sqrt{3}}{6}(M+2N)$	$\frac{M}{2}$	0
$\mathbf{B_4}$	$-\frac{\sqrt{3}}{6}(M+2N)$	$-\frac{M}{2}$	0
$\mathbf{B_5}$	$-\frac{\sqrt{3}}{6}(M-N)$	$-\frac{M+N}{2}$	0
$\mathbf{B_6}$	$\frac{\sqrt{3}}{6}(M+2N)$	$-\frac{N}{2}$	0

Where the coordinates of the Base and side`s labels have been shown in Figure 5-3:

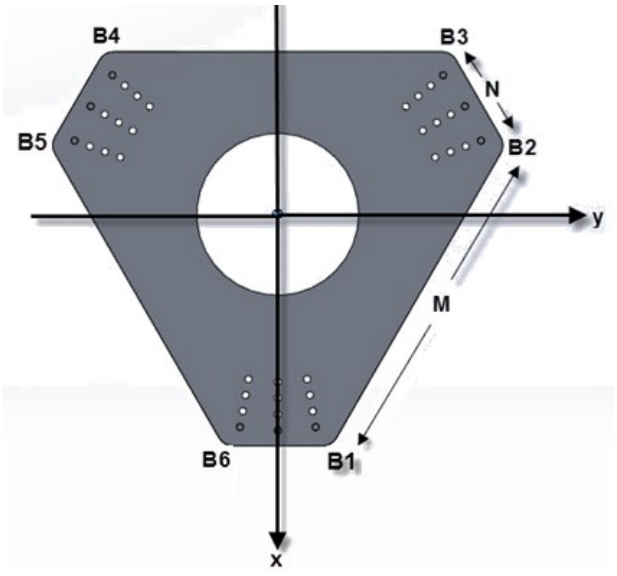

Figure 5-3: Schematic of semiregular hexagon Base platform including side length and coordinate reference

The position of Top vertices has been calculated based trigonometric relations and they are presented in Table2:

Table 5-2: Coordinates of Top joints with respect to the side`s dimensions

Top joints	X	Y	Z
$\mathbf{T_1}$	$-\frac{\sqrt{3}}{6}(2M+N)$	$\frac{N}{2}$	0
$\mathbf{T_2}$	$\frac{\sqrt{3}}{6}(M-N)$	$\frac{M+N}{2}$	0
$\mathbf{T_3}$	$\frac{\sqrt{3}}{6}(M+2N)$	$\frac{M}{2}$	0
$\mathbf{T_4}$	$-\frac{\sqrt{3}}{6}(M+2N)$	$-\frac{N}{2}$	0
$\mathbf{T_5}$	$\frac{\sqrt{3}}{6}(M-N)$	$-\frac{M+N}{2}$	0
$\mathbf{T_6}$	$\frac{\sqrt{3}}{6}(M+2N)$	$-\frac{M}{2}$	0

Focusing the attention on a single leg, it is composed by two links connected each other by a cylindrical joint and connected to the top and to the base by two respective universal joints. The potential centres of instantaneous rotations (CIR) allowed by the cylindrical joint are on the axis of the joint, while the potential CIR allowed by the TOP universal joint are in the centre of the joint. The combination of these CIR subspaces is coincident with the axis of the cylindrical joint because it intersects the centre of the universal joint. The same kinematical behaviour can be obtained with a prismatic joint (that substitutes the cylindrical joint) and a spherical joint (that substitutes the top universal joint). Thus we can observe that the proposed UCU parallel robot is kinematically equivalent to a Stewart platform. The homogeneous transformation matrix from the TOP to the BASE is described by the following transformation matrix [89, 95]:

$$T_{BASE}^{TOP} =$$

$$\begin{bmatrix} \cos\beta\cos\gamma + \sin\alpha\sin\beta\sin\gamma & -\cos\beta\sin\gamma + \sin\alpha\sin\beta\cos\gamma & \cos\alpha\sin\beta & Px \\ \cos\alpha\sin\gamma & \cos\alpha\cos\gamma & -\sin\alpha & PY \\ \sin\beta\cos\gamma + \sin\alpha\cos\beta\sin\gamma & \sin\beta\sin\gamma + \sin\alpha\cos\beta\cos\gamma & \cos\alpha\cos\beta & PZ \\ 0 & 0 & 0 & 1 \end{bmatrix} \quad (5.2)$$

With respect to this homogeneous transformation and the trajectory of *Xp*, the coordinates of the vertices of the top and base were calculated online based on the time history by the following equation:

$$\begin{bmatrix} X_{Ti} \\ Y_{Ti} \\ Z_{Ti} \\ 1 \end{bmatrix} = \mathrm{T}_{\mathrm{BASE}}^{\mathrm{TOP}}(px, py, pz, \alpha, \beta, \gamma) \begin{pmatrix} x_{Ti} \\ y_{Ti} \\ z_{Ti} \\ 1 \end{pmatrix} \tag{5.3}$$

Where $\boldsymbol{P}_i = [X_{Ti}, Y_{Ti}, Z_{Ti}]$ representing the position of the top joints with respect to the base and $\boldsymbol{p}_i = [x_{Ti}, y_{Ti}, z_{Ti}]$ representing the position of the top joints with respect to the end-effector's coordinate reference. In another approach, Equation 5.3 can be rewritten by the following equation:

$$\boldsymbol{X}_{Ti} = \Re x_{Ti} + \boldsymbol{t} \tag{5.4.a}$$

$$\boldsymbol{Y}_{Ti} = \Re y_{Ti} + \boldsymbol{t} \tag{5.4.b}$$

$$\boldsymbol{Z}_{Ti} = \Re z_{Ti} + \boldsymbol{t} \tag{5.4.c}$$

Where t and $\Re$ represent the translation and rotation of the moving platform with respect to the base. Since the coordinates of the base and top have been calculated, the length of the actuators can be found by the following equation:

$$\boldsymbol{S} = \boldsymbol{q} + \boldsymbol{t} - \boldsymbol{b_i} \tag{5.5.a}$$

And

$$\boldsymbol{q} = \Re \boldsymbol{p}_i \tag{5.5.b}$$

Where $\boldsymbol{b_i}$ is the *i*th connection point at the Base.

$$\boldsymbol{S}_i = (X_{Ti} - X_{bi}) + (Y_{Ti} - Y_{bi}) + (Z_{Ti} - Z_{bi}) \qquad i \in \{1 \dots 6\} \qquad (5.5.c)$$

$$L_i = \sqrt{(X_{Ti} - X_{bi})^2 + (Y_{Ti} - Y_{bi})^2 + (Z_{Ti} - Z_{bi})^2} \qquad i \in \{1 \dots 6\} \qquad (5.5.d)$$

The position of moving platform and top joints during the foot trajectory calculates through inverse kinematics. Inverse kinematics identifies the positions of the platforms and the joints' position through the motion of defined rehabilitation exercises. However, applying the structural limitations of design identifies points existing in the workspace. The constraints of the robot include the length of the strokes and the joints' range of motion. The position of the joints on the hexapod for the motion of the foot during different exercises has been calculated. Therefore, the stroke of each actuator has been calculated by the length of each actuator's position vector. The angle between the joints and the actuators for the base has been calculated by the following equation:

$$\alpha_{bi} = cos^{-1}\left(\frac{\boldsymbol{M_X} \cdot \boldsymbol{S_i}}{|\boldsymbol{S_i}|}\right) \qquad i \in \{1 \dots 6\} \qquad (5.6.a)$$

$$\beta_{bi} = cos^{-1}\left(\frac{\boldsymbol{N_y} \cdot \boldsymbol{S_i}}{|\boldsymbol{S_i}|}\right) \qquad i \in \{1 \dots 6\} \qquad (5.6.b)$$

Where, M_X and N_y are the axes of the joints on the base; S_i is the actuator position vector; α_{Bi} is the angle of the joint with its x-axis and β_{Bi} is the angle of the joint with its Y-axis. For the top:

$$\alpha_{Ti} = cos^{-1}\left(\frac{\boldsymbol{m_X} \cdot \boldsymbol{S_i}}{|\boldsymbol{S_i}|}\right) \qquad i \in \{1 \dots 6\} \qquad (5.7.a)$$

$$\beta_{Ti} = cos^{-1}\left(\frac{\boldsymbol{n_y} \cdot \boldsymbol{S_i}}{|\boldsymbol{S_i}|}\right) \qquad i \in \{1 \dots 6\} \qquad (5.7.b)$$

Where, m_X and n_y are the axes of the joints after the motion and α_{Ti} is the angle of the joint with its X-axis and β_{Ti} is the angle of the joint with its Y-axis of the moving platform; m_X and n_y are changed with respect to M_X and N_y based on the rotational motions that applied for the system.

To consider the singularity points of the robot, the unit vector along the actuator was calculated by the following equation:

$$\boldsymbol{s_i} = \frac{\boldsymbol{S_i}}{|\boldsymbol{S_i}|} \qquad i \in \{1 \dots 6\} \qquad (5.8)$$

With respect to the force plate used in the gait laboratory, the applied forces by the foot were measured and analysed during all exercises. This force has been used as an external force which will be applied on the top platform. The actuator forces (**F**) is calculated based on the Newton-Euler formulation developed by Dasgupta in 1998 [81] and given by $= [\, F_1 \quad F_2 \quad F_3 \quad F_4 \quad F_5 \quad F_6 \,]^T$, where $[F_1, F_2, \dots, F_6]$ represent the actuator force for actuators [1, 2, ..., 6]. So the resultant force and momentum for the system are given by the following equations respectively:

$$\mathbf{R} = \sum_{i=1}^{6} \boldsymbol{s}_i F_i \qquad (5.9)$$

$$\mathbf{M} = \sum_{i=1}^{6} (\mathbf{b}_i \times \boldsymbol{s}_i) F_i \qquad (5.10)$$

With respect to the following equation, the output force system is related to the input forces:

$$[\mathbf{R} \quad \mathbf{M}]^T = \mathbf{HF} \qquad (5.11)$$

And

$$\mathbf{H} = \begin{bmatrix} \boldsymbol{s}_1 & \boldsymbol{s}_2 & \boldsymbol{s}_3 & \boldsymbol{s}_4 & \boldsymbol{s}_5 & \boldsymbol{s}_6 \\ \mathbf{b}_i \times \boldsymbol{s}_1 & \mathbf{b}_i \times \boldsymbol{s}_2 & \mathbf{b}_i \times \boldsymbol{s}_3 & \mathbf{b}_i \times \boldsymbol{s}_4 & \mathbf{b}_i \times \boldsymbol{s}_5 & \mathbf{b}_i \times \boldsymbol{s}_6 \end{bmatrix} \qquad (5.12)$$

Where **H** is a 6×6 transformation matrix which describes the relation between the input forces and output forces. When **H** is singular, the extra load will be created on the platform which cannot be supported by the actuator forces. The singularities were identified while the value of determination of the matrix **H** was zero. The static singularity will appear when:

$$\det[\mathbf{H}(\boldsymbol{Xp})] = 0 \qquad (5.13)$$

Equation 5.13 shows the singularity manifold for the 6 DoF Stewart platform which consists of continuous hypersurfaces which separate the task space into two or more disjointed segments. To follow the trajectory of the foot during different exercises, an algorithm was developed in MATLAB to calculate the length of the actuators and the required force for each actuator based on kinematics, dynamics, singularity and workspace of the designed robot. The foot trajectory was simulated by a Vicon system and it was imported to the control system of the robot. The CAD model of the robot was designed in a SolidWorks environment and it was linked to MATLAB in order to follow the foot trajectory. As it is shown in Figure 5-4, the centre of the moving platform of the CAD model was moved along the scaled down trajectory of the foot.

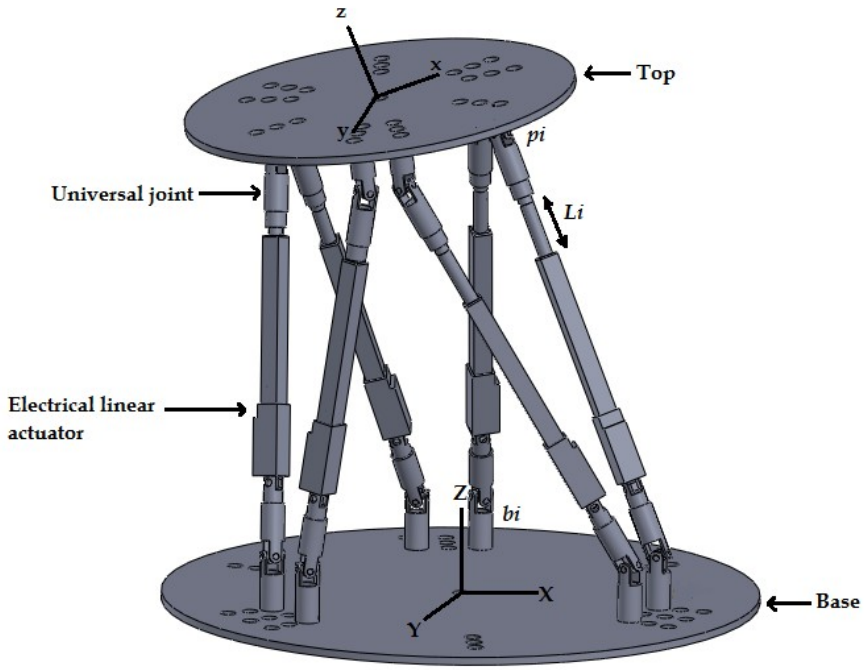

Figure 5-4: The CAD model of the robot designed in SolidWorks

5.2.3 Simulation

Based on the kinematics and dynamic analysis of the robot, the prototype of the 6 DoF UPU parallel robot was designed and built in the Robotic Laboratory at the University of Birmingham, Birmingham, UK. Six servo actuators with a stroke size of 150mm were used and the actuators were connected to the top and base by 12 universal joints. A SSC-32 micro controller was used to control the position of the moving platform.

A Graphical User Interface (GUI) was designed and created in MATLAB to control the movements of the hexapod. The GUI included a data base library with four different exercises. The control system of the robot was designed in such a way to follow the trajectory of a foot during different exercises. Before the robot performed the exercise, its workspace, the required force for each actuator, the length of the actuators, the path motion and singularly points were calculated and the results displayed on the monitor.

Based on the geometry and exact dimensions of all components, the CAD model of the robot was designed in SolidWorks. Due to the stroke limitation of the prototype`s actuators, the measured foot trajectories in the gait laboratory were scaled down to three times of the recorded trajectory by the Vicon system; except for in the ankle exercise where the foot trajectory was not scaled down. Then, the scaled-down trajectory was simulated by the motion analysis tool box in SolidWorks. The CAD model of the hexapod was moved along all of the trajectories and the required force of the actuators was calculated by motion analysis in SolidWorks. The external force applying on the moving platform was calculated by the force plates in the gait lab and this force utilized in motion analysis as an external force during different exercises. The CAD model was linked to MATLAB and by moving the CAD model the physical prototype executed the same motion.

5.2.4 Tracking the foot trajectory by a Kinect camera

To validate the movement of the physical model with the obtained results of the CAD model, a Kinect camera was used as an optical sensor to track and detect the position of the physical hexapod during performance of the exercises. A skeleton model of a lower limb was placed on the moving platform and the movements of the foot were recorded by two Kinect cameras during all exercises. Blue, red and green paper markers were placed on anatomical landmarks of the foot, similar to the anatomical landmarks which were used in the gait laboratory. It is worth mentioning that Kinect camera has some difficulties in detecting the transparent, reflective or absorptive objects because the infrared pattern is not visible or reflected correctly [132]. In [38] it was explained how the depth was calculated by the Kinect.

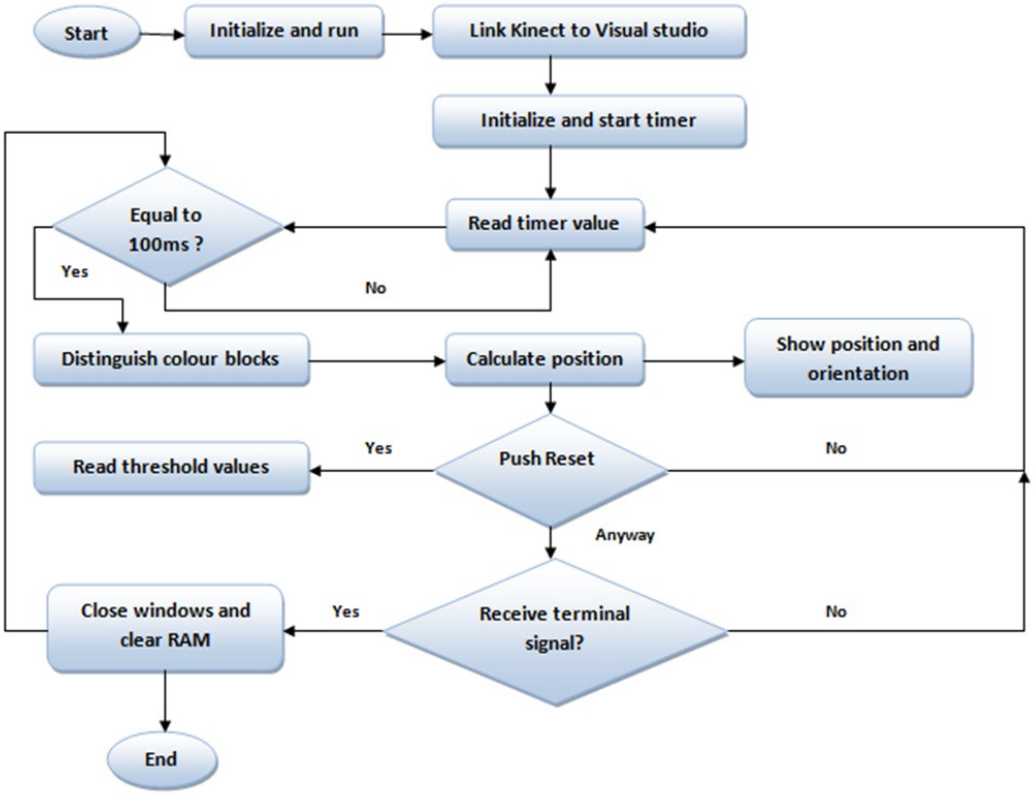

Figure 5-5: Logical flowchart demonstrating color detection by Kinect camera

As it is shown in Figure 5-5, to detect a color point, first the Kinect was linked to the visual studio, then the timer read the value. If that value is equal to 100ms then the camera distinguishes the color block and it measures the position of the marker. By pressing the RESET button, a closed loop was created in order to detect the position continuously.

In order to calibrate and measure the accuracy of the camera, a ruler with a resolution of 0.1mm was used. The centre point of a blue marker was placed in different positions along the X and Y axes and the measured values were compared with those measured by the ruler. As it can be seen in Figure 5-6, ten trials were performed along the Y axis from 0-300mm with increments of 30mm.

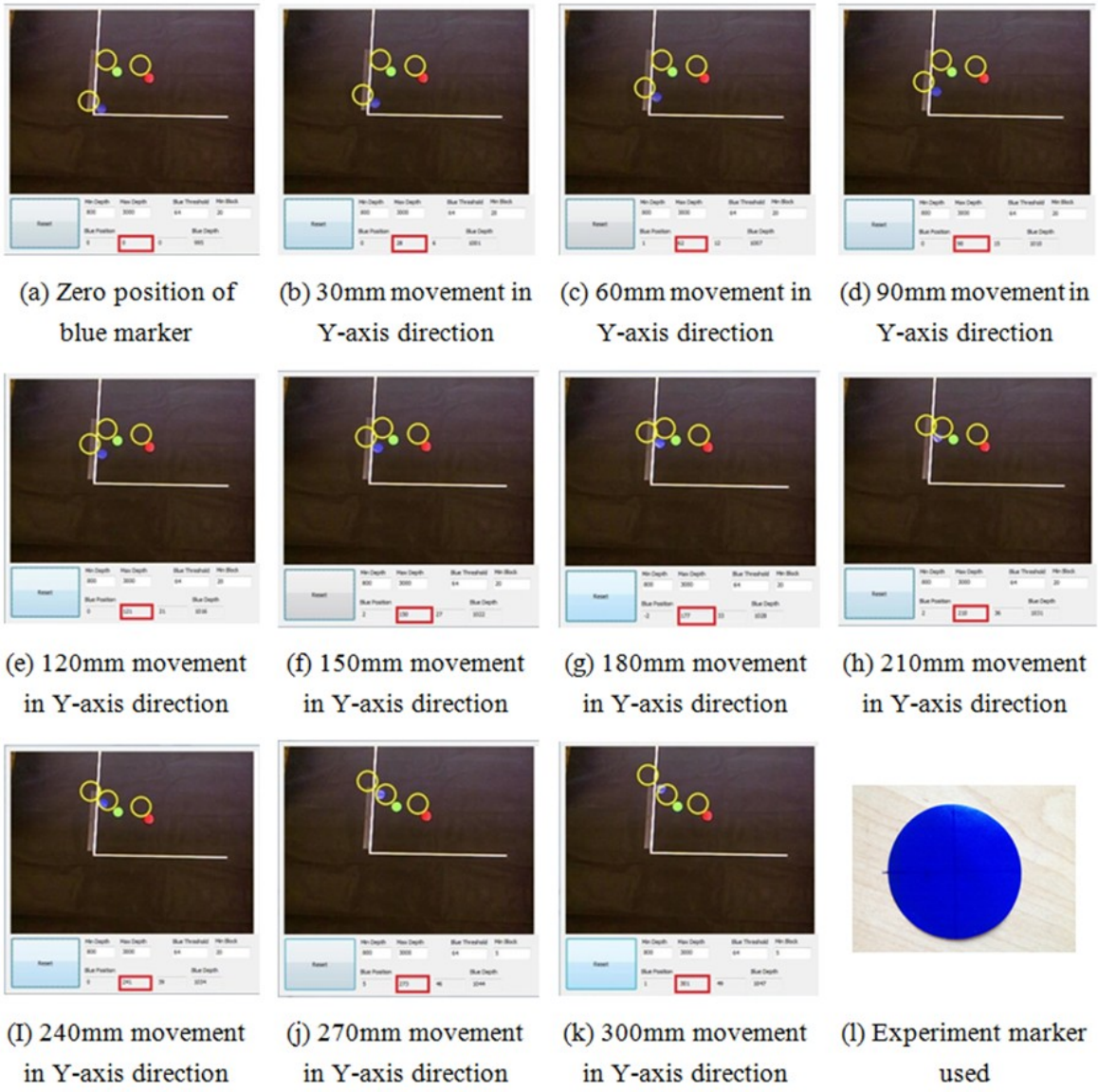

Figure 5-6: Calibration of Kinect camera: (a-k) along Y axis for every 30mm from 0mm-300mm, (I) Experimental blue marker

As it can be seen in Figure 5-7, a black background was used to reduce the noises created by light. The green, red and blue markers have been detected by the Kinect camera and they have been marked by yellow circles. The positions of the markers were measured with respect to the coordinate reference shown in Figure 5-7. A skeleton model of a leg was connected to a flexible holder from the hip joint and its foot segment was attached on the centre of the moving platform by double-sided

sticky tape. The joints used in the knee and ankle of the skeleton model give a wide range of movement to the skeleton model for performing different exercises. The position error of the Kinect camera was calculated by comparing the results of the Kinect camera with a Vicon camera. One of the cameras tracked the movement of the robot in the sagittal plane and another one tracked it in the coronal plane; while data received from the Kinect was stored in real-time.

Figure 5-7: Color marker detection by Kinect camera using KinectColourBlock software

5.3 Results and discussion

5.3.1 Required force of actuators

Based on dynamic analysis, the required forces for all the actuators have been calculated in all cases (Figure 5-8). The weight of the leg was considered as the external force applied on the moving platform. The mean value of the weight of the right leg was 15.4kg ±1.44. In stair climbing, the force of actuator number 3 started from 52N and it reached to its maximum of 130N after 4.33s. The trend of the forces were increased for four of the actuators while this trend decreased for the other two; this shows that by increasing the stroke lengths and changing the orientation of the moving platform how the robot performed this exercise. In marching, the required force of actuator 1 started from 84N and it reached to its maximum of 121N after 1.34s. The fluctuations in the trend of the forces were caused by changing the orientation of the moving platform and the stroke size of the actuators. In the ankle dorsiflexion/plantar exercise, actuator number 1 reached to its maximum of 96N after 2.34s. In the ankle exercise, the trend of the force of the actuators (1,4), (2,5) and (3,6) are similar to each other, which shows that actuators 1 and 4 had the largest stroke size with larger forces compared to the other actuators. In the hip flexion/ extension exercise, actuator number 3 reached to its maximum of 101N after 0.46s. In the last exercise, the variation of the trend of the force for 4 and 5 was less than for the other actuators and the trend of the force for 3 and 6 was similar to each other.

The type and amount of actuators required for the rehabilitation of lower limbs can be better understood with respect to the obtained results. It is worth mentioning that for lower limb rehabilitation in a standing position, usually an unweighting harness will be used which helps to reduce the weight of a patient by up to 60%; so, the external force will be decreased and a lower amount of actuator force will be required to lift the leg.

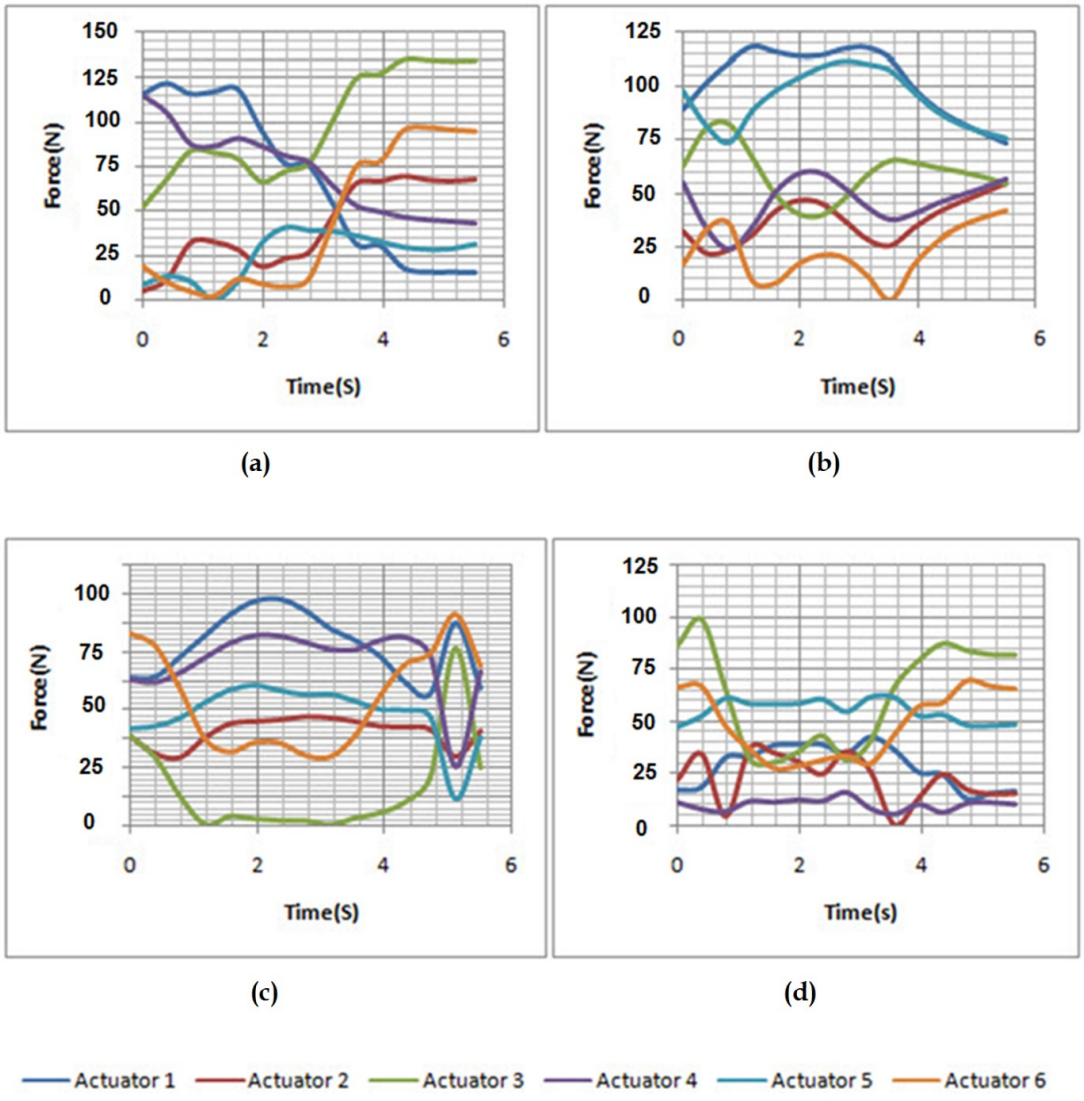

Figure 5-8: Actuator forces in (a) Stair climbing, (b) Marching, (c) Ankle dorsiflexion/plantar flexion, (d) Hip flexion/extension

5.3.2 Workspace of the robot

The structural limitations and singularity points of the robot have been considered along the path motion. As it is shown in Figure 5-9, the workspace of the robot was simulated in MATLAB software based on the developed numerical method in MATLAB, the structural limitation of the robot and Cartesian and polar algorithms. The resolution of simulation can be increased by

increasing the number of mesh points. The robot was able to move 240 mm along the X and Y axes and 140mm along the positive Z axis.

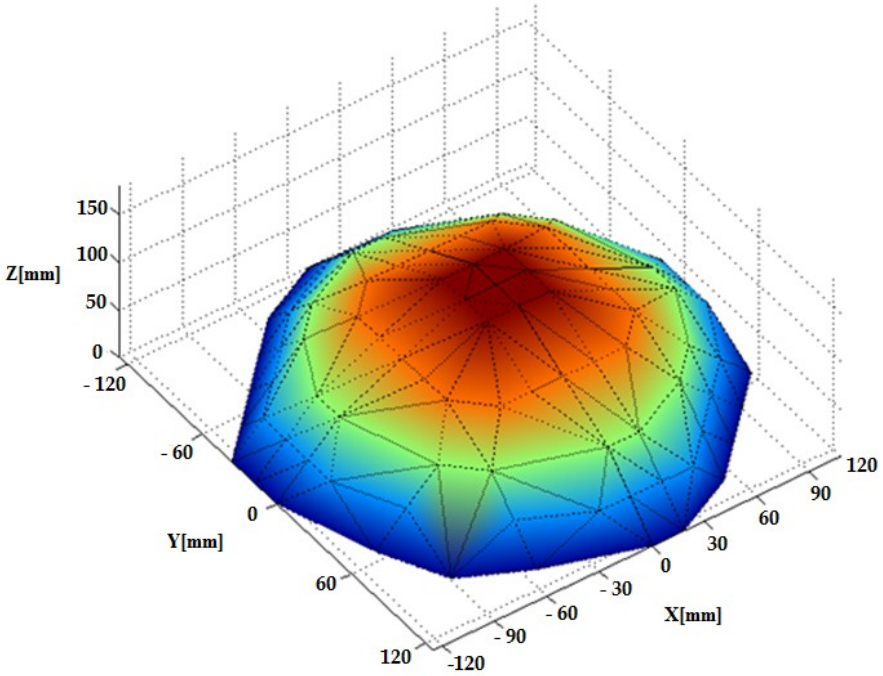

Figure 5-9: Calculated workspace of the robot in MATLAB

All foot trajectories during different exercises were simulated in MATLAB. The lengths of the actuators were calculated based on Equation (5.6.a.). The singularity condition of the robot was checked within the workspace by the developed program in MATLAB based on Equations 5.11 and 5.12. As it is shown in Figure 5.10, the ranges of motions for different trajectories have been illustrated and it can be found that the end-effector moved along the paths inside the workspace. The range of movement for all exercises except the ankle exercise was out of the workspace of the robot, so the trajectory of motion for the marching, hip and stair climbing exercises has been scaled down three times compared to the recorded trajectory in the gait. In the ankle exercise, the moving platform reached the maximum of 6cm along the Z axis and then returned to the home position (Figure 5-10 (a)). In the hip exercise, the robot simulated the flexion/extension movement for the leg and it reached the maximum of 138mm along the Z axis (Figure 5-10 (b)). In the marching

exercise the robot reached the maximum of 140mm along the Z axis and the variation of movement along the X axis were between 0-10mm (Figure 5-10 (c)). In stair climbing, the robot simulated the movement of the foot during one step and it reached the maximum of 110mm along the Z axis (Figure 5-10 (d)).

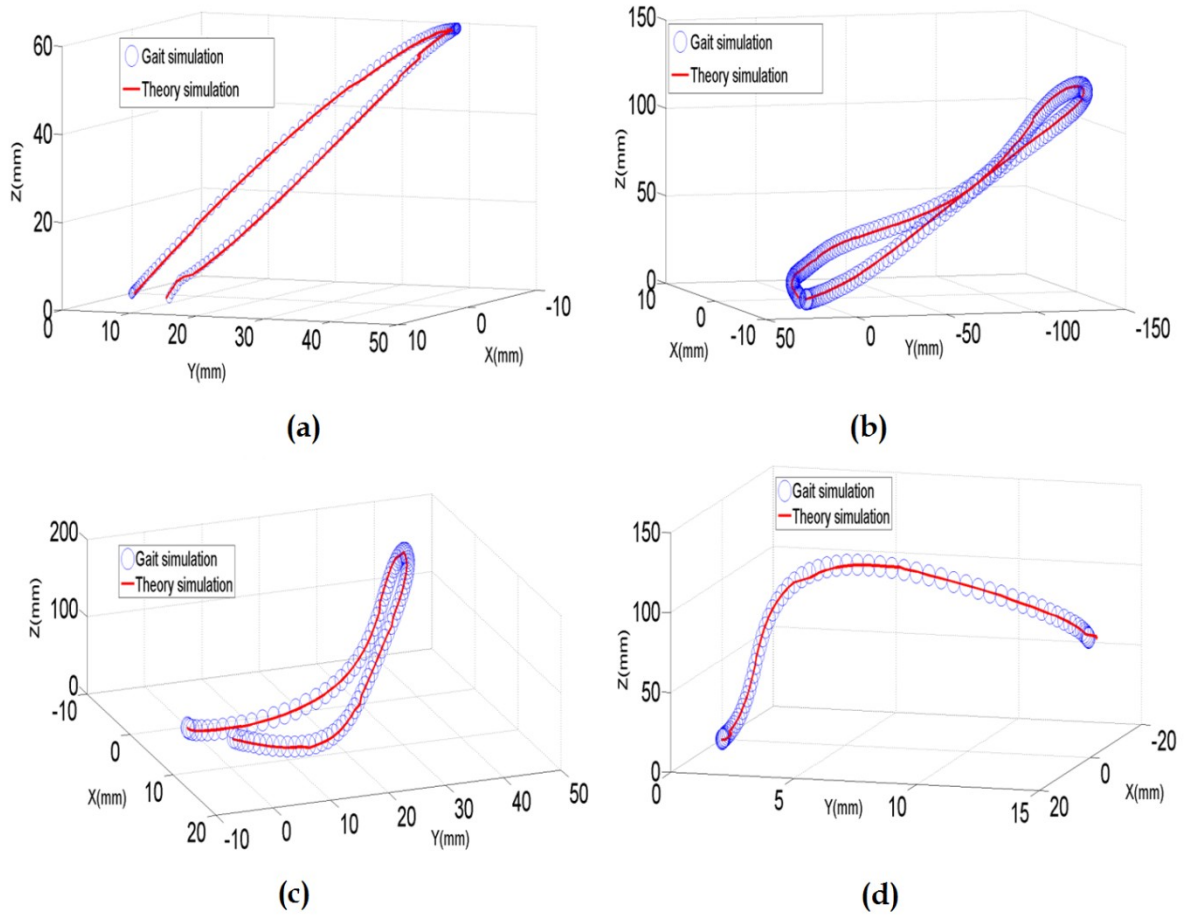

Figure 5-10: Foot trajectory (blue circles) versus robot`s trajectory (red line) during 4 different exercises : (a) Ankle exercise, (b) Hip exercise, (c) Marching, (d) Stair climbing

Based on the MATLAB simulation results, the trajectories of the foot during all exercises have been simulated by the CAD model of the robot during the performance of the exercises in SolidWorks. Table 5-3 presents the position error of the trajectory recorded by Vicon with the trajectory of the CAD model of the robot during four different exercises.

Table 5-3: Position error of CAD simulation

Type of exercise	Maximum position error(mm)			Minimum position error(mm)		
	X	Y	Z	X	Y	Z
Marching	1.22	1.24	1.05	0.23	0.35	0.19
Ankle exercise	1.05	1.07	1.09	0.34	0.73	0.94
Hip exercise	1.08	1.09	1.39	0.27	0.36	0.47
Stair climbing	1.15	1.19	1.89	0.78	0.48	0.95

With respect to Table 5-3, the maximum position error observed in the ankle stair climbing exercise was 1.89mm along the Z axis. The minimum position error observed in the marching exercise was 0.19mm along the Z axis. The mean position errors for all the exercises were 0.68mm, 0.54mm and 1.02mm respectively in the X, Y and Z axes. These small position errors are negligible for the purpose of lower limb rehabilitation and they might be caused by inaccuracy in measuring the position of the joints of the physical model. As shown in Table 5-1, the position error along the Z axis was more than on the other axes, which can be caused by the position feedback received from the servos. Also the position error in the Y axis was more than in the X axis.

5.3.3 Robot execution and Kinect detection

In this section, it will be explained how the exercises were executed by the robot and how the position errors were measured by the Kinect camera. As an example, one of the exercises will be discussed here. As shown in Figure 5-11(b), the trajectory of the foot and the ground reaction force during marching were measured and analysed. The constructed robot followed the scaled-down trajectory of the foot during the marching exercise and it is shown in Figure 5-11(a).

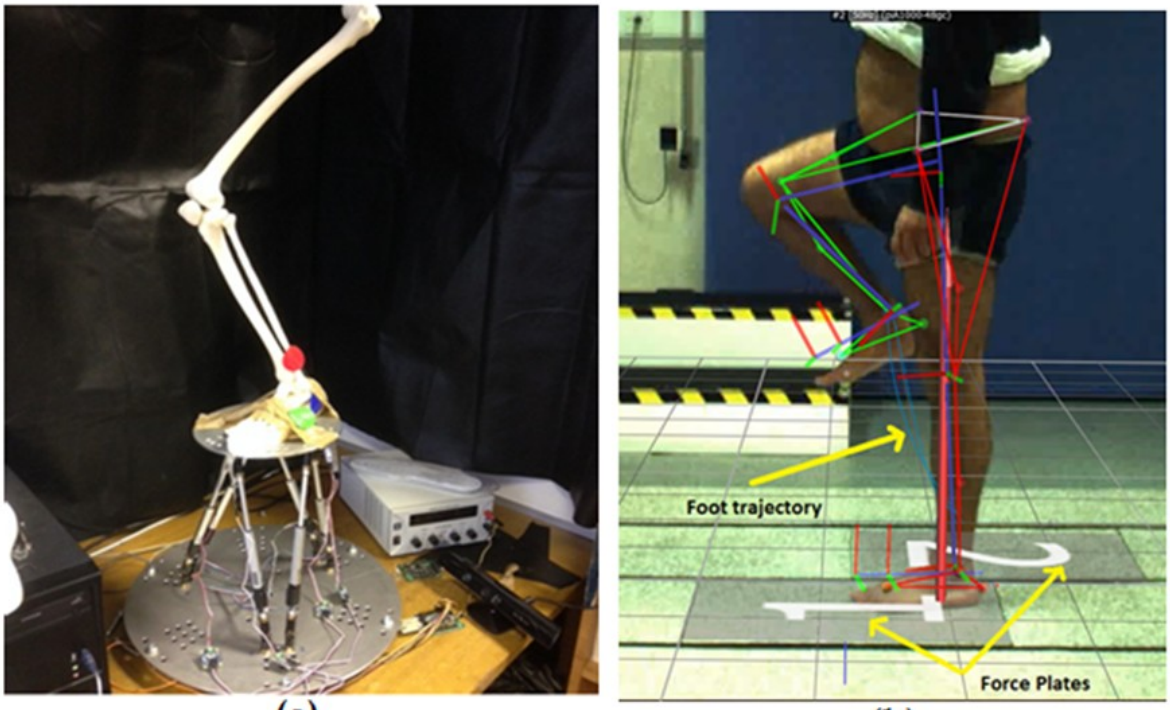

Figure 5-11: Performing marching exercise (a) by the robot, (b) Performing marching exercise by healthy subject

Working with a Kinect camera in a laboratory environment was much easier, faster and cheaper than using Vicon cameras in a clinical environment. Based on the calibration test mentioned in section 2.4, the mean value of the position error was 2.6mm. In this experiment, the movements of the skeleton model of the foot and moving platform were measured by the Kinect camera. The position error between the results obtained by the Kinect camera and Vicon camera has been reported in Table 5.2.

Table 5-4: Position error of Kinect camera during movements of skeleton model of foot by hexapod

Type of exercise	Maximum position error(mm)			Minimum position error(mm)		
	X	Y	Z	X	Y	Z
Marching	34.15	32.78	34.05	11.75	10.81	12.04
Ankle exercise	32.02	33.06	33.25	10.75	10.95	11.80
Knee exercise	33.54	31.65	31.84	11.02	10.75	10.84
Stair climbing	33.24	35.02	33.54	11.46	12.34	11.99

As shown by Table 5-4, the position error has been increased significantly in comparison with the results obtained in Table 5-3. The maximum and minimum position errors were 34.15mm in the X axis in marching and 10.75mm in the X axis in the ankle exercise respectively. Since two cameras were used to track the movements of the robot, one of them tracked the movements in the X and Z axes and the other one was used to track the movements in the Y and Z axes. The position error can be decreased by better synchronization between the two cameras. Also these two cameras were placed 1m away from the robot in order to capture the whole of the movements of the robot without relocating the position of the cameras; this might be another reason for the position error. In this study, a black background was used in order to reduce the light reflection and detect the markers with better resolution; some preliminary tests proved this issue. The robot repeated execution of each exercise 12 times and the mean position error along different axes were presented in Table 5-3. Considering the Kinect camera as a partly accurate and cheap replacement for a Vicon camera was another achievement of this chapter and the error of using a Kinect camera during rehabilitation experiments was addressed fairly. The most important factors in reducing these errors are increasing the number of cameras and preparing a proper location based on light reflections.

5.4 Conclusion

In this chapter, different rehabilitation exercises have been simulated by a prototype of a 6 DoF parallel robot. The ability of the robot during the performance of these exercises has been investigated; however, the trajectory of the foot, for the marching and stair climbing and hip exercises was scaled down due to the stroke limitation of the actuators used. Based on the work volume of the robot, the maximum movements of the end-effector was ±240mm along the X and Y axis and 140mm along the positive Z axis. The robot followed all the trajectories without facing any singularity points. In this experiment, the accuracy of the Kinect camera in detecting the colour markers has been investigated. The Kinect camera was calibrated and the results showed that it has the mean position error of 2.6mm in detecting the colour markers. Then the Kinect camera was used to track the position of a skeleton model during all exercises and the results showed the maximum and minimum position errors were about 28 times and 23 times the position error calculated by the MATLAB simulation. The maximum position error of 1.89mm was observed between the results of the developed CAD model of the robot and the Vicon camera. The Kinect results showed that the position error was increased by 29%, 30% and 24% in the X, Y and Z axes for all exercises, in comparison with the results of the CAD simulation. However, by adjusting the light the accuracy of the Kinect will be increased. It was found that the Kinect camera can be a cheap and easy replacement for the expensive Vicon system. The outcome of this research approves the abilities of a 6 DoF parallel robot as an accurate rehabilitation system for performing various rehabilitation exercises.

Chapter 6

Lower limb robotic rehabilitation using patient data

6.1 Introduction

The ability of 6 DoF parallel robot in tracking the foot trajectory of healthy participants was investigated and kinematics of the prototype of the robot was studied. The aim of chapter 6 is to find out if a 6 DoF parallel robot is capable of tracking the movement of a paretic leg during a single stride. To reach this goal, the foot trajectories of nine post-stroke patients including both males and females have been measured by a Vicon system in the gait laboratory. The force plates were used to measure the ground reaction force created by an individual patient's in vivo gait. Based on kinematic and dynamic analysis of a 6 DoF UPS parallel robot, an algorithm was developed in MATLAB to calculate the length of the actuators and their required force during all trajectories. The work space and singularity points of the robot were investigated in nine different cases. Based on the results, a UPS parallel robot with 6 DoF and high repeatability was designed and built in order to simulate a single stride [133].

6.2 Gait Analysis

6.2.1 Participants

As it is shown in Figure 6-1, a total of nine patients including four females and five males attended the West Midlands Rehabilitation Centre for the first session of physical rehabilitation after a stroke. In this experiment small sample size have been studied due to limited number of post-stroke patients admitted with WMRC, although other patients with lower limb disability with different diseases were admitted by WMRC which other control groups have not been considered in this study. In this pilot study, the average age of the group was 49.3 years ranging from 21 years to 68 years. Participants completed informed consent to participate in this study, which had been approved by the NHS Trust. Three females shown in Figures 6-1(a), 6-1(g) and 6-1(h) and three males shown in Figures 6-1(d), 6-1(f) and 6-1(i) were paralysed on the right side of their body and the rest shown in Figures 6-1(b), 6-1(c) and 6-1(e) were paralysed on the left side. One of the male participants shown in Figure 6-1(c) and one of the female participants shown in Figure 6.1(a) used a walker during gait analysis. Except for one of the males shown in Figure 6-1(e), all other participants wore shoes during the test. The participants will be recalled by their (a-i) captions of Figure 6-1 throughout the text.

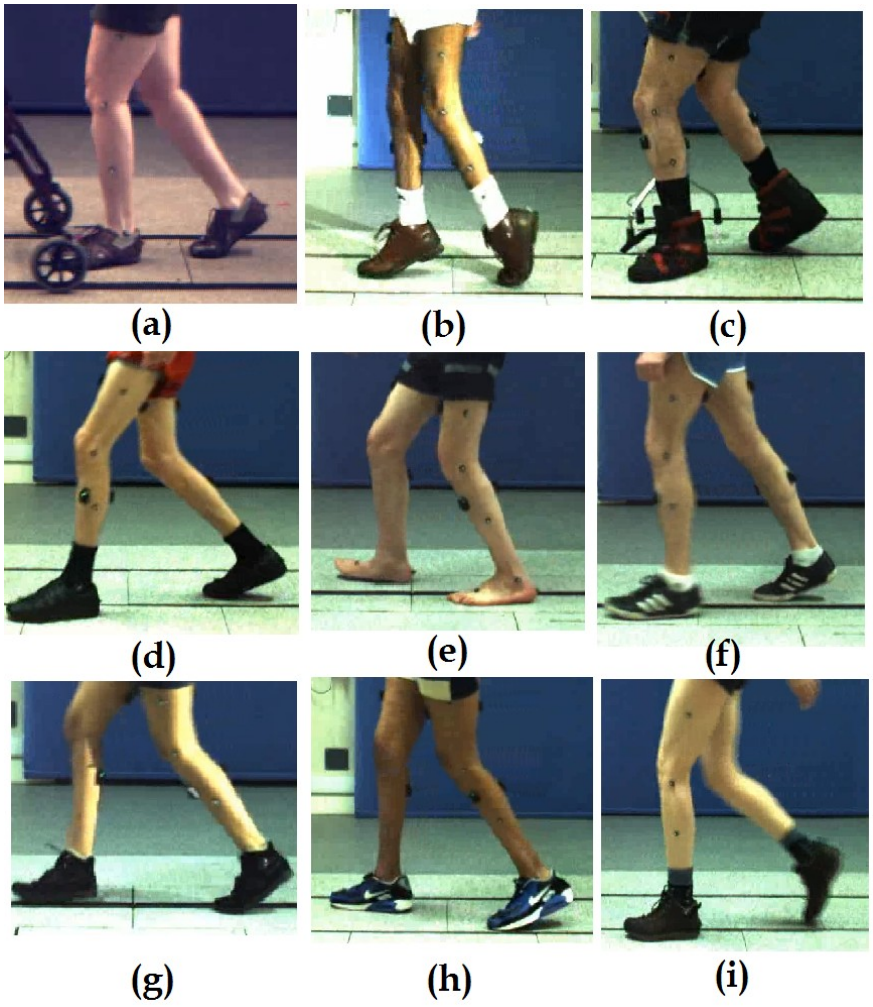

Figure 6-1: Gait analysis of nine post-stroke patients

6.2.2 Measurements

The laboratory was equipped with 12 Vicon cameras including six MX3+ and six MX T40 cameras. The Vicon cameras collected data in 100Hz. Two digital cameras were used in the sagittal and lateral planes and they collected data in 50Hz. The Vicon cameras were synchronized with two force plates (Kistler and Ampti Optima) which were used in the laboratory to collect data with a sampling frequency of 2000Hz. Before data collection, the cameras were calibrated within a $2.8m^2$ calibration volume. Sixteen reflective markers were placed on the participant`s right and left leg to

record the gait parameters. The position of the markers measured by the Vicon system and temporal spatial parameters, linear velocity and acceleration of the markers were calculated. Based on the Cardan angle system, the joint moments were calculated. The resultant force of the joints was calculated by applying inverse dynamic. The data for each leg was averaged over the successful trials.

A set of three markers were attached to the thigh, shank and foot segments. Before starting the experiment the height, mass and all anthropometric dimensions of the participants were measured including pelvis depth, knee width, hip breath and sphyrion height. Each participant was asked to walk on a 10m walkway with self-speed. Six successful trials were collected for each leg, in total 12 trials for each participant. As it is shown in Figure 6-2, the trajectory of the foot segment was calculated with respect to the measured trajectory of attached markers 1, 2 and 3 which were placed on the heel, ankle joint and toe respectively. The normal vector of the plane created by these three markers was calculated by equation 5.1.

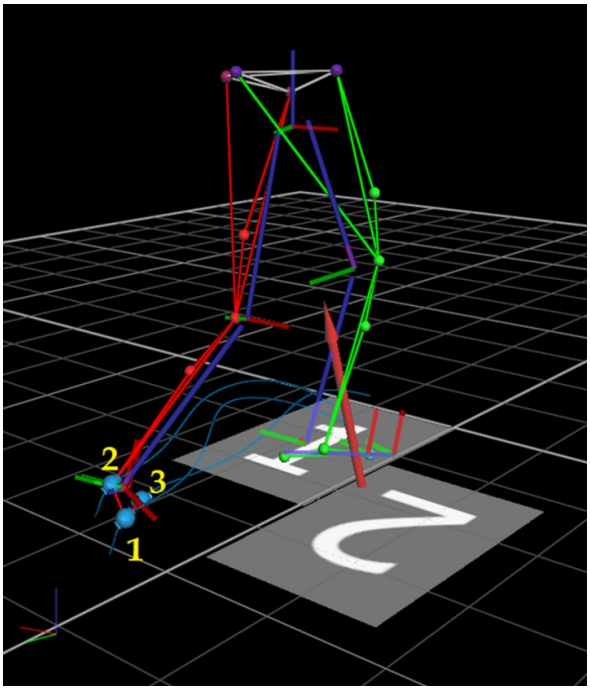

Figure 6-2: Foot trajectory of paretic leg with respect to the attached markers

6.3 Analysis of parallel robot

6.3.1 Kinematics and dynamics of parallel robot

The kinematics of the parallel robot has been investigated in [134], based on orientation ranges and linear translation of the foot segment. The length of the actuators of the parallel robot has been calculated based on a study carried out in [87]. In the current study, the fixed platform and moving platform have been called the base and top respectively. The actuators which have been called legs (L_i) are connected to the top by six spherical rolling joints (Hephaist-SRJ016C) and to the base by six universal joints. The global coordinate reference (X, Y, Z) was placed at the centre of the base and the local coordinate reference was placed at the centre of gravity of the top (x, y, z). The terms (α, β, γ) represent the rotation of the top frame around the X-axis, Y-axis and Z-axis respectively; $[P_X, P_Y, P_Z]$ represent the position of centre of the top frame with respect to the base frame; $X_{p-o} = [P_X, P_Y, P_Z, \alpha, \beta, \gamma]^T$ represents the position and orientation of the upper platform; $\boldsymbol{P}_i = [X_{Ti}, Y_{Ti}, Z_{Ti}]$ represents the position of the top joints with respect to the base and $\boldsymbol{p}_i = [x_{Ti}, y_{Ti}, z_{Ti}]$ represents the position of the top joints with respect to the end-effector's coordinate reference; where t and $\mathfrak{R}$ represent the translation and rotation of the moving platform with respect to the base (Figure 6-3). Since the coordinates of the base and top have been calculated, the length of the actuators can be found by the following equations 5.5.a and 5.5.b. The unit vector along the actuator is given by:

$$\boldsymbol{S} = \frac{\boldsymbol{S}}{\boldsymbol{L}} \tag{6.1.a}$$

And

$$\boldsymbol{L} = \|\boldsymbol{S}\| \tag{6.1.b}$$

And the sliding velocity between the two parts of the leg was calculated by the following equation:

$$\dot{\boldsymbol{L}} = \boldsymbol{s}.\dot{\boldsymbol{S}} \tag{6.2}$$

Since the actuator has no axial rotation, the angular velocity of the actuator will be:

$$\boldsymbol{V} = \boldsymbol{s} \times \dot{\boldsymbol{S}}/_{L} \tag{6.3}$$

The following equation represents the angular acceleration of the leg. With respect to the following equation some other parameters will be calculated, such as position, velocity and acceleration of the actuator:

$$\boldsymbol{J} = (\boldsymbol{s} \times \ddot{\boldsymbol{S}} - \boldsymbol{2}\dot{L}\boldsymbol{V})/L \tag{6.4}$$

To calculate the kinematics and dynamic of each actuator, the frame M and N have been attached to the top joint and base joint of each actuator. The transformation matrix from the moving frame to the fixed coordinate of the actuator (attached to the base) is given by the following equation:

$$\boldsymbol{T} = [\boldsymbol{s}, \frac{(\boldsymbol{K}\times\boldsymbol{s})}{\|\boldsymbol{K}\times\boldsymbol{s}\|}, \boldsymbol{u} \times \frac{(\boldsymbol{K}\times\boldsymbol{s})}{\|\boldsymbol{K}\times\boldsymbol{s}\|}] \tag{6.5}$$

For the transformation matrix of the upper frame the actuator vector ($\boldsymbol{\zeta} = [L\ 0\ 0]^T$) will be added to the previous transformation matrix. M and N represent the centres of gravity of the upper and lower part of the actuator and their position vectors are represented by r_{N_0} and r_{M_0}respectively. They are transformed to the fixed actuator coordinates by the following equations:

$$\boldsymbol{r}_N = \boldsymbol{T}\boldsymbol{r}_{N_0} \tag{6.6.a}$$

$$\boldsymbol{r}_M = \boldsymbol{T}(\boldsymbol{\zeta} + \boldsymbol{r}_{N_0}) \tag{6.6.b}$$

So, the acceleration and moment of inertia for the lower part (N) and upper part (M) can be calculated by the following equations [81, 89]:

$$\boldsymbol{a}_N = \boldsymbol{J} \times \boldsymbol{r}_N + \boldsymbol{V} \times (\boldsymbol{V} \times \boldsymbol{r}_N) \tag{6.7.a}$$

$$\boldsymbol{a}_M = \ddot{\boldsymbol{L}}\boldsymbol{s} + \boldsymbol{J} \times \boldsymbol{r}_M + \boldsymbol{V} \times (\boldsymbol{V} \times \boldsymbol{r}_M) + 2\dot{\boldsymbol{L}}\boldsymbol{V} \times \boldsymbol{s} \tag{6.7.b}$$

$$\boldsymbol{I}_N = \boldsymbol{T}\boldsymbol{I}_{N_0}\boldsymbol{T}^T \tag{6.8.a}$$

$$\boldsymbol{I}_M = \boldsymbol{T}[\boldsymbol{I}_{M_0} + \boldsymbol{m}_M\boldsymbol{L}^2\boldsymbol{diag}(0,1,1)]\boldsymbol{T}^T \tag{6.8.b}$$

Where $\boldsymbol{I}_{N_0}$and $\boldsymbol{I}_{M_0}$represent the moment of inertia of the lower part and upper part in their local coordinates. So the actuator force will be calculated by the following equations:

$$\mathbf{F} = \left(m_M\boldsymbol{s}\,.(\boldsymbol{a}_M - \boldsymbol{g}) + C_p\dot{\boldsymbol{L}}\right) - (\boldsymbol{s}.\mathbf{F}_s) \tag{6.9.a}$$

$$\mathbf{F} = D - x \tag{6.9.b}$$

Where C_p represents the moment of friction at the prismatic joint and $\mathbf{F}_s$ represents the component of force at the spherical joint along the leg. The term $\mathbf{F}_s$ is given by the following equation in terms of the unknown x:

$$\mathbf{F}_s = x\boldsymbol{s} + (\mathbf{C} \times \boldsymbol{s})/\boldsymbol{L} = x\boldsymbol{s} + \boldsymbol{\chi} \tag{6.10}$$

Where unknown x will be calculated by [81]:

$$\mathbf{C} = \mathrm{m_N}\mathbf{r_N} \times \mathrm{a_N} + \mathrm{m_M}\mathbf{r_M} \times \mathbf{a_M} - (\mathrm{m_N}\mathbf{r_N} + \mathrm{m_M}\mathbf{r_M}) \times \mathbf{g} + (\boldsymbol{I}_N + \boldsymbol{I}_M)J + \boldsymbol{V} \times (\boldsymbol{I}_N + \boldsymbol{I}_M)\boldsymbol{V} + C_u\boldsymbol{V} + \mathbf{f} \tag{6.11}$$

And

$$\mathbf{f} = C_s(\boldsymbol{V} - \boldsymbol{\omega}) \tag{6.12}$$

Where **f** is the moment of viscous friction at the spherical joint and in the current study is assumed to be zero. The term $\mathbf{F}_s$ represents the constraint force at the spherical joint applying on the actuator. The constraint moment at the universal joint has been expressed by the following equation [81]:

$$M_u = s.\mathbf{C}. \tag{6.13}$$

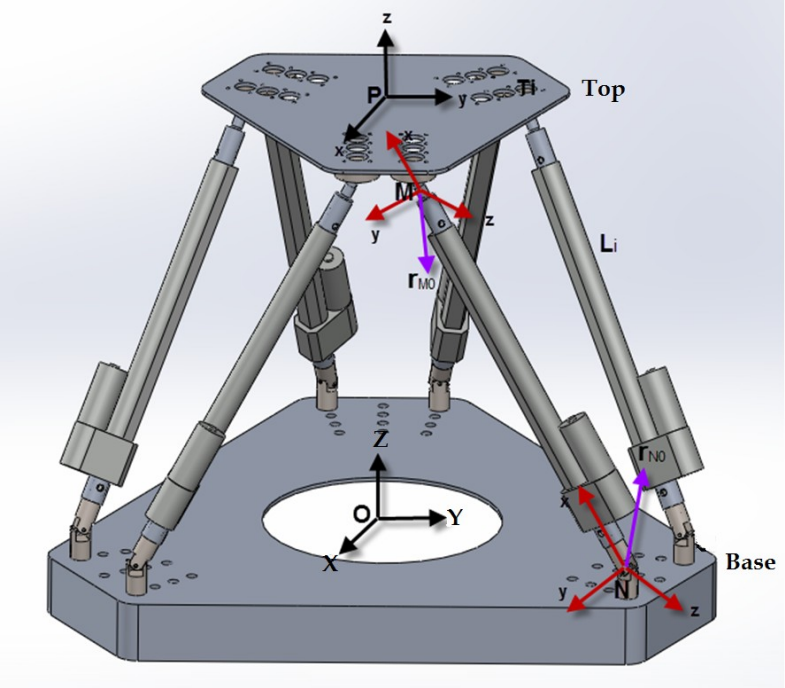

Figure 6-3: CAD model of hexapod designed in SolidWorks

6.3.2 Singularity analysis

With respect to the measured ground reaction force of the leg in vivo gait, the external force of the system applying on the top platform is available as F_{leg} and a moment M_{leg} where these vectors were transformed to the global basis by the rotation transformation.

The Newton`s equation for the top is expressed by the following equation in terms of linear and angular accelerations of the platform [81]:

$$\sum_{i=1}^{6}[x_i\,\mathbf{s}_i] = \Re \boldsymbol{F_{leg}} + \boldsymbol{M}(\boldsymbol{g}-\boldsymbol{a}) + \sum_{i=1}^{6}\boldsymbol{K_i} \qquad (6.14)$$

Where $\Re F_{leg}$ is the transformed external force vector of the leg from the top to the base, x_i represents the unknown x for the ith leg and K_i is the stationary axis of the universal joint at ith leg. The Euler`s equation of the platform [89], based on moments about the platform reference point is:

$$\sum_{i=1}^{6}[x_i\,\boldsymbol{q_i}\times\boldsymbol{s_i}] = M\boldsymbol{P_R}\times(\mathbf{g}-\mathbf{a}) - \mathbf{I}\boldsymbol{\alpha} - \boldsymbol{\omega}\times\mathbf{I}\boldsymbol{\omega} + \Re\mathbf{M}_{\text{leg}} - \sum_{i=1}^{6}[\boldsymbol{q_i}\times\boldsymbol{K_i} - \mathbf{f}_i] \qquad (6.15)$$

Where P_R is the transformed position vector of the centre of gravity of the upper platform from the Top to the Base and $\boldsymbol{\omega}$ is the angular velocity of platform. By combining equations 16 and 17, the following equation with six equations and six unknowns will be created:

$$\begin{bmatrix} \boldsymbol{s1} & \boldsymbol{s2} & \boldsymbol{s3} & \boldsymbol{s4} & \boldsymbol{s5} & \boldsymbol{s6} \\ \boldsymbol{q1}\times\boldsymbol{s1} & \boldsymbol{q2}\times\boldsymbol{s2} & \boldsymbol{q3}\times\boldsymbol{s3} & \boldsymbol{q4}\times\boldsymbol{s4} & \boldsymbol{q5}\times\boldsymbol{s5} & \boldsymbol{q6}\times\boldsymbol{s6} \end{bmatrix} [x1 \quad x2 \quad x3 \quad x4 \quad x5 \quad x6]^T =$$

$$\begin{bmatrix} \Re\boldsymbol{F_{leg}} + \boldsymbol{M}(\boldsymbol{g}-\boldsymbol{a}) - \sum_{i=1}^{6}\boldsymbol{K_i} \\ M\boldsymbol{P_R}\times(\mathbf{g}-\mathbf{a}) - \mathbf{I}\boldsymbol{\alpha} - \boldsymbol{\omega}\times\mathbf{I}\boldsymbol{\omega} + \Re\mathbf{M}_{\mathbf{leg}} - \sum_{i=1}^{6}[\boldsymbol{q_i}\times\boldsymbol{K_i} - \boldsymbol{f_i}] \end{bmatrix} \qquad (6.16.a)$$

Hence

$$\mathbf{HX} = \mathbf{c} \qquad (6.16.b)$$

So x has been computed by the above equation and the required input forces have been calculated by the following equation:

$$\mathbf{F} = \mathbf{D} - \mathbf{X} \qquad (6.17)$$

Where **F** is the actuator force and **D** is considered in Equation 16. If matrix H is singular, then the linear system does not have any solution and the robot will be in a singular configuration with an

extra degree of freedom. The condition number will be considered for proximity of the matrix to singularity. To find the singularity of the system, the mentioned algorithm was imported to MATLAB software to solve the equations.

To follow the trajectory of a foot during a gait cycle, an algorithm was developed in MATLAB to calculate the length of the actuators and the required force for each actuator based on kinematics, dynamics, singularity and workspace of the designed robot [135]. The desired trajectory was measured in the gait lab and it was imported to the control system of the robot. A CAD model of the robot was linked to MATLAB to follow the same trajectory. In the case where the robot faces any kind of constraint or singularity points or workspace limitation, it searches for the next reachable point along the trajectory.

6.3.3 Repeatability of the Robot

An experiment was conducted to evaluate the repeatability and reliability of the robot's positioning in Static Mode. The experimental procedure is as follows: The robot was first positioned to (0, 0, 120) mm in the z-axis to allow it to translate freely across is X and Y-axes. Then, the robot moved to -100 mm in the x-axis. Once it had stopped moving, the robot moved to +100 mm in the x-axis, and then moved back to -100 mm again. The stroke length of the shortest actuator was measured with a set of Vernier callipers. The motion was repeated and the stroke measured another three times to produce 4 sets of data for the desired position. Several other stroke lengths were measured within the workspace area of the robot and finally the robot was moved back to the translation co-ordinate (0, 0, 120) mm. This procedure was repeated for all axis of translation.

6.4 Results and discussion

The range of motion for the ankle joint in plantarflexion /dorsiflexion movement is (35˚, 25˚), in adduction/abduction is (30˚, 30˚) and in inversion/eversion is (40˚, 15˚) respectively [38]. In this study, the average range of motion of the participants` ankle joints during a gait cycle in plantarflexion /dorsiflexion was (8˚, 7.74˚), in adduction/abduction was (10.08˚, 3.35˚) and in inversion/eversion was (16.07˚, 3.65˚) respectively.

In section 6-1, it was explained how the trajectory of the foot was calculated based on coordinates of the attached markers. Foot trajectories of all participants have been measured through the Vicon system and the data were analysed by Vicon Nexus software. The obtained trajectory of the paretic leg was normalized for each participant during a single stride. The mean averaged trajectories over six trials were calculated for individual patients in order to import them to the control system of the robot. As a sample, the foot trajectory of participant (a) has been normalized in time and shown in Figure 6-4(a). The foot trajectory reached to a maximum of 120mm along the Z-axis when the foot reached to 68% of the trajectory. The ground reaction forces and moment of the paralyzed leg was measured by the force plate. As shown in Figure 6-4(b), the range of variation of force in the X and Y axes changed between 0N to 98N; while this value changed between 0-810N in the Z-xis. The peak force in the Z -axis happened when both heel and toe were in contact with the force plate. At 40% of the trajectory both heel and toe touched the force plate and at 52% of the trajectory the heel lost its contact with the force plate. The maximum ground reaction forces in different axes will be used as an external force in order to calculate the actuator forces during the foot trajectory.

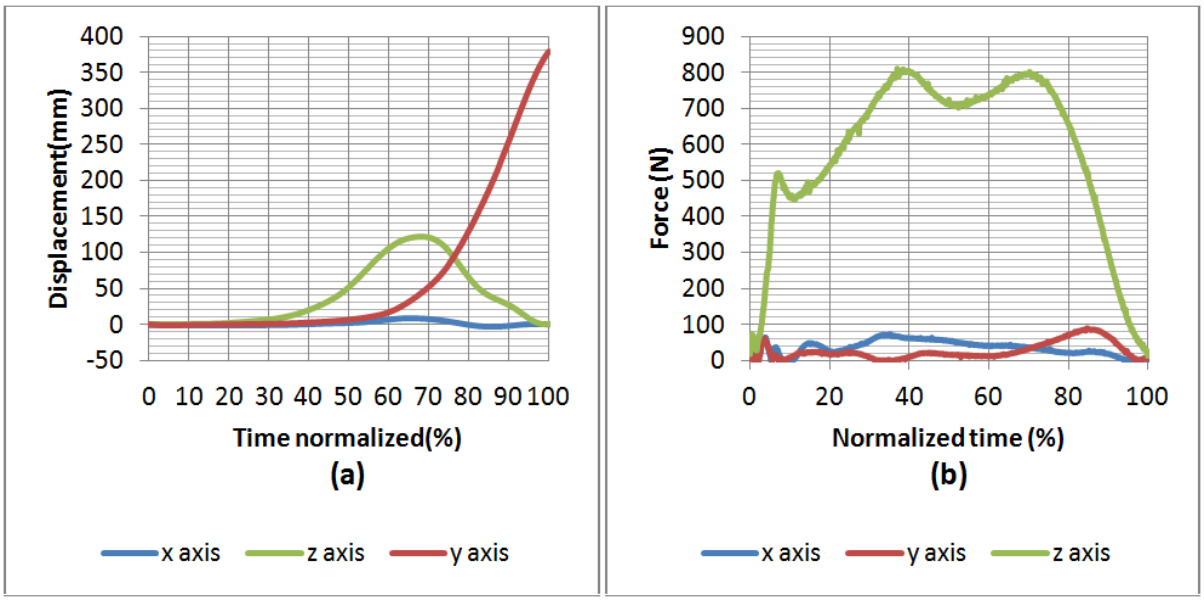

Figure 6-4: Gait results for participant-a (a) paralyzed foot trajectory in x, y, and z axes, (b) ground reaction force in x, y and z axes

6.4.1 Development of physical model

Based on kinematics and dynamics' analysis, a six DOF hexapod was built and is shown in Figure 6-5 using six linear servo actuators with a stroke of 30cm, operating speed (12V) of 55.88mm per second, dynamic trust (12V) of 11.33Kg and static trust (12V) of 226.79Kg connected to the top and base by six rolling spherical joints (SRJ016C) and six universal joints. Ultra light G6 polycarbonate foot wear with adjustable straps was placed on the top platform. A micro control SSC-32 was used to control the movements of the UPS robot. With respect to FEA analysis which was applied to Stewart platforms with different configurations, Stewart robot with platform of semi regular hexagons showed more stability in compare with other structures [136].

Figure 6-5: The constructed 6 DoF UPS parallel robot

6.4.2 Kinematics and dynamic results

As shown in Figure 6-6, the workspace of the robot was simulated in MATLAB with respect to the maximum length of the actuators and joint constraints in order to find the reachable boundary of the moving platform. The maximum translations of the end-effector in the X, Y and Z axes were 556mm, 556mm and 290mm respectively.

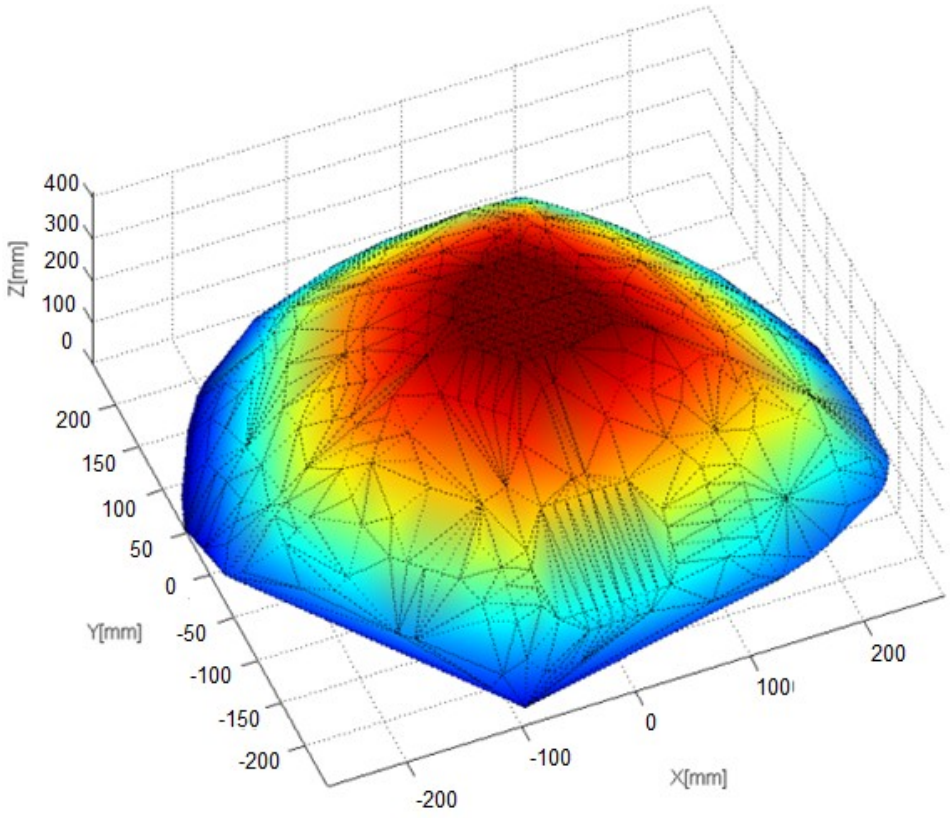

Figure 6-6: The workspace of robot simulated in MATLAB

The trajectory of the foot of participant (a) was applied to the developed program in MATLAB in order to find the length of the actuators for that particular motion. The calculated lengths have been transferred to the interface program (VBA) in order to modify the motors that are developed in the assembled CAD model in SolidWorks. A dynamic algorithm was developed in MATLAB to calculate the force of the actuators during the movements of the robot based on measured data in vivo gait and kinematic analysis. The actuators' forces were calculated for individual cases and the average value for all participants' trajectories were calculated in 5.5s and shown in Figure 6-7. The required forces for actuator 1 and 4 started from 293N and 243N respectively and they reached their maximum amounts of 450N and 370N respectively during the swing phase of the gait cycle. The trend of the force for actuators 2 and 5 started from 348N and 346N and were decreased gradually;

however, after 4s they increased to reach to their maximum value of 435N and 449N respectively. The trend of the forces for actuators 3 and 6 fluctuated in the stance phase of the gait, in a time range of 0s - 0.9s and then both of them reached their maximum values of 100N and 50N at 4.4s respectively.

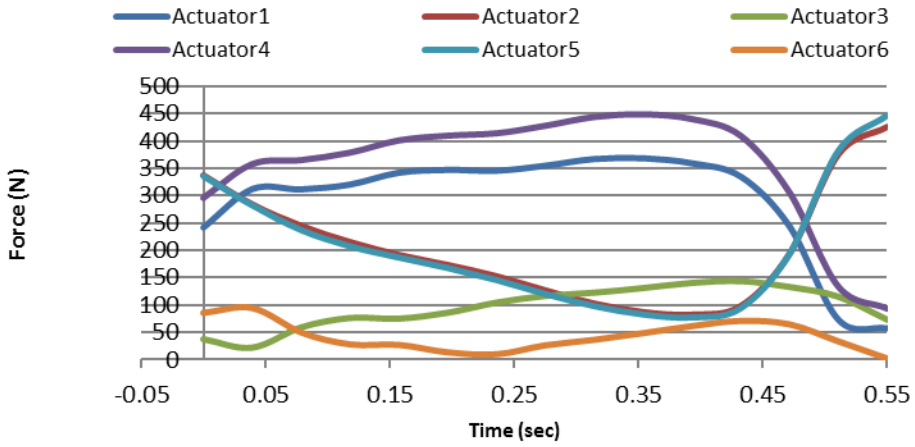

Figure 6-7: Average required force of six actuators during a single stride

The trajectory of the foot during a gait cycle has been followed by the end-effector for all nine participants. As shown in Figure 6-8, the trajectory of the foot in gait vivo (illustrated with the blue circles) was compared with a simulated trajectory of the robot in MATLAB (which was illustrated with the red line). The illustrated foot trajectory for each participant is the average of six successful trials. The measured paralyzed foot trajectories of the patients during a single stride have been scaled down in the Y-axis two times from the original foot trajectory in order to be within the workspace of the robot. The robot is able to move 278mm in the positive Y-axis while the maximum scaled down trajectory is 263mm in the Y-axis (Figure 6-8(e)). The robot was able to track the foot trajectory of all nine patients during a single stride, although their foot trajectories were different from each other. The robot started its movement from the home position, while all the actuator`s stroke sizes were zero. First, the robot calculated the length of the actuators with

respect to the pre-defined trajectories and then it calculated the required force of the actuators with respect to the applied GRF. With respect to the joint constraint and workspace of the robot, the singularities of the robot during its movement have been investigated. If there was not any singularity point during the trajectory of the robot, then it started its movement. The speed of the actuators during its movement was 2.71cm/s and this was constant all along the trajectory. In Figure 6-8(a), the robot reached 66mm in the Z-axis and this was the time that the foot reached its maximum position during a single stride. The patients were asked to walk as much as possible in a straight line; as a result, the variation of data in X was between -10mm - +10mm for all cases. As it can be seen, the trend of the foot trajectory was very similar between all cases, so the robot moved along similar trajectories. However, it is very important to personalize the trajectory of motion for individual patients since small movements out of the range of motion of the joint cause serious injury to the patient during robotic rehabilitation.

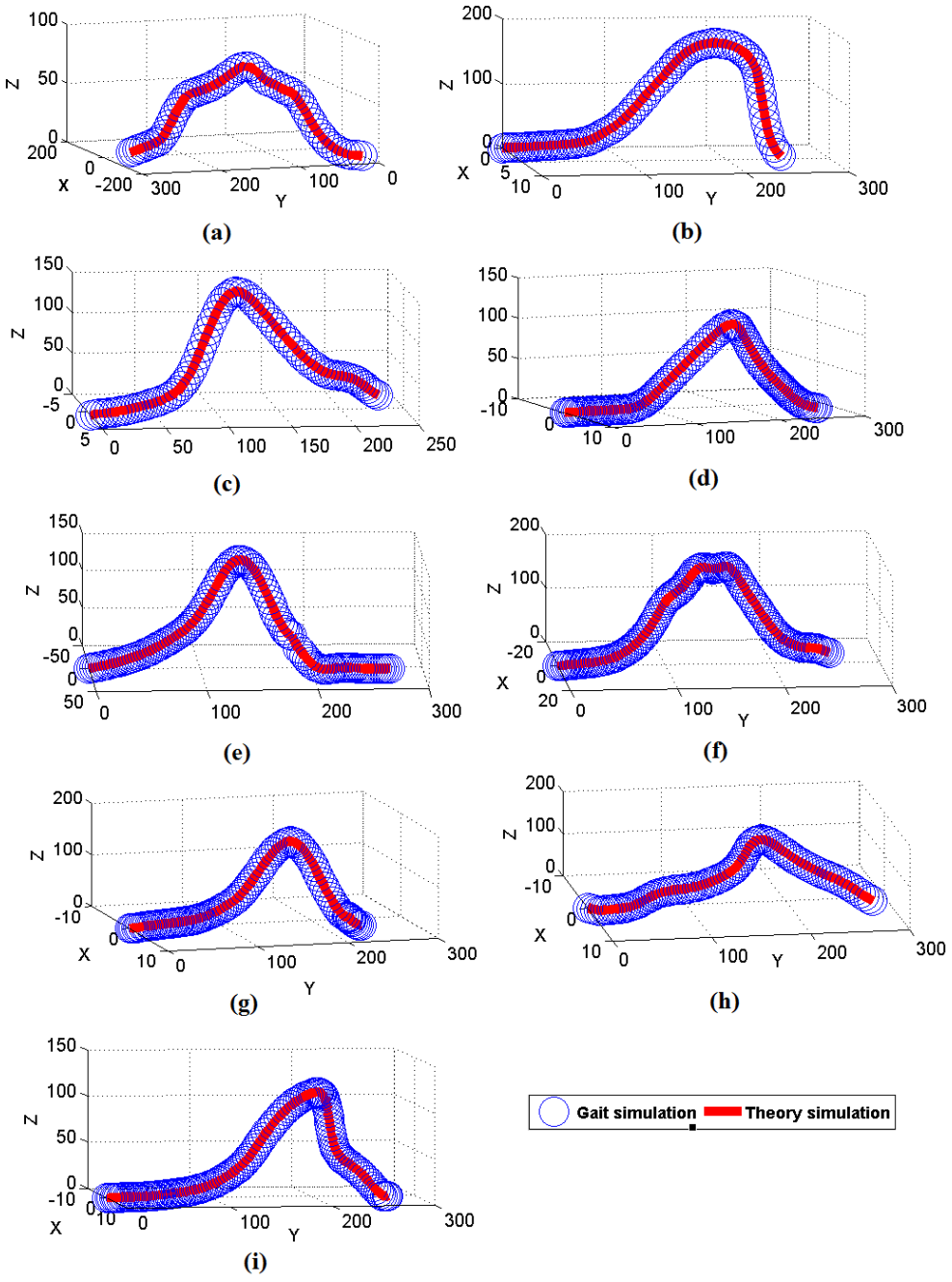

Figure 6-8: (a-i) represents the trajectory of the foot trajectory based on gait results with respect to the trajectory of the robot during performance of the exercise. Blue circles show the trajectory of the foot measured in vivo gait and the red line represents the trajectory of the robot during performance of the exercise.

The mean position error of the robot has been calculated while the robot tracked the foot trajectory.

The position of the end-effector has been calculated based on the servo feedback of the actuators

and then the results have been compared with the gait results. The mean values of the position error over the nine participants were 0.7mm, 1.2mm and 0.95mm in all X, Y and Z axes and are shown in Figure 6-9. The results revealed that the 6 DoF UPS parallel robot is a very precise device for ankle rehabilitation.

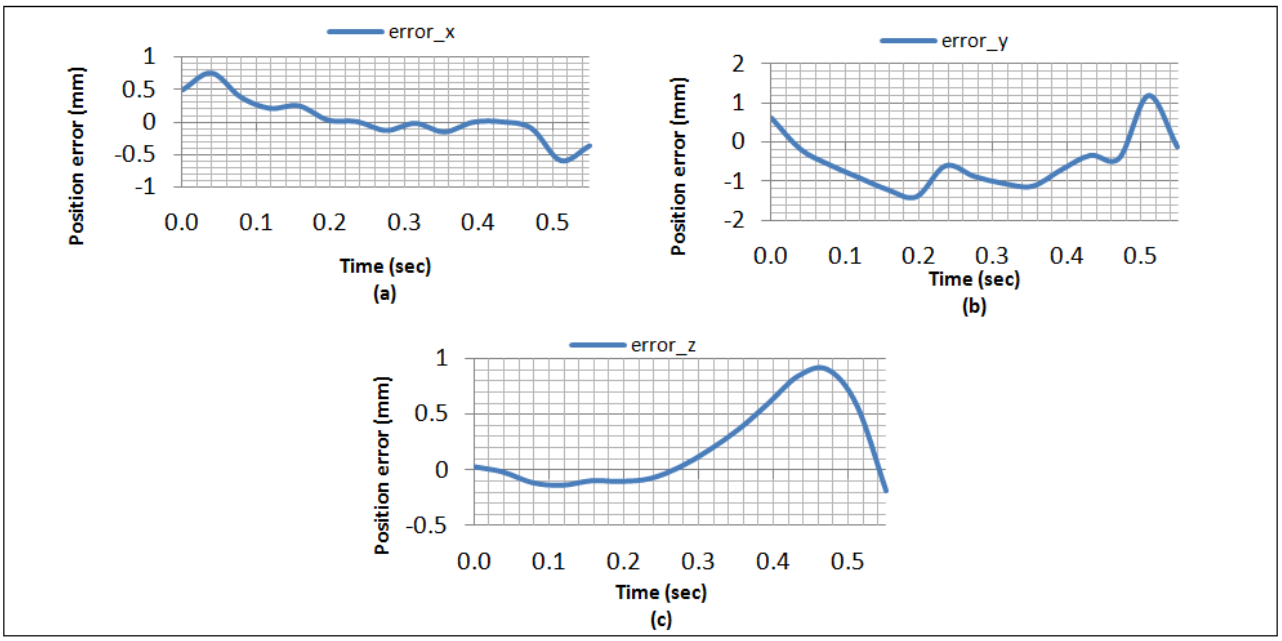

Figure 6-9: (a) position error of end-effector in X-axis, b) position error of end-effector in Y-axis, c) position error of end-effector in Z-axis

As shown Figure 6-10(a), the position error in the X-axis was zero when the robot was passing 50% of the trajectory. The position error in the Y-axis fluctuated and it reached to its maximum of 1.2mm after passing 95% of the trajectory; this maximum position error was caused by the joint constraint of the robot. The position error in the Z-axis started from zero and after 0.26s, it reached zero; this means that the position error in the Z-axis was zero when the foot trajectory reached its maximum position. Then, this error was increased radically up to 0.95mm and then it was decreased

to zero by the end of the trajectory. Since the stroke size was increasing along two axes, the position error was expected to increase as well.

6.4.3 Reliability results

As shown in Figure 6-10, the charts for the translations in the X and Y co-ordinates show an apparent similarity between them, with both deviations showing a peak at around 225 mm displacement (Figure 6-6(a) and 6-6(b)) and coming to a plateau beyond the peak point (0.55 and 0.43 mm for X and Y respectively). The stroke lengths at 225 mm displacement for all six actuators were (202.9, 212.0, 80.7, 91.6, 159.2, 139.5) mm. For comparison, at a displacement of 150 mm in the X-axis, the stroke lengths are (166.1, 89.7, 172.4, 135.7, 82.5, 122.2) mm. The average stroke lengths are marginally longer at 225 mm, with a couple of strokes reaching over 200 mm in length. This is closer to approaching the maximum stroke of the actuator of 250 mm compared to the stroke lengths at 150 mm. One can conclude that the unreliability increases with the stroke of the actuators. In theory, if all of the actuators are of equal performance, there should be no variation between the data generated from the translations between the X and Y-axis translations; however, small errors in the measurement procedure such as inconsistent lengths along the clevis of the actuators will bring rise to differences between the axes.

As expected, translations in the Z-axis showed a trend distinct to that of the X-Y translations, as the vertical displacement occurs on a different plane. Comparing the absolute values of standard deviation on the Z-axis with that of the other translations, it shows that the actuators can be up to 3.65 times more reliable in purely vertical translations compared to lateral movements. The standard deviations only peak at 0.171 mm (Figure 6.10.a) as opposed to 0.420 and 0.624 mm for the other 2 axes of translation.

Translations purely in the Z-axis have a different characteristic in that all of the actuator lengths are theoretically equal at all positions. Due to this characteristic, all of the actuators are only required to move together at the same speed, as opposed to other translations which require some actuators to move in sequence with each other. This is what gives rise to the higher reliability of movement in the Z-axis. The controller used in the platform (Lynxmotion SSC-32) is programmable to synchronise movement across all actuators; however due to the fixed duty cycle on the actuator hardware it is not possible to achieve this synchronisation.

In contrast to the reliability of the actuators under translation, rotational movements showed fluctuating reliability; however the trend is not random as all three axes of rotation show peaks of unreliability between 15 to 20 degrees of rotation and a similar plateau beyond that range. The three rotations are visually similar in 'phase' and characteristics.

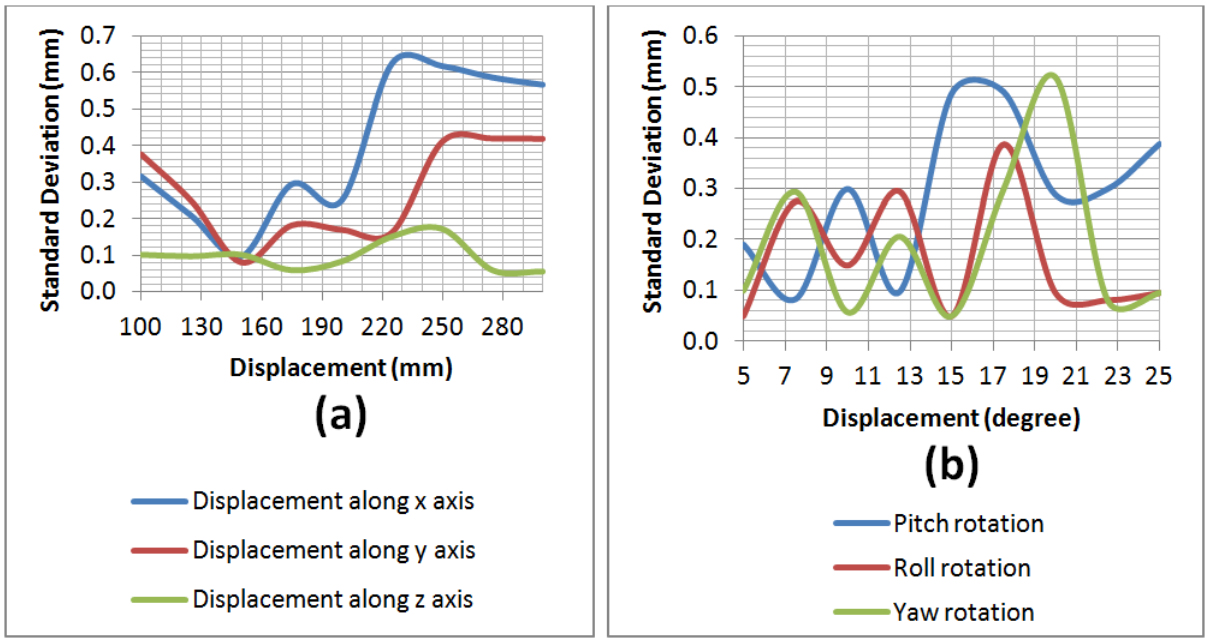

Figure 6-10: Robot repeatability test (a) reliability of actuators for displacement along x, y and z axes, (b) Reliability of actuators for roll, pitch and yaw rotations

6.5 Conclusion

In this chapter, the capability of a 6 DoF parallel robot for lower limb rehabilitation using foot trajectories of a number of post-stroke patients has been investigated. The paretic foot trajectories of all patients have been simulated in the gait and then it was used by the robot to track the same trajectory. The repeatability of the moving platform translation in the X and Y axes are very reliable, as at the worst, the errors are no more than 0.712% of the displacement. However, the reliability of the robot in the Z-axis was more than the two other axes and the repeatability of the parallel platform movement was very high, especially for purely translational movements in static mode. Based on kinematic/dynamic analysis, the trajectory of the robot during the following of the foot trajectories of all patients has been simulated in MATLAB and the results showed that the robot was able to track all the trajectories within the workspace of the robot. Then a physical model performed the exercise with the maximum position error of 1.2mm in the X-axis. With respect to the precision, low cost and high repeatability of the robot it can be a proper replacement for traditional physiotherapy.

Chapter 7

Unilateral and Bilateral Lower Limb Robotic Rehabilitation System

7.1 Introduction

The overall aim of this chapter is to develop a safe, accurate and reliable robotic system for lower limb rehabilitation of early-stage post-stroke patients. The initial phase of the investigation has been completed by the identification and measurement of human leg segmental motion characteristics (signatures) during different exercises in the gait laboratory. Based on kinematic, dynamic analysis of a 6 DoF parallel robot, the length of the actuators, actuator forces and position of the end-effector have been calculated during different trajectories. The designed robot in chapter 6 was used in this study and the robot was able to lift 200kg with an average speed of 2.7 (cm/s). The movement of the robot during three different unilateral exercises has been tracked by a Kinect camera. Based on the functionality of the active robot for unilateral rehabilitation and obtained data from chapter 4, a novel bilateral rehabilitation system has been proposed for rehabilitation of paretic patients. The bilateral system includes both active and passive platforms where the passive parallel mechanism is also used in conjunction with the robot to follow the motions of the healthy leg; hence creating a bilateral mode of operation suitable for gait training or stair climbing. As a preliminary test, the biomechanical relationship between the left and right legs was analysed; this was used to relate the human biomechanical motion to the robotic device [136].

7.2 Methodology

In this study, in order to find the differences between the trajectory of a healthy leg and a paretic leg, the foot trajectory of ten post-stroke patients, including five male and five female, have been measured during four different exercises in the gait laboratory. The characteristics of the patients have been shown in Table7-1. The results will be used to train the parallel robot to simulate normal walking.

Table 7-1: Characteristics of patients

	Age (year)	Weight (kg)	BMI	Height (m)	Step length (m)	Step time (s)	Stride length (m)	Stride time (s)	Walking velocity (m/s)
Male (n=5)	46.1 ±4.1 years	86.2 ±6.03 kg	24.42 ±2.01	1.76 ±7.92m	0.67 ± 0.034 m	0.50 ± 0.028 s	1.34 ± 0.059 m	1.01 ± 0.05 s	1.32 ± 0.081 m/s
Female (n=5)	45.76 ±5.39 years	72.63 ±3.59 kg	23.42 ±1.69	1.68c±4. 54m	0.56 ± 0.114 m	0.46 ± 0.321 s	1.12 ± 0.142 m	0.91 ± 0.01 s	1.34 ± 0.15 m/s
Overall (n=10)	45.5±2. 74 years	79.415±3 .81 kg	23.92 ±2.85	1.72±4.2 3	0.615 ± 0.024 m	0.48 ± 0.114 s	1.23 ± 0.124 m	0.96 ± 0.035 s	1.33 ± 0.155 m/s

7.2.1 Foot trajectory of post-stroke patients during different exercises

In this study, ten post-stroke patients with the right leg affected participated. All of the participants had their first stroke between 9-12 months before the test. Prior to the experimentation ethical approval was granted to the WMRC and all subjects completed a data collection consent

form and a health declaration form. The foot trajectories of all participants have been measured by a Vicon system at the gait laboratory of the West Midlands Rehabilitation Centre (WMRC). The gait laboratory was equipped with 12 Vicon cameras including six MX3+ and six MX T40 cameras collecting data in 100Hz. Two digital cameras have been used in saggital and lateral planes and they collected data in 50Hz. Two force plates, a Kistler force plate and an Ampti Optima force plate, with sampling frequency of 2000Hz was used to measure the ground reaction forces. Before starting the experiment, the cameras were calibrated within a $2.8m^2$ calibration volume. An Oxford foot model with sixteen reflective markers was placed on the participants' lower limbs. The position of the markers was measured by the Vicon system and the temporal spatial parameters, linear velocity and the acceleration of the markers were calculated. The joints' moments and resultant force of the joints were calculated based on the Cardan angle system and inverse dynamics. Two types of exercises were tested by the patients: (I) bilateral exercises where both legs will be engaged during the exercise; (II) unilateral exercises in which the exercise will only be performed by the paretic leg.

The purpose of the unilateral exercises was to record the signature of motion of the healthy leg, in order to be simulated by the robot for the affected leg. In the first exercise shown in Figure 7.1.a, participants were asked to sit on a bar while they grasped the support bar and both their feet were placed on the force plates. Then, the participants were asked to perform hip flexion/extension with one leg while the other leg remained on the force plate. In the second exercise shown in Figure 7.1.b, participants were asked to sit on the support bar to perform an ankle dorsiflexion exercise; while both feet were placed on the force plates and both their hands were free. For the third exercise, a two-step platform was placed in the middle of the gait laboratory`s walkway. In the last exercise shown in Figure 7.1.c, participants were asked to stand on the force plate while both feet were placed on the right and left force plates. Then participants were asked to bend their knees with one foot on each of the right and left force plates. This exercised is called marching due to its

similarity to military marching. In each exercise, the maximum applied force by the leg was measured by the force plate and it was used as an external force which was applied on top of the parallel robot.

A set of three markers was attached to the thigh, shank and foot segments. All anthropometric dimensions have been measured before the experiment. The trajectory of the foot segment was simulated with respect to the measured trajectory of the attached markers placed on the heel, ankle joint and toe respectively. The normal vector of the plane, created by these three markers, was calculated by equation 7.5.1. The calculated normal vector will be used by the robot to follow the foot motion.

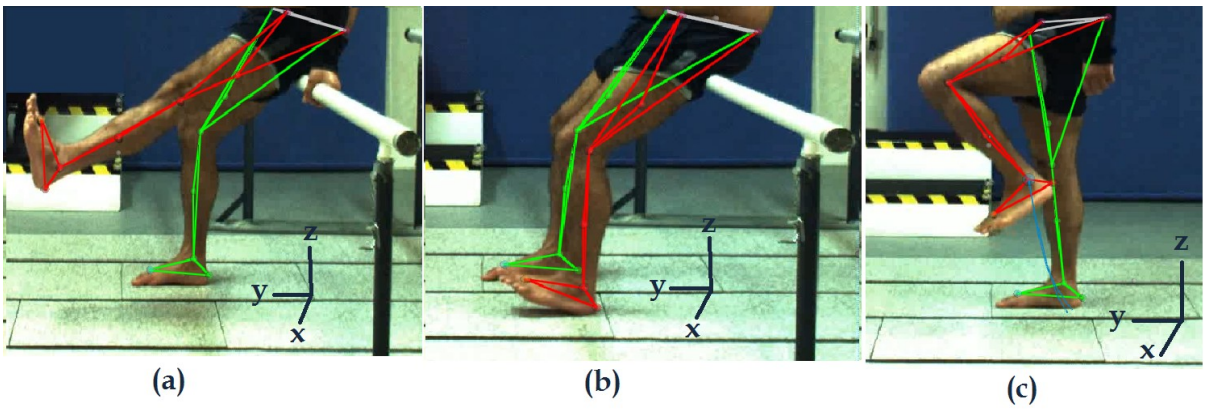

Figure 7-1: Unilateral exercises (a) Hip flexion/extension, (b) Ankle dorsiflexion/plantarflexion, (c) Marching

7.2.2 Robot analysis

A high degree of stiffness, good power to volume ratio and the flexibility of a 6 DoF parallel robot were the reasons to select the architecture of this system for rehabilitation of lower limbs [54]. The length of the actuators and the position of the end-effector during different exercises have been calculated based on the geometry of the robot [72].

Point P with coordinate system (*X, Y, Z*) was placed on the centre of the fixed platform with the Z axis pointing vertically upwards, called the base frame. The end-effector's coordinate system O=(*x, y, z*) was attached to the centre of the moving platform (top) with the Z axis perpendicular to the end-effector, pointing upwards; [*L1, L2,..., L6*] represent the lengths of the actuators; $t = [Px, Py, Pz]^{T}$ representing the location of the moving platform (top) with respect to the base and $\Re$ =(α , β , γ) representing the rotation angles of the top frame: first around the X axis to α degrees, then around the Y axis to β degrees and lastly around the Z axis to γ degrees (Figure 7.2(a)). It is worth mentioning that all of the angles have been calculated based on the right hand sided rule. Therefore the position and orientation of the moving platform have been expressed by $\boldsymbol{Xp} = [px, py, pz, \alpha, \beta, \gamma]^{T}$. With respect to Equation 5.2, the homogeneous transformation matrix has been used to describe the position of joints on the top platform with respect to the fixed/base platform.

With respect to this homogeneous transformation and the trajectory of *Xp*, the coordinates of the vertices of the top and base were calculated online based on time history by equation 5.3. Then, the lengths of the actuators have been calculated by equation 5.5.d. The actuator forces during different exercises have been calculated and presented by Equation 4 [41]. The measured force by the force plates have been considered as an external force in the calculation (Equation 6.9.a).

With respect to the following equation, the output force system is related to the input forces [89]:

$$[\mathbf{R} \quad \mathbf{M}]^{T} = \mathbf{HF} \tag{7.1}$$

Where $\mathbf{F} = [f_1, f_2, f_3, f_4, f_5, f_6]^{T}$ and $[f_1, f_2, f_3, f_4, f_5, f_6]$ represent the magnitude of the actuator force of the actuator 1-6; R and M present the resultant force and moment at the platform and **H** is a 6×6 transformation matrix which describes the relation between the input forces and output forces.

When **H** is singular, extra load will be created on the platform which cannot be supported by the actuator forces. The singularities were identified while the value of determination of the matrix **H** was zero. The static singularity will appear when:

$$\det[\mathbf{H}(\boldsymbol{Xp})] = 0 \qquad (7.2)$$

Equation 7.2 shows the singularity manifold for the 6 DoF Stewart platform which consists of continuous hypersurfaces which separate the task space into two or more disjointed segments. The work volume of the robot has been calculated based on calculated joint constraints and the length of the actuators [145].

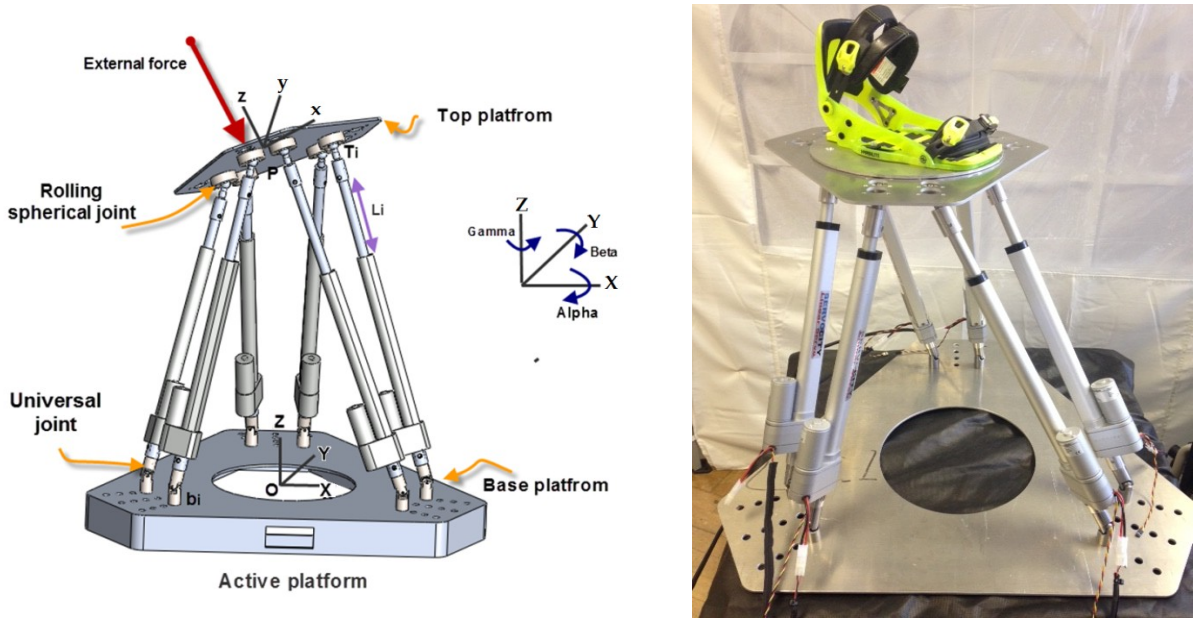

(a) **(b)**

Figure 7-2: (a) CAD model of robot, (b) Physical model of the robot

7.2.2.1 Unilateral active robot

The Figure 7-2(b), a six degrees of freedom (DOF) UPS parallel robot has been designed and built in the Robotics laboratory at the University of Birmingham. Six servo linear actuators with a stroke size of 30cm and static force of operating speed (12V) of 55.88mm per second, dynamic trust (12V) of 11.33Kg and static trust (12V) of 226.79Kg were connected to the top and base by six rolling spherical joints (SRJ016C) and six universal joints. Ultra light G6 polycarbonate foot wear with adjustable straps was placed on the top platform. A micro control SSC-32 was used to control the movements of the UPS robot. In order to increase the pivot angle of the rolling spherical joints from 35˚ to 65˚, another component was designed in SolidWorks and then 6 of them were printed by a 3D printer. The rolling spherical joint was connected to the moving platform by 6 of these components. Figure 7-3 demonstrates the printed component:

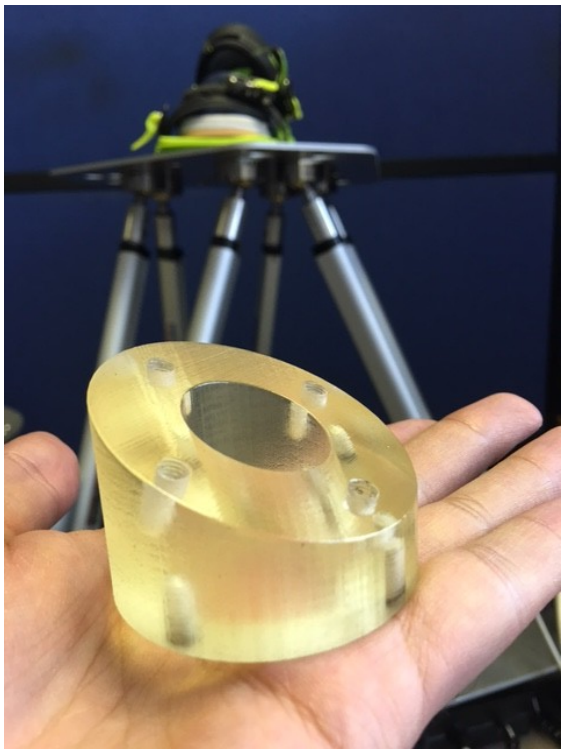

Figure 7-3: The external component was designed and printed using 3D printer in order to increase the pivot angle of the Rolling spherical joints

Active-passive and assistive/resistive control system using either backdrivable actuators or through impedance control have the advantage of offering resistive motion to the patient; hence allowing for active force participation by the patient's affected leg. However, in this study all of the required forces for performing the exercise will be provided by active (assistive) actuators. With respect to the workspace of the robot and limitation of the patient's joints and muscles, different exercises have been defined for the robot, ranging from flexibility and a range of motion exercises to strength and muscle endurance exercises.

7.2.2.2 Load test of hexapod parallel robot

As shown in Figure 7-9, the load test was performed in order to quantify the vertical movement speed of the robot and time taken by the robot under varying levels of load on its upper platform. In the first step, the robot started its movement from the home position along a displacement of +200 mm in the Z-axis and the time taken for the forward movement was measured. Then in the second step, the robot went back to the home position and the time taken for the backward movement was measured. In the third step, the robot was loaded with a 5kg mass on its upper platform approximately in the centre to distribute its load evenly across all six actuators. The first and second steps were repeated for this load to measure the forward and backward vertical movement speeds of the robot at the specified load. Time measurements were repeated for loads in 5 kg intervals through to 200 kg. The average speed was calculated by measured stroke length over movement time.

7.2.3 Robot`s graphical user interface

To control the robot a graphical user interface (GUI) has been designed by use of MATLAB. The robot is able to be manually translated/rotated using the sliders on the GUI. The sliders each have their own call-back method, which is triggered when the user manipulates them. The call-back method updates the co-ordinates and rotations displayed under the 'Position of upper platform' section, according to the value of the moved slider, and then it calls the 'Point to point mode' method to move the robot to the new location. This allows the robot to move as soon as the slider is released. The range of motion for each axis is defined by the minimum and maximum slider values. These limits define the safe working range for each of the axes. With respect to the kinematic and dynamic analysis of the robot, the length of the actuators, actuator force and stiffness of the robot will be calculated during different trajectories and they will be illustrated in the GUI. The Stewart -platform workspace can be calculated directly from the GUI. The calculation method will plot the resulting tetrahedral mesh at the end of its function. Also another option has been added to the GUI to control the robot, with an Xbox controller. Both translation and orientation buttons have been defined for the controller. With respect to the workspace of the robot, the controller vibrates when the end-effector reaches to the work volume`s boundaries. The robot can be manually translated/rotated using the sliders on the GUI.

As it is shown in Figure 7-4, the robot can be controlled in two different modes through the GUI: (I) Point to point mode (low level) – taking values of the desired co-ordinates and rotation angles from the input fields under the 'Position of upper platform' area, the values are passed onto a method that calculates stroke lengths of all six legs of the hexapod. The stroke lengths are then passed onto a method that sends the appropriate signal to the SSC-32 servo controller to move the leg servos to their correct stroke lengths. (II) Continues Mode (High level) – this mode defines the process behind how the robot moves through all of the exercises. Fundamentally the robot moves

through each co-ordinate using the 'Point to point mode' at a given rate (a function of the speed defined in the GUI) in this mode. To optimise the real-time movement of the robot, all stroke lengths for every step of the exercise is calculated beforehand and stored in a single 2D matrix, with stroke lengths for each leg displayed in each column of the matrix. Depending on the exercise, the pre-calculations take up to 20 seconds to complete. This is to avoid the robot waiting for new stroke lengths to be calculated as it moves through the exercise path.

The stroke lengths are then passed on to a method that operates the servo legs (as in Static Mode) one row at a time. The servos can be programmed to move in a specified duration, or if no duration is specified the servos will move to their desired locations.

Three different speeds, slow, medium and fast have been defined for the robot. With respect to the severity of the injury, the therapist is able to select the appropriate speed for rehabilitation of the lower limb. To optimise the real-time movement of the robot, all stroke lengths for every step of the exercise are calculated beforehand and stored in a single 2D matrix, with stroke lengths for each leg displayed in each column of the matrix. Depending on the exercise, the pre-calculations take up to 10 seconds to complete. This is to avoid the robot waiting for new stroke lengths to be calculated as it moves through the exercise path. The stroke lengths are then passed on to a method that operates the servo legs (as in 'Point to point') one row at a time. The servos can be programmed to move in a specified duration, or if no duration is specified, the servos will move to their desired locations as quickly as possible. The number of cycles for performing the exercises can be defined in the GUI. Repeatability and variety of tasks encourage the user to use the device for longer. Also, there is an option to demonstrate the live 3D model of the hexapod during performance of the exercise. The Kinect camera as a depth camera was used to track the trajectory of the robot during its motion and

to validate the trajectory of motion. Blue, red and green paper markers were placed on the moving platform and KinectColorBlock software was used to track the color markers.

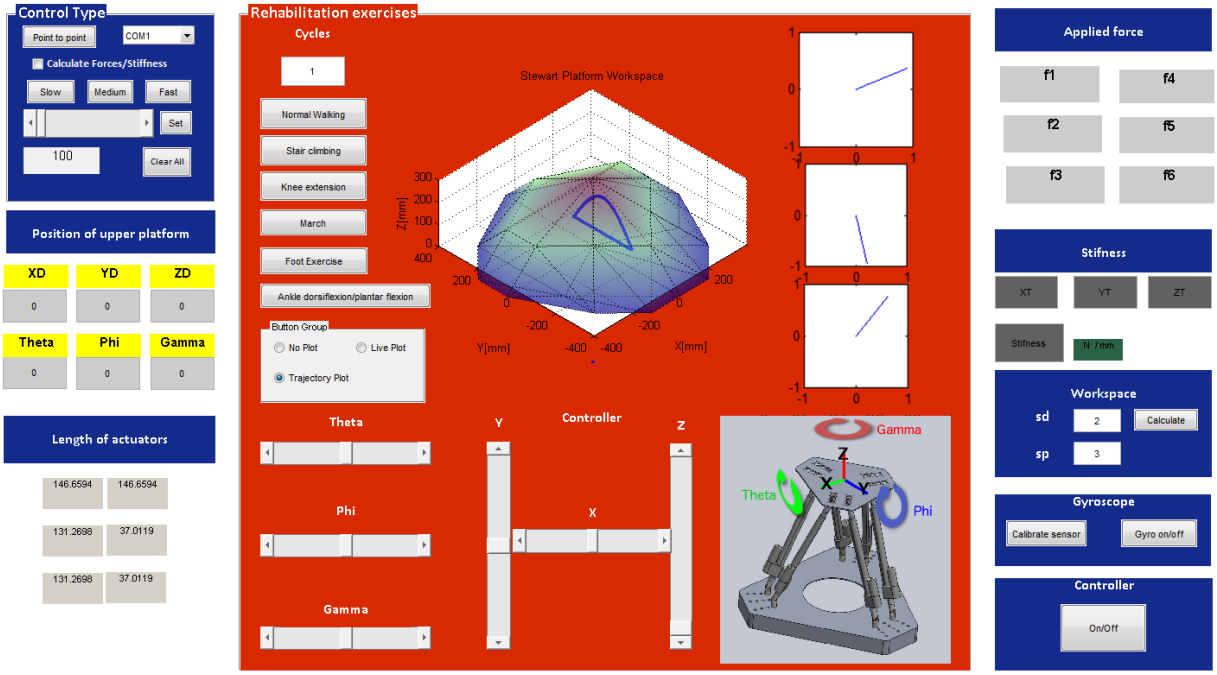

Figure 7-4: Designed GUI including a rehabilitation library in order to perform different exercises

7.3 Results

7.3.1 Gait analysis

Unilateral exercises- The average foot trajectory of patients during all exercises has been calculated. With respect to the averaged value, the general model for the movement of the robot can be presented. However, the personalized trajectory for individual patients has been calculated based on foot trajectory of the healthy leg. For instance, the average foot trajectory in the Z axis during the unilateral exercises has been shown in Figure 7-5:

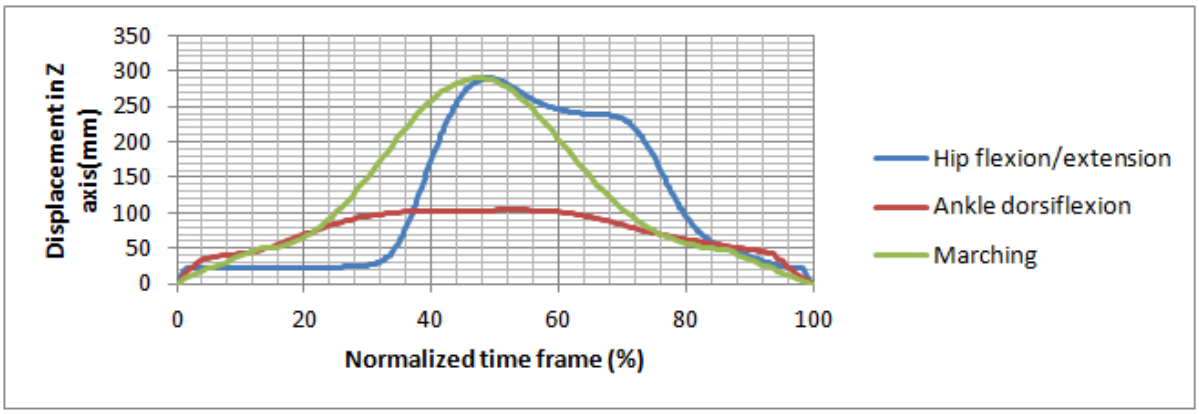

Figure 7-5: Averaged foot trajectory of ten post-stroke patients during three unilateral exercises

The variation of the data in the X axis was less than in the two other axes. In Figure 7-5, time was normalized in order to display all three exercises under one graph. With respect to the normal vector calculated in Equation 5.1, the trajectories of the foot during all exercises have been calculated. The maximum displacement values for both marching and hip exercises were similar to each other; while this value was 200cm less in the ankle exercise. All of the measured data in all axes were less than 300mm, which means the robot is able to reach to the maximum foot`s position during performance of the exercises. Although, the capability of the robot for performing different exercises depends on different constraints and some of them will be investigated in the next section. There are no significant differences in the foot trajectory of the right leg and left leg during performance of simple tasks by healthy subjects; it was the main reason for defining these three simple exercises in this study, in order to simulate the foot trajectory of a healthy leg by the robot.

7.3.2 Kinematics and dynamics of robot

The length of the actuators and position of the end-effector during different exercises were calculated. Based on measured foot trajectories in the gait laboratory, the end-effector's motion during different exercises were simulated by MATLAB and are shown in Figures 7-6(a.1), 7-6(b.1) and 7-6(c.1). The developed MATLAB program calculated the actuator forces and then checked the singularity locus of the robot during those specific trajectories. Based on the obtained results, the robot was able to follow all the of the given trajectories. As mentioned previously, the variation of displacement in the X and Y axes were much less than in the Z axis, especially for the marching and hip exercises. All of the trajectories were inside the workspace of the robot. However, for hip and marching exercises the trajectories needed to be scaled down in order to be within the workspace of the robot due to the stroke size of the actuators used in the robot. Based on the simulation results the positional errors between the gait results and theoretical results for all three exercises are illustrated in Figures 7-6(a.2), 7-6(b.2) and 7-6(c.2). The maximum error of 1.5mm in Z axis was observed during hip flexion extension, which may have been caused by the robot`s joints constraints. The positional errors in all axes during Ankle exercise were less than 1mm, while the corresponding values for Marching exercise were less than 1.2 mm. The robot's Computer Aided Design (CAD) model was developed in SolidWorks. The CAD model was used to measure the location of joints in order to be used as input for the developed inverse kinematic algorithm in Matlab. Use of the data extracted from the CAD model can also be a contributory factor in the positional errors.

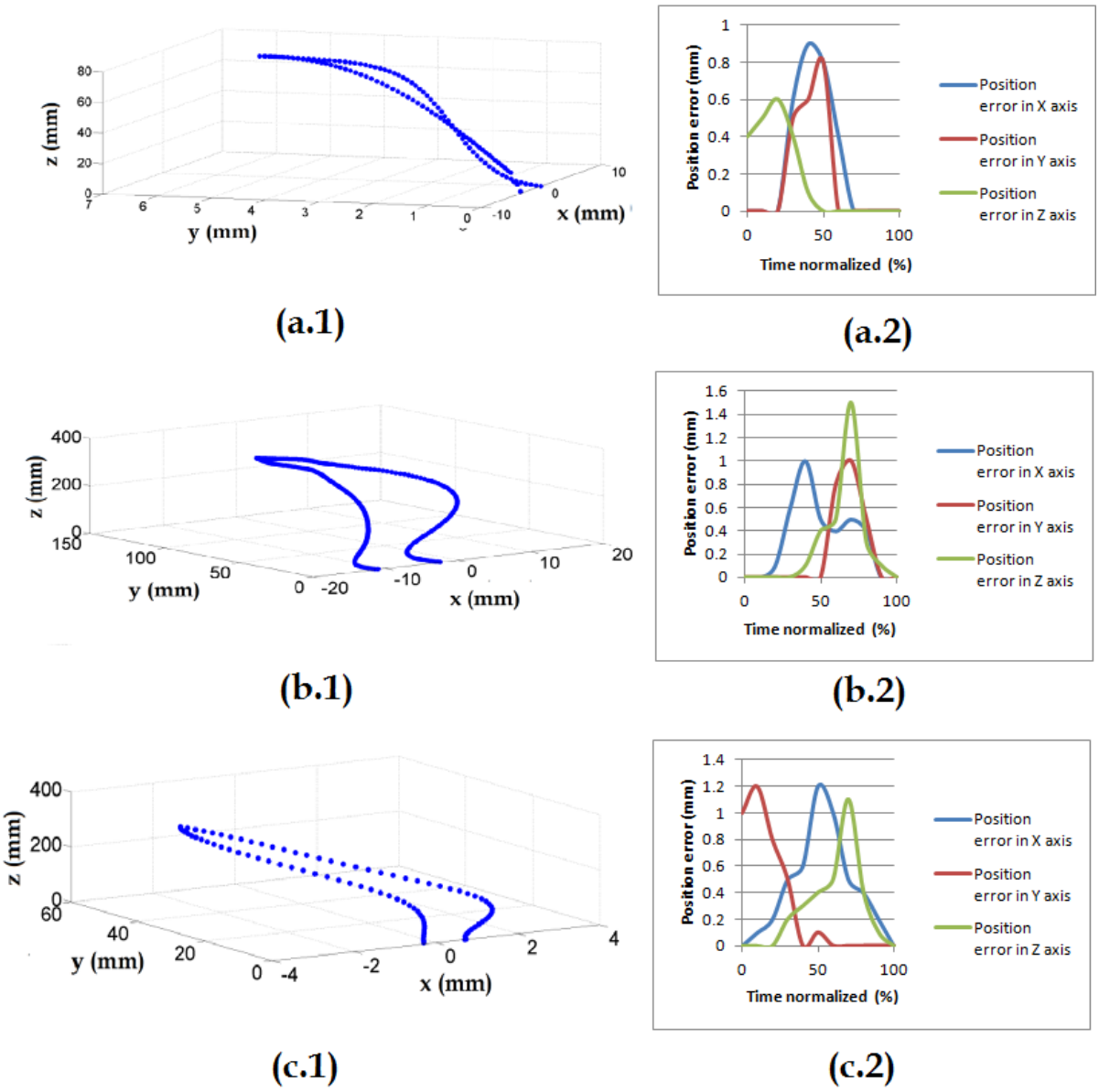

Figure 7-6: Position of end-effector during performing: (a.1) Ankle dorsiflexion/plantarflexion, (b.1) Hip flexion/extension, (c.1) Marching – this is illustrated based on theoretical results. The corresponding position errors between theoretical results and gait results are shown in Figures (a.2), (b.2) and (c.2) respectively.

A Kinect camera was used to track and validate the trajectory of the end-effector during different exercises. The Kinect`s measured data has been compared with simulation results in order to calculate the positional error. As shown in Figure 7-7, the maximum position error was 2.5cm in the Z axis during the ankle dorsiflexion/plantarflexion exercise; while the error increased to 2.9cm in the Z axis during the Hip flexion/extension exercise and this value was 3cm during marching. The maximum errors in the X axis were 2.4cm, 2.9cm and 2.8cm in the Ankle, Hip and Marching exercises respectively, while the corresponding values in the Y axis were 2.6cm, 2.8cm, and 2.9cm respectively.

In order to track and record the position of the robot during its movement by the Kinect, a program was developed in MATLAB. Each exercise was repeated three times in order to measure the displacement along each axis individually. As can be seen in Figure 7-7, the positional error in the X and Y axes were similar to each other during the ankle exercise and this error was raised to its maximum when the foot trajectory reached midway. Also the maximum error in the Z axis observed after tracking 60% of the trajectory during the hip exercise. In marching, the positional error in the Y axis was between 60%-80% more than the other two axes of the trajectory.

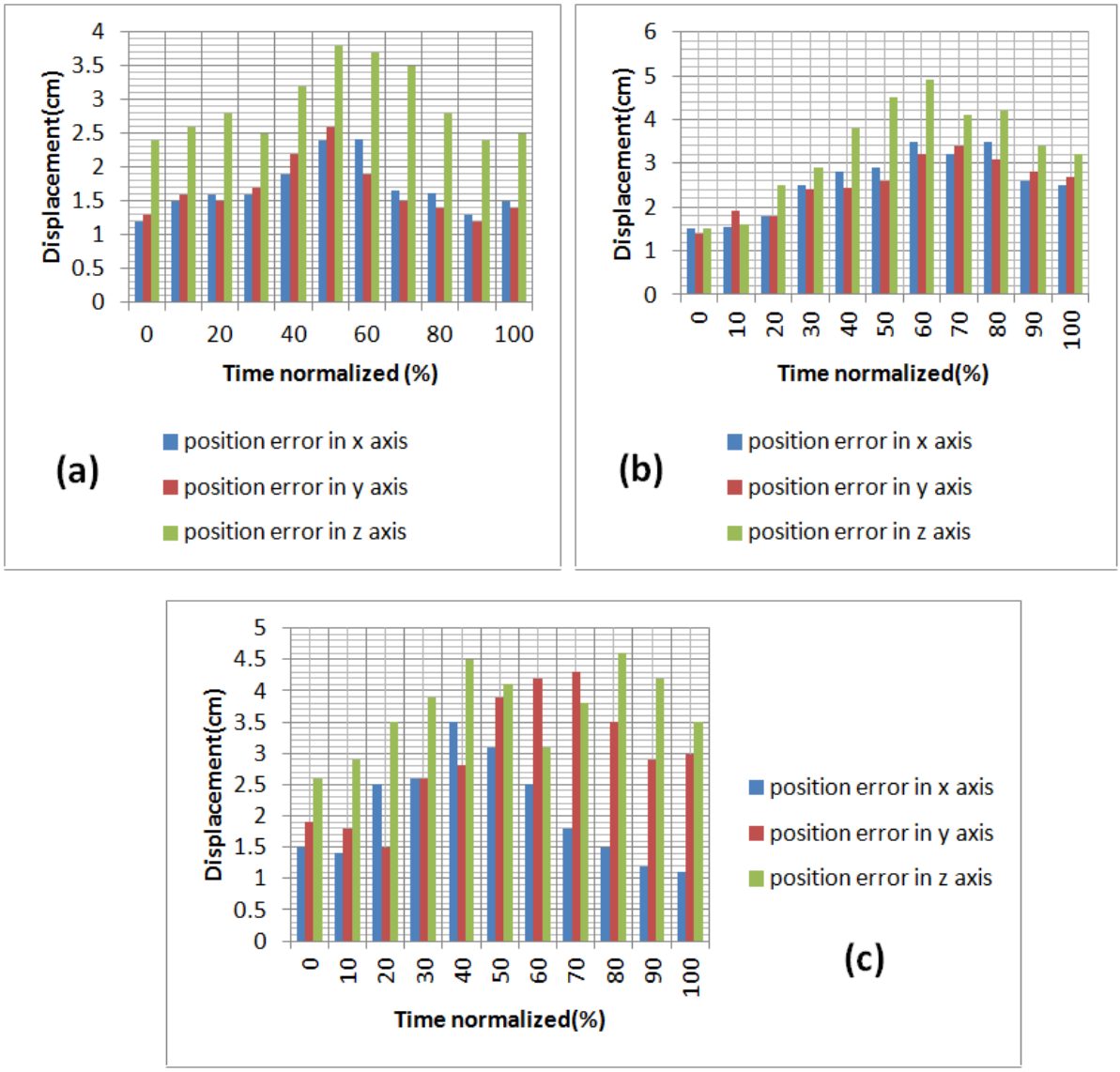

Figure 7-7: Position error between Kinect`s measurements and theoretical results in (a) Ankle dorsiflexion (b) Hip extension/flexion, (c) Marching

Based on dynamic analysis, the actuators' forces have been calculated in MATLAB during different exercises. The force profile measured by the force plates in the Gait Measurement lab was assumed to be an external force for all exercises. For instance, Figure 7-8 shows the actuators' forces during three unilateral exercises when the external force of 30kg is applied on the moving platform. The singularities of the robot during different trajectories have been analysed based on the dynamic

results. The maximum required actuator forces were 15.69N, 39.34N and 43.46N in the Ankle, Hip, and Marching exercises respectively.

As shown in Figure 7-8(a), two of the actuators worked with higher force in order to perform the ankle dorsiflexion movement while the rest were working with lower power, although in this exercise the external force was much less than in the two other exercises. Based on the gait measurements most of patients' weight was supported by the supporting bar and the affected side of the body. In Figure 7.8(b), the actuators required more force in order to lift the leg and perform the exercise. In this exercise two of the actuators were working with high power. In Figure 7.8(c), four of the actuators worked with similar power in a time frame between 20%-60%; which shows the external force was distributed normally all around the top platform and the robot was moving with a constant speed.

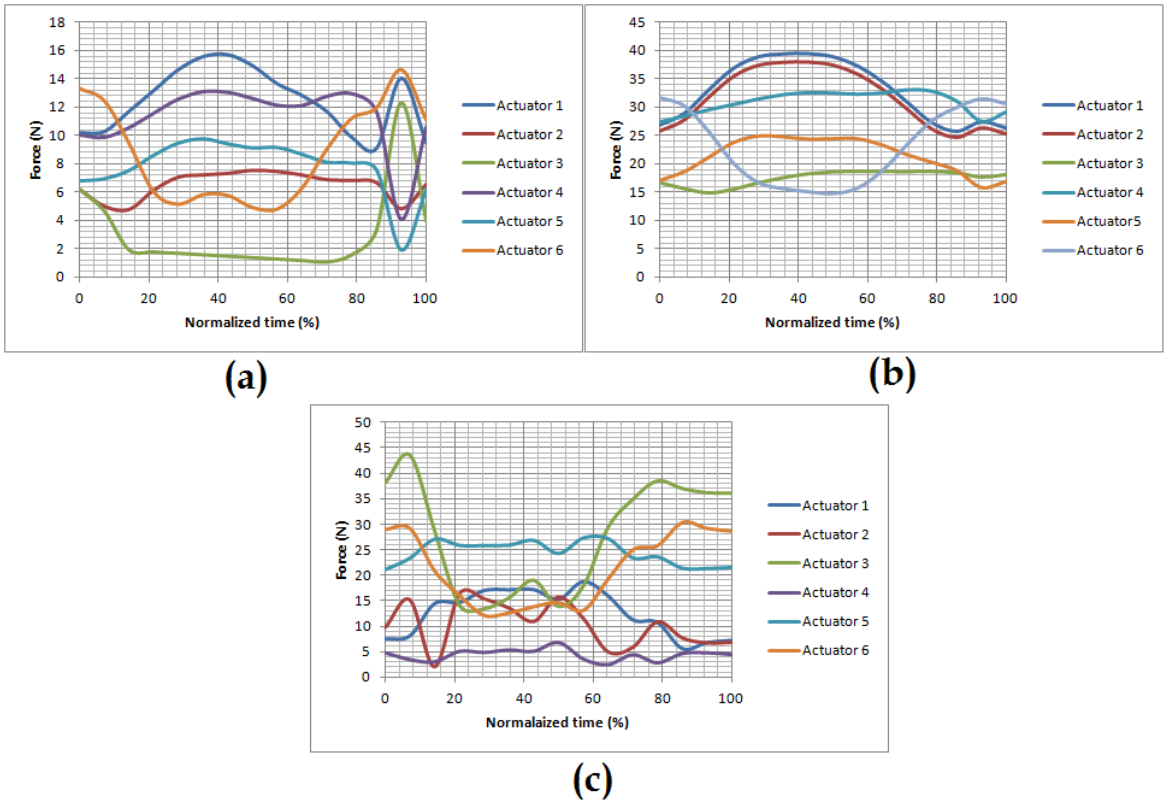

Figure 7-8: Actuator force in (a) Ankle dorsiflexion/plantarflexion, (b) Marching, (c) Hip flexion/extension

7.3.3 Load test of physical model

According to the translation of 200 mm in the Z axis, the stroke length calculates to approximately 188 mm in all actuators. This Figure will generate the correct stroke speed as opposed to dividing the displacement by the movement time. With reference to Figure 7-9(a)'s forward speed trend-line, there appears to be a strong linear relationship between the platform load and the speed taken for the robot to undergo vertical displacement. The coefficient of determination is 0.977, further enhancing this suggested relationship. Therefore, the function of the vertical movement speed is as follows:

$$V_{avr} = -0.0043 \times M + 3.5449 \quad (7.3)$$

Where V_{avr} and M represent the $Average\ speed\ (cms^{-1})$ and $Load\ capacity\ (kg)$ respectively. The relationship of the speed and load justifies through the assumption that the power produced from the linear actuators is constant. In the general sense, power is a product of the force and velocity. Newton's Third Law of Motion states that the average force generated from the actuators must equal that of the total load. Therefore, the power produced is also the product of load capacity and the average speed. So, there is a linear inverse proportion between load capacity and average stroke speed, as suggested in the linear negative gradient of the trend-line in Figure 7-9(a).

In the reverse direction, the speed is almost constant as the deviations between the mean times with respect to load capacity are a maximum 210 milliseconds. The elapsed time was recorded with a physical timer, therefore reaction time and human error must be taken into consideration, with the maximum deviation being slightly lower than the average human reaction time of around 250

milliseconds. Therefore, any deviation smaller than it can be considered due to human error and not an effect of the load on the actuator stroke speed. The mechanism of the linear actuator is such that in the reverse direction, the meshing of the worm and spur gears inside holds the load of the actuators. Therefore, no active power is used to carry the load downwards on the platform. This also means that the load has a negligible effect on the speed of the actuators as it retracts back to a shorter stroke length; a theory justified by the lack of correlation in the data for reverse movement speeds. The actuators run at full speed in the reverse direction regardless of the load. With respect to the peak speed of the actuators in this hexapod configuration, the maximum average speed achieved by the strokes is 3.73 cm/s; whereas the manufacturer's stated actuator speed rates are at approximately 7 cm/s under zero loads.

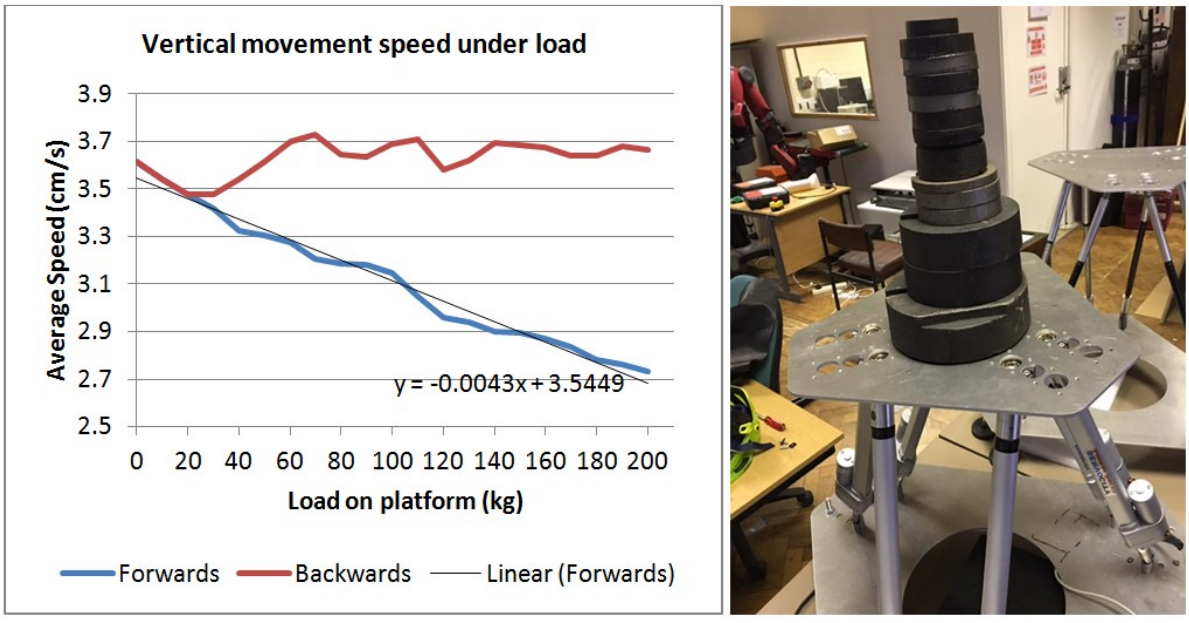

Figure 7-9: Loading test; (a) Effects of load on time and speed of movement of the robot (b) Robot loaded under 30kg load

7.4 A proposed conceptual design of a bilateral rehabilitation system

The advantages of using combined unilateral/bilateral upper limb rehabilitation over individual unilateral or bilateral trainings have been demonstrated by Lum, P, 2006 [60]. In this section we propose to develop a new functional lower limb robot-assisted rehabilitation system for paretic patients, especially those at an early stage of recovery. The system is aimed at providing a step-change capability that will allow self-learning, patient-directed, repetitive therapeutic exercises with the aim of accelerating the rate of recovery by increasing therapy time at affordable costs. We propose to enhance the robot described in Figure 7-2(b) to operate in conjunction with a similarly structured passive (Non-actuated) platform to form a bilateral rehabilitation system. Use of the suspension unweighting frame to support patient's weight and balance will be made as an integral part of the overall system. In Bilateral mode, walking can be simulated in a similar fashion to stepping on treadmill. The system will be integrated with a virtual reality environment to simulate normal walking as a task oriented exercise. The passive platform starts its motion by the healthy leg from home-position. As the healthy leg touches the ground in the virtual environment, the active platform starts its movement by assisting the affected leg to follow the generated foot trajectory created by the personalized relationship between the affected leg and healthy leg. This relationship has been explained in section 4.1 and 4.2. The level of assistance of the robot can be adjusted by the therapist depending on the degree of impairment of the leg. Once the affected leg starts its movement, the user slides back his healthy leg to the home position.

7.4.1 Preliminary determination of the trajectory of paretic leg

In chapter 4, it was explained that how the relation between the right and left leg can be formulated and utilized by the robot. In this section, the relation between right and left leg for two other exercises (Stair climbing and Treadmill walking) will be explained:

Normal walking - Barefoot participants were asked to walk with self-speed along a walkway. The start point and end point were marked on the floor. Each participant had six good trials with the right leg foot strike on the force plate completely and data was averaged for each leg over the successful trials.

Stair climbing - Stair climbing was started with the participants' right foot for the first six trials and their left foot in the next six trials. The height of each step was 209mm and the reflective markers were placed on the edges of the step platform to define the location of the stairs.

Treadmill walking – Treadmill walking was performed by the patients over 12 trials and each trial took minimum of 15s. A safety harness was used on the unweighted frame in order to create balance for the patients during walking.

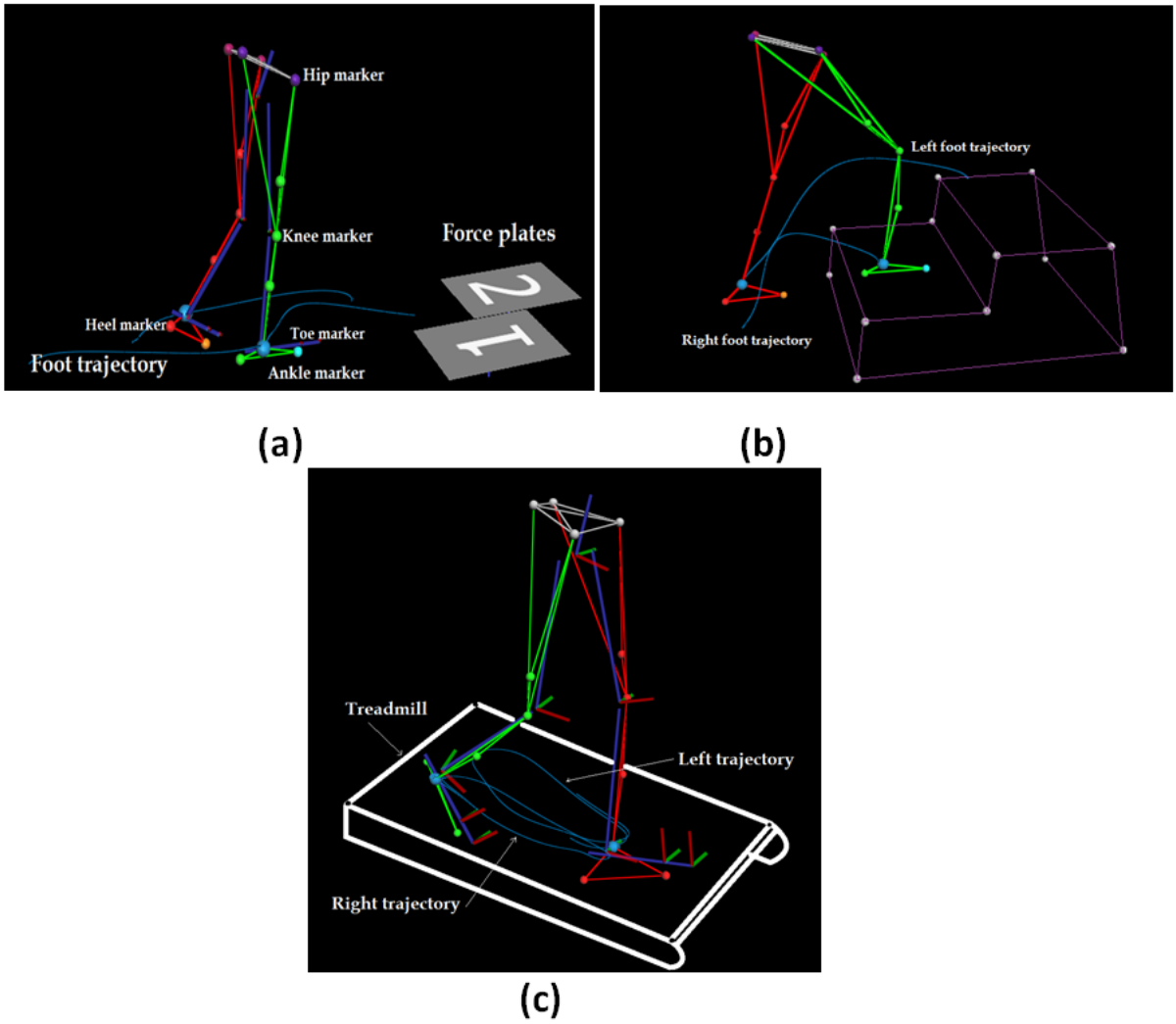

Figure 7-10: 3D simulation of lower limb during (a) Normal walking, (b) Stair climbing, (c) Treadmill walking

In normal walking, the foot trajectories of both legs have been measured in four consecutive steps 1-4 (Figure 7-11(a)). The first step started with the left leg and the last step finished with the right leg. In the second step the right leg was placed on the force plate number 1 and in the third step both legs have been placed on both force plates 1 and 2.

The profile of the ground reaction force was measured in both single support and double support phases. The walking velocity, cycle period and double stance duration were calculated during each

trial. Each patient had 12 trials including 6 trials started with the right step and 6 trials started with the left step. In all trials, patients had a good right and left foot strike on both force plates.

As it is shown in Figure 7.11(b), in treadmill walking, the position orientation of both the healthy leg and paretic leg was simulated and analysed by the Vicon system. In this exercise, the GRF was not evaluated because it was performed on the treadmill. The results of this exercise will be fed to the control system of the robot.

The mean value of the translation and orientation of the foot trajectory during left strides and right strides have been calculated over 12 trials for individual patients. The trajectory of the left stride and right stride have been shown by $P_L = [x_i, y_i, z_i, \alpha_i, \beta_i, \gamma_i]$ and $P_R = [x_j, y_j, z_j, \alpha_j, \beta_j, \gamma_j]$; $P_R^L = [(x_i - x_j), (y_i - y_j), (z_i - z_j), (\alpha_i - \alpha_j), (\beta_i - \beta_j), (\gamma_i - \gamma_j)]$ or on the other hand, $P_R^L = [x_{ij}, y_{ij}, z_{ij}, \alpha_{ij}, \beta_{ij}, \gamma_{ij}]$ represent the personalized relation between the right and left stride during bilateral exercises; $[x, y, z]$ represents the translation of the motion and $[\alpha, \beta, \gamma]$ illustrates the orientation of the motion; i and j show the time frame of the left stride and right stride respectively.

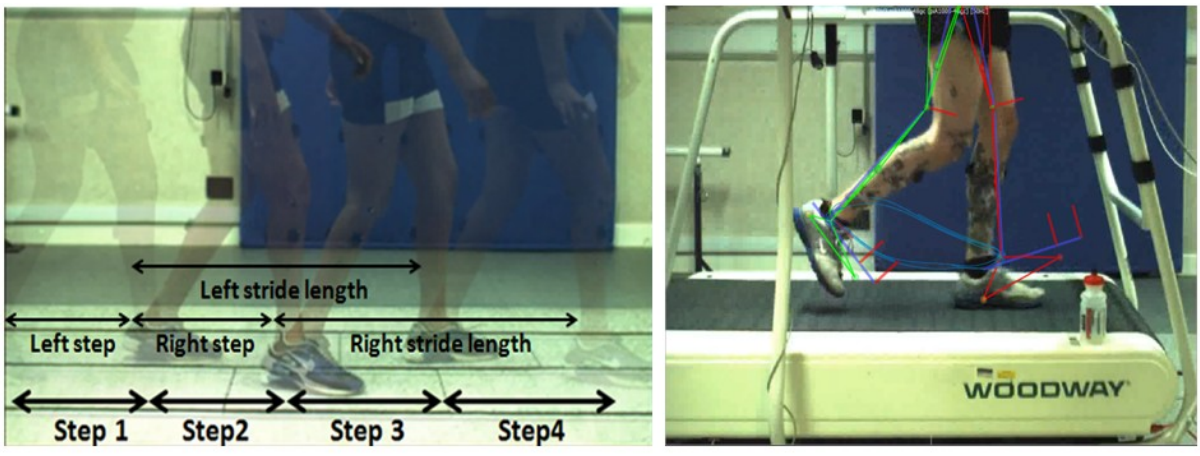

Figure 7-11: Analyzing the foot trajectories of post-stroke patients during (a) Normal walking, (b) Treadmill walking

With respect to the gait measurements, the P_R^L values were calculated and personalised for all of the patients. Therefore, when the passive platform starts its movement by the healthy leg, the position and orientation of the passive platform will be transferred to an associated PC, where a new trajectory will be generated for the active platform based on the personalized P_R^L relationship.

7.4.2 Some bilateral exercises

In bilateral exercises, the foot trajectory has to be personalised for individual patients; while in unilateral exercises, based on symmetry hypothesis between legs, the motion of a healthy leg will be simulated by the robot for the affected leg.

To demonstrate the personalized P_R^L relationship, the results of the analysis for one patient are discussed in this section. The average of the right and left strides' foot trajectories for (female, age=45years, height=1.7m, weight=73.45kg) is shown in Figure 7-12. Both right and left strides have been plotted with respect to the time frame during normal walking (Figure 7-12(a)) and treadmill walking (Figure 7-12(b)). The time frame has been normalized in percentages for both left and right strides. The relation between the right and left strides in the X, Y and Z axes (z_{ij}, x_{ij}, y_{ij}) has been shown with dotted lines and $\alpha_{ij}, \beta_{ij}\ and\ \gamma_{ij}$ have been calculated in the same way. With respect to this simple method, only by the known trajectory of the healthy leg and the relation between the right and left leg, the trajectory of the affected leg can be calculated and simulated by the robot.

As it is shown in Figure 7-12(a), the trends of motion in the Z axis are very similar to each other while this trend for the X axis is different. In addition, the trend of motion in the Y axis is very similar except between 45%-90% of the normalized time. These differences are caused by asymmetry between the range of motion of the healthy leg and paretic leg.

Figure 7-12(b) represents the foot trajectories in X, Y and Z axes during treadmill walking. This cycle started as the toe of the healthy leg touched the treadmill till the foot was lifted from the treadmill and the corresponding foot trajectory of the paretic leg in that cycle is shown in Figure 7-12(b). Reverse trends of displacement along the Z axis state that as soon as the healthy leg touched the treadmill surface, the other leg was lifted. The trend of displacement in the X axis was very similar for both legs and the trend of displacement on the Y axis was perfectly matched and overlaid. It is worth mentioning that these trends will be different with respect to the range of motion of joints for different patients. The relation between the healthy leg and paretic leg in the translation and orientation of the trajectory has been calculated.

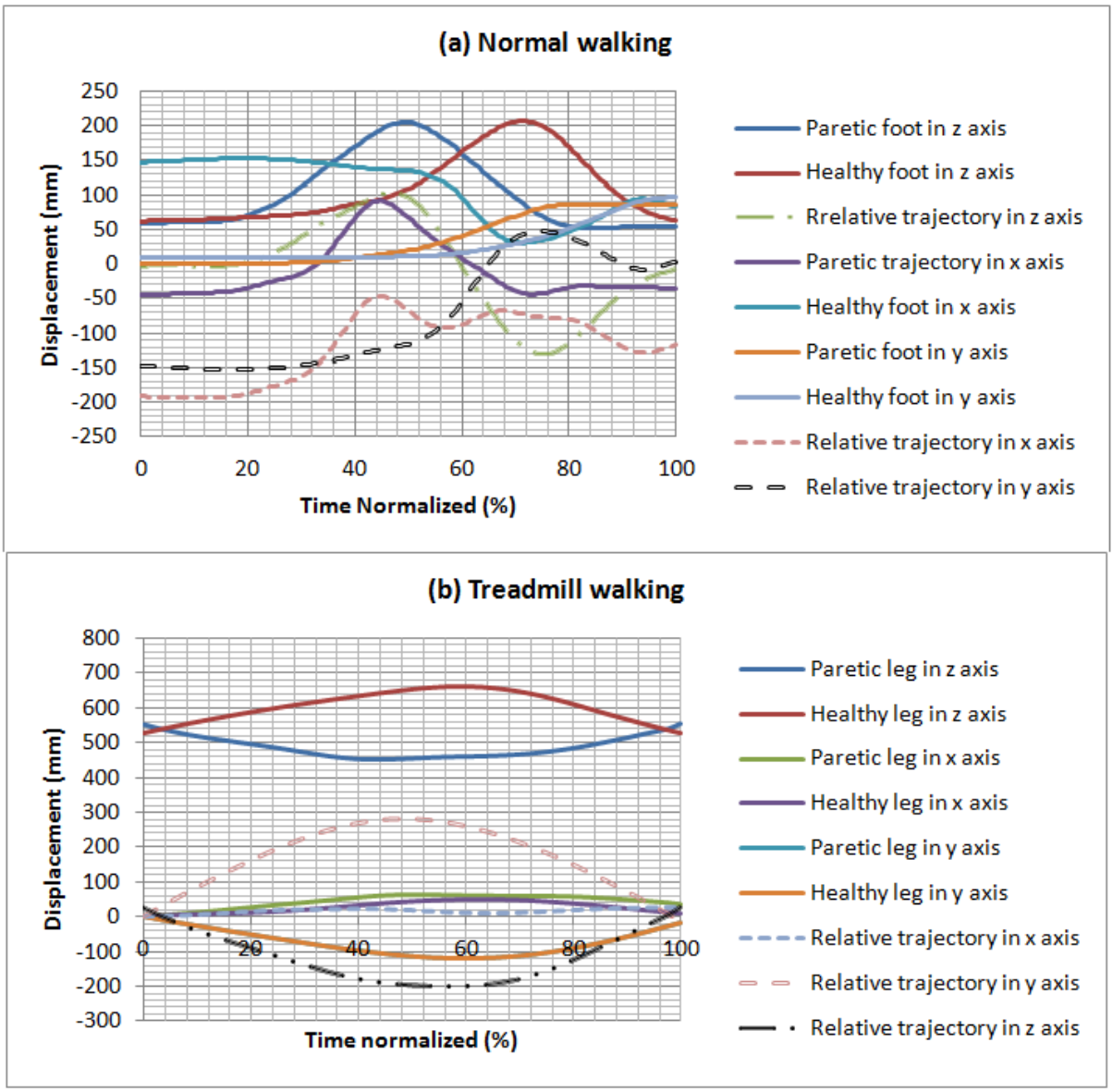

Figure 7-12: Averaged trajectory of foot during right and left stride length in Z axis

For the same participant, ground reaction force (GRF) in the X, Y and Z axes have been measured by two force plates in the gait laboratory and the results are shown in Figure 7-13. The data obtained from the force plates will be used by the robot at different states of the exercise to provide the required actuation in order to support the weight of the user. The maximum load in Z axis reached 763N on the force plate number 1, which was struck by her affected leg. The corresponding value on the force plate number 2, struck by her healthy leg, reached 760N.

Especially the measured force profile of force plate 1 illustrates the required force for the actuators of the active platform in order to support the patient`s weight. In the same way, the foot trajectory and the relation between the right and left foot have been calculated during stair climbing. The measured data by the Kistler force plate will be used by the active platform and the GRF was increased radically after the foot strike in the Z axis. A locking system will be designed for a passive platform in the future and the measured data by the Optima force plate will be used by this system in order to make a balance between the two applied forces of both legs during performance of the exercise. As shown in Figure 7-13, the variation of force in the X and Y axes was much less than the applied force on the Z axis. It is worth mentioning that the relation between the GRF of the right and left leg can be calculated similar to the position and orientation. It means that the GRF will be personalized for individual patients and by knowing the GRF of one of the legs and the relation between the right and left legs, the personalized GRF for the other leg can be calculated.

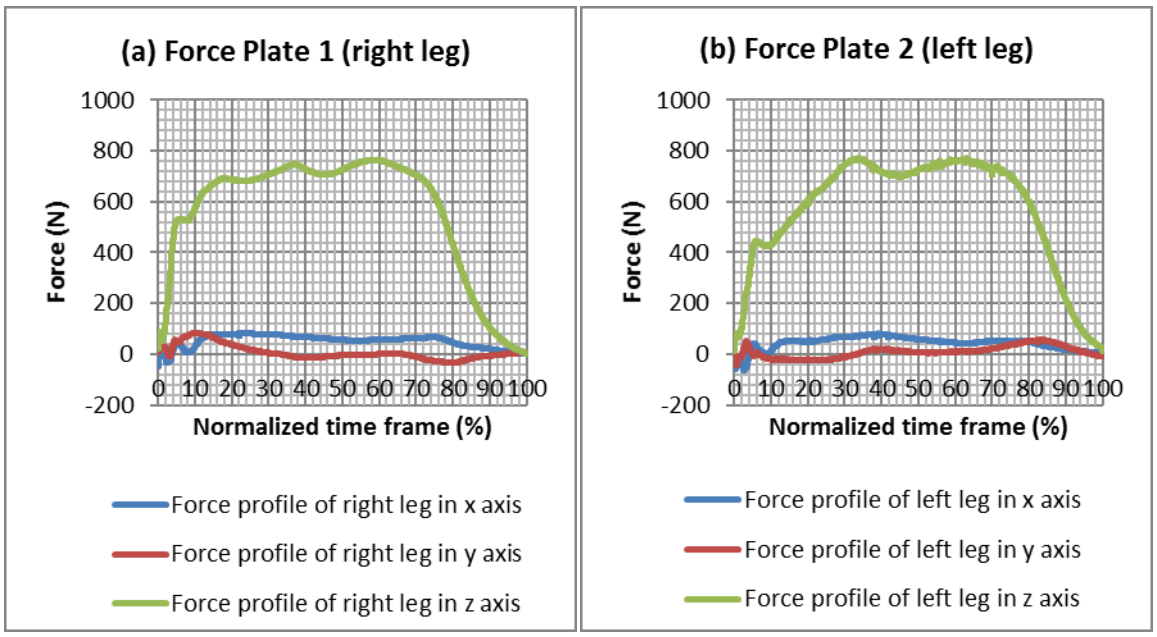

Figure 7-13: Measured ground reaction force for force plates 1 and 2

7.4.3 Bilateral model description

The bilateral robotic rehabilitation systems, which will be used by the patient in order to perform the proprioceptive exercises (like normal walking), try to keep the balance in both unilateral and bilateral stances. Therefore, the robotic device must be powerful enough to support the weight of patient during different movements.

In order to perform the bilateral exercises, another platform has been designed as a passive platform to follow the motion of the healthy leg. The structure of the passive platform is similar to the corresponding active Stewart platform with the same height. Although, in this platform, six gas struts with a stroke size of 30cm with an adjustable pressure switch have been utilized. The gas struts are connected to the top platform by six rolling spherical joints and to the fixed platform using six universal joints. The gas inside the struts was discharged in order to lift the platform with minimum load. Another binding shoe has been placed on the platform which has been equipped with a safety lock to release the foot in emergency cases. The required force for lifting the passive platform was 0.986kg. In future the material of the top platform will be changed to carbon fibre in order to reduce the weight of the platform. Also in the future an intelligent locking system will be embedded onto the passive platform and the measured GRF data of another force plate will be used by this system.

The 9 DOF Razor IMU with three sensors including ITG-3200c (MEMS triple-axis gyro), ADXL345 (triple-axis accelerometer) and HMC5883L (triple-axis magnetometer), has been used in order to measure nine degrees of inertial measurement. The outputs of all sensors have been processed by an on-board ATmega328 and output over a serial interface. The power of the 9DoF sensor was supplied by a 3.3VDC battery. An Xbee Pr 60mW Wire Antenna and USB Bluetooth were used to make a simple and reliable wireless communication between the 9DoF sensor and the

computer. Both the 9DoF sensor and Xbee antenna were placed under the centre of the passive moving platform in such a way so that the axes of the 9DoF sensor matched with the pre-defined axes of both platforms.

As shown in Figure 7-4, the measured angles by the gyroscope have been displayed in the GUI. The gyroscope calculation takes the code from the MATLAB_ARDUINO script written separately to the control system. The calibration button is a push button that triggers the calibration method. The second button is a toggle state switch. It is designed such that when the button is ON, the data from the gyroscope is constantly being polled through the serial port. Displacement angles for all three axes are calculated to simulate a dial by taking the sines and cosines of the angles to plot a rotating line. In the future, a dial graphic will show the exact angle of the lines. To optimize performance (essential for the real-time reporting of the displacements), the dials are plotted once and then using the set method the dial's data values are updated in real-time to change the 2nd state. This is a much less processor-intensive approach to plotting the dial in real-time.

In order to use these two platforms for the purpose of walking simulation, the minimum distance between them should be considered. Two robots were modelled in SolidWorks and motion analysis was used to find the minimum distance between the two platforms. This distance will prevent collision between the two platforms during the simulation. Although the required workspace of the robot should be considered for performing the exercise, it should be compact enough to be easily deployed. The torque output of active platform should be enough to support the load in different orientations. As it is shown in Figure 7-14, the minimum distance between the two platforms' edges and two platforms' centres were 25cm and 14cm respectively.

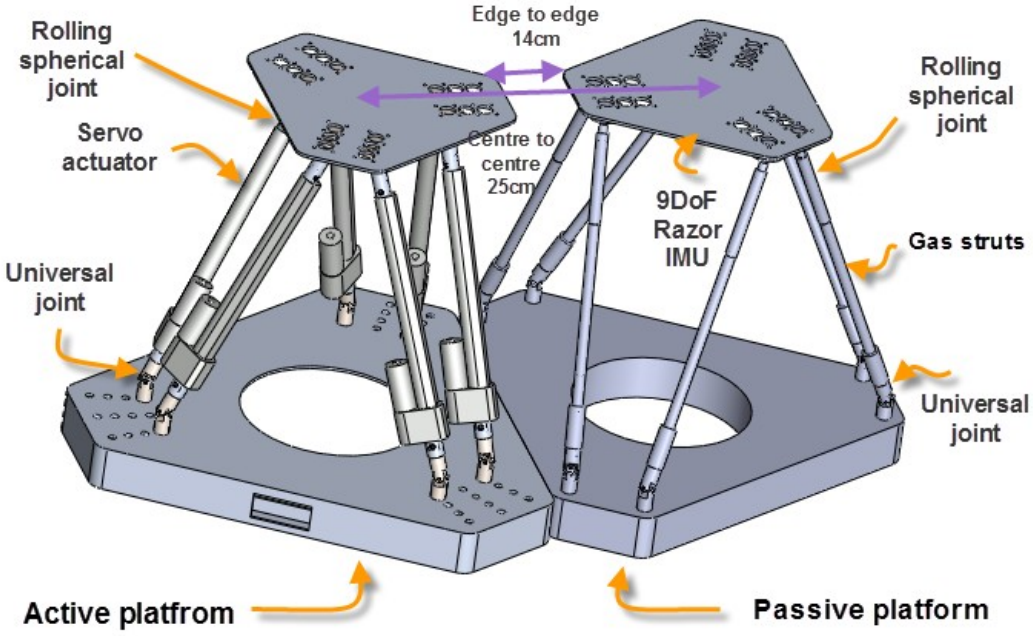

Figure 7-14: The minimum distance between two platforms

In bilateral mode, walking will be simulated similar to stepping on a treadmill. The active robot will be moved with respect to the position of the passive platform. The user starts the exercise when both platforms are in the home-position and they both support the weight of the user. When the healthy leg starts its stride, the control mode of the active platform will be changed from its position to force the control to support the weight of the user. Upon lifting the healthy leg, the position of the moving platform will be transferred to the PC by the Xbee antenna in order to find the corresponding trajectory for the affected leg by the pre-defined trajectory of P_2^1. As soon as the swinging foot hits the virtual ground, the active platform switches back to position control. Then the active platform follows the generated trajectory of P_2^1 to take another stride. As soon as the affected leg starts its movement, the user slides back his healthy leg to the home position. It is worth mentioning that a few training cycles, with full support of an unweighting harness and a therapist are required before starting the real test. The utilized control interface has the responsibility of

changing the control mode and sliding the active platform backwards and coordinating the trajectory of the active platform with respect to the motion of the passive platform. The state of both platforms will be sent to the PC and this information will be transformed to walking through the virtual environment. Using the suspension unweighting frame is necessary in order to unload up to 60% of a patient`s weight, especially when the patient`s weight will fully shifted from one foot to another. It is worth mentioning that the current active platform is able to lift 200kg without any restriction.

Based on the results of chapter 3 and 4, it was found that laterality affect on the range of movements of the joints and the trajectory of foots. In virtual reality, usually user will be asked to hit some targets which their locations were pre-defined already. Therefore, in these kinds of exercises the target will affect of natural movements of the extremities and they prevent the user to react naturally to the actions. While, in some other exercises, patient encourages to reacts naturally like crossing an street in virtual environment. So bilateral exercises should be designed to help the patients to use their own natural sensory information in order to prevent the effects of laterality.

As shown in Figure 7-15, finally the proposed rehabilitation system has been built in the Robotics laboratory, in the School of Mechanical Engineering, the University of Birmingham.

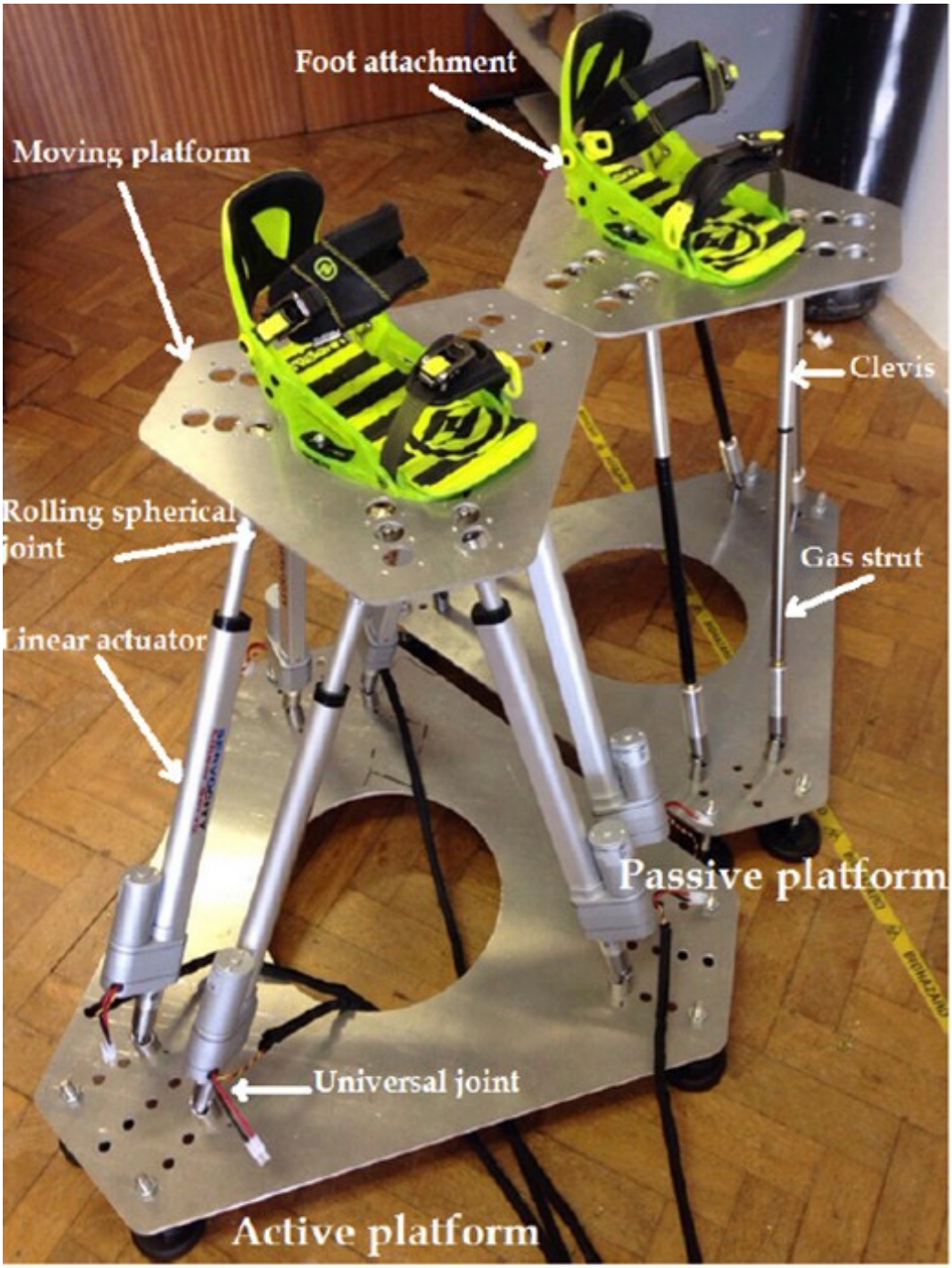
Foot attachment
Moving platform
Clevis
Rolling spherical joint
Gas strut
Linear actuator
Passive platform
Universal joint
Active platform

(a)

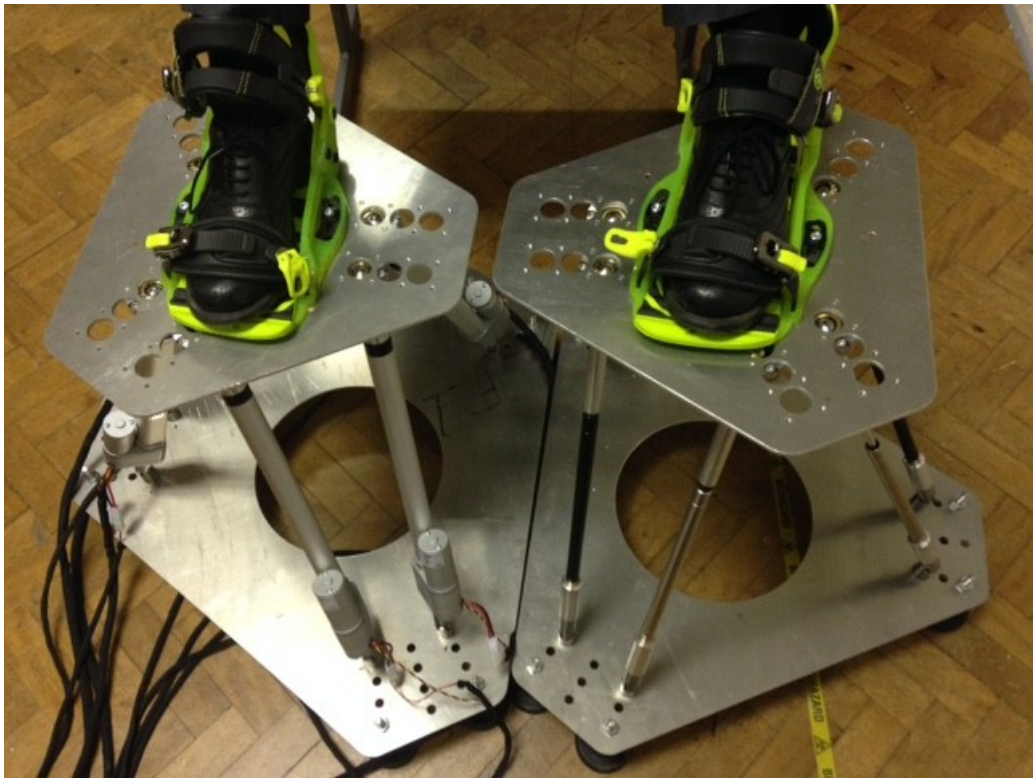

(b)

Figure 7-15: **(a,b) Views of the existing prototype of robot-assisted rehabilitation system developed at the University of Birmingham including an active parallel robot platform and a similarly-articulated passive platform**

Although clinical tests require more developments along with the external peripheral devices such as an unweighting frame, haptic device, virtual environment. The successful development of a failsafe mechanism is paramount. Therefore, a novel bespoke safety-critical solution will be developed to prevent out of range motions and velocities and provide singularity free/protected hardware/software situations. In addition, the safety of the system should be improved in order to be used by patients in clinics. In future haptic technology with force feedback will be added to the system to give more control ability to the user. An optimised adaptive/cognitive control strategy

will be designed to integrate the stiffness in the loop, leading to impedance control. This will allow the robot to offer a range of resistive/assistive combinations depending on the level of severity of the patient's impaired leg. In order to evaluate the progress of rehabilitation, EMG sensors can be used to evaluate the muscle activities during different exercises. The Methodologies of both unilateral and bilateral rehabilitation system have been briefly illustrated in Figure 7-16 as follow:

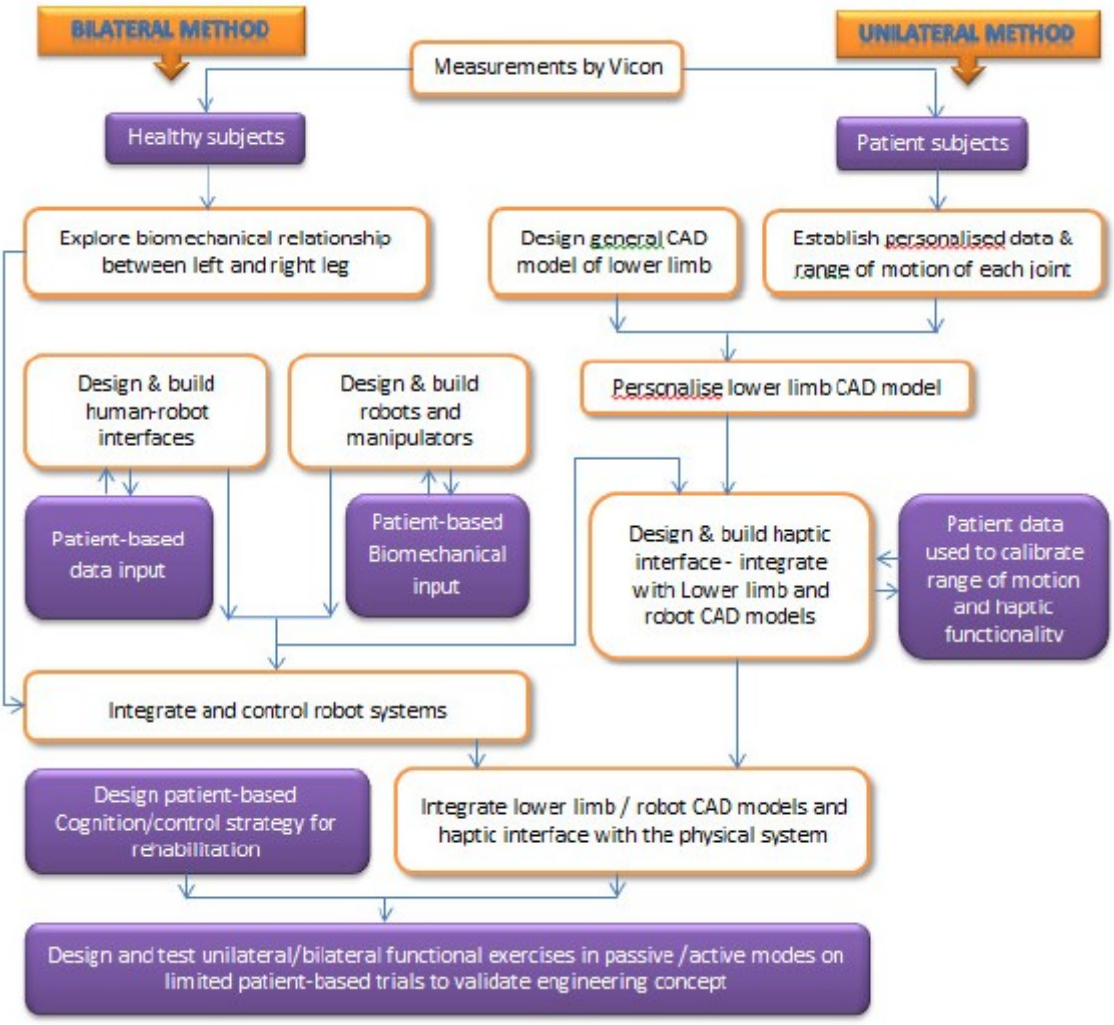

Figure 7-16: The proposed unilateral and bilateral robotic rehabilitation methodologies

7.5 Conclusion

In this chapter, a Stewart platform with 6 DoF was used in order to perform the unilateral exercises for lower limb rehabilitation. Based on measured gait data, a robot was able to move along different foot trajectories in order to simulate different exercises. Based on inverse kinematic and joint constraints, it was concluded that the designed robot is able to move 556mm in X and Y axes and 290mm in the Z axis. Using dynamic analysis, it was found that the robot is able to lift the load of 200kg with an average velocity of 2.7 (cm/s). A Kinect camera was used to validate the trajectory of the robot with simulated results in MATLAB. The position error between the Kinect results and simulation results showed that there were a maximum position error of 4.9cm in the Z axis during hip flexion/extension exercise and a minimum position error of 1.1cm in the X axis during the ankle exercise; this error can be improved by adjusting the light and resolution of the camera. With respect to the measured GRF data, the robot would be able to lift a leg easily during lower limb rehabilitation. A novel, self-learning bilateral rehabilitation system has been proposed with the hypothesis that it would lead to accelerated improvement in patient condition due to its self-directed therapeutic intervention. This is achieved through establishing a personalised spatial relationship between the paretic and healthy legs. Although, the bilateral system should be improved in order to be ready for the clinical tests, it can be a challenging concept in the area of lower limb robotic rehabilitation.

Chapter 8

Conclusion

8.1 Introduction

The aim of this research is to develop a robotic system for rehabilitation of patients with lower limb disability. The robot would be able to track the personalized foot trajectory of a patient during different rehabilitation exercises. In order to personalize the foot trajectory of participants, different exercises were defined and the trajectory of lower limb joints for both legs for individual participant were analysed using Vicon system. With respect to the obtained data the biomechanical relationship between two legs was developed. The kinematics and dynamics of parallel robot were investigated in order to build a parallel robot to track the foot trajectory of participants. Based on the designed CAD model of parallel robot, a physical prototype was built and was used to track the foot trajectory of healthy participants during various movements. A Kinect camera was used to track the movements of the robot in order to validate the position of centre of moving platform with the obtained data from the gait lab. Next, another larger parallel robot in real-scale was developed and built in order to track the foot trajectory of patients with lower limb disability. With respect to ability of robot to perform different exercises, a bilateral system was proposed based on concept of self-learning.

8.2 Overview of the research

The robotic therapy would allow treatment of people with severe impairments at any time post-stroke that would be more consistent, predictable and measurable. In this research a rehabilitation system has been developed that can provide a combination of both assistive motion and resistive force to the impaired leg, encouraging patient's motor function as required.

In the first experiment, the lower limb`s movements of 28 healthy subjects were recorded and simulated using Vicon system. First, the foot trajectories of healthy subjects during normal walking in two different phases, Targeting and non-Targeting, were studied and analysed. Laterality is one of the main issues which should be considered in defining the rehabilitation exercises. Results showed that laterality doesn`t affect the angular rotation of lower limb`s joints in both Targeting and non-Targeting tests; hence, no significant asymmetry observed between the lower limb joint`s motions.

In the next experiment, Vicon was used to simulate the lower limb`s motion of 8 healthy subjects during normal walking in both Targeting and non-Targeting modes. The statistical results reveals that gender has no significant effect on step difference between the left and right leg; while the position of the foot strike has a significant effect on step length during the Targeting test. The step length before the force plate was significantly different ($p<0.001$) with corresponding value after the force plate in Targeting. As it was expected, Both gender and positions were non-significant effects on step difference. Based on results, Targeting is an important factor which therapists should consider in order to have a better gait interpretation.

Based on gait results, the mathematical relationship between the right and left leg of healthy subjects has been modelled in Matlab. The biomechanical relationship will be used to map the motion signatures from healthy leg to the affected leg using bilateral robotic rehabilitation system. In bilateral robotic rehabilitation, the concept of self-learning was emphasized in order to perform natural and personalized movements during rehabilitation. It was concluded that gait analysis should be performed without Targeting in order to obtain natural signatures of motions for lower limbs. With respect to the non-Targeting results, a realistic and natural kind of motions was mapped from the healthy leg to the paretic leg. In chapter 4, the biomechanical relationship between the foot trajectory of left leg and right leg during normal walking was developed. The results will be used in control system of bilateral robotic rehabilitation system.

In order to design and build the prototype of the parallel robot, the inverse kinematic was used to calculate the length of actuators along the foot trajectories. With respect to 10cm stroke size of actuators, the foot trajectories were scaled down and used by the control system. The workspace of the robot along X, Y and Z axes were 240mm, 240mm and 140mm respectively. Based on inverse dynamic, the actuator forces were calculated along 4 different rehabilitation exercises including Marching, stair climbing, hip flexion/extension and ankle dorsiflexion/plantarflexion. The singularity of the robot along different trajectories was investigated using developed Matlab algorithm. The CAD model of the robot was designed in SolidWorks and the exercises were simulated in CAD environment. Based on kinematic and dynamic analysis a 6 DoF UPU Stewart platform was designed and built using 6 servo linear actuators with stroke size of 10cm. Kinect camera was used to validate the movements of the end-effector along different exercises. Results illustrated that Kinect had the maximum position error of 34.15mm.

In order to increase the workspace of the robot, 30cm stroke servo linear actuators were used to build a new 6 DoF UPS Stewart platform. By increasing the length of actuators the workspace of the new robot was increased 316mm along X and Y axes and 150mm along Z axis. The foot trajectories of post-stroke patients were recorded and simulated using Vicon system. The trajectories were simulated by the CAD model of the robot in Solidworks and then executed by the robot. The maximum position error of 1.2mm was observed in the X axis. The GUI was designed in Matlab in order to demonstrate the length of actuators, actuator forces, workspace, control velocity, stiffness, motion database and live plot of the robot. Two different control system was designed for the robot; (I) Point to point, (II) continuous trajectory. The designed GUI make user capable of controlling the movements of the robot along different trajectories with different velocities. The FEA results show that the robot is able to lift the weight of 200kg.

Results showed that 6 DoF parallel robot was able to accomplish different unilateral rehabilitation exercises. A passive parallel platform was designed and built in order to perform bilateral exercises, such as walking, stair climbing and treadmill walking. Initially, six gas struts with 10cm stroke were used in order to build a prototype of 6 DoF UPU parallel passive platform. The bilateral training system comprises of an assistive/resistive parallel robot under the impaired leg, and a passive similar parallel platform placed under the healthy leg, to provide simulated gait training and other similar exercises. The bilateral robotic system was proposed based on concept of self-learning and some preliminary tests were performed based on biomechanical relationship between the right/left leg during different exercises.

8.3 Contribution of the thesis

The main contribution of this research is developing a rehabilitation system which can be controlled based on the personalized foot trajectory of participants. The range of motion of lower limb joints is different for each patient during performing various exercises, so it is necessary to personalize the exercises for individuals. In this method the foot trajectory of patients were recorded and analysed during different exercises over number of trials. Also, the ground reaction forces were measured by the force plates in the gait lab and the results were utilized in the developed dynamic model. As a result, a personalized database including different rehabilitation exercises was created for individual participants. This database was used by the developed parallel robots in order to follow the foot trajectories during different motions. Albeit, the foot trajectories of patients were scaled down, but both robots could track the motions within the workspace of the robot successfully. Based on the designed GUI, therapist can select the appropriate exercise for the patient and robot performs the exercise repeatedly. The therapist would not require to have any physical intervention and can even monitor the progress of recovery remotely.

8.4 Future development

Proposing a novel rehabilitation system based on concept of self-learning has been reckoned as another significant achievement of this research. Learning from patient`s own natural signature of motion can be a challenging topic in the field of rehabilitation. The proposed bilateral robotic rehabilitation system can be a start point to answer to the following questions:

I. How the affected side of paretic patients can be rehabilitated by learning from the motions of healthy side of the body using bilateral robotic rehabilitation system?

II. How patient would be able to create his own desired rehabilitation exercises using robotic rehabilitation system?

III. How a robotic rehabilitation system can be developed in order to:

- Provide extra hours of treatment within the patient`s home in order to improve the functional motion recovery of the affected limb.
- Be intelligent, small and cheap enough to be used in homes, local clinics and hospitals.
- Accelerate the functional recovery by providing movements and exercises that are derived from the patient's own motion, rather than a set of standard movements.

A future work on back-drivable linear actuators can be developed and used so that the robot platform becomes a resistive/assistive device. An optimised adaptive/cognitive control strategy will be designed to integrate the stiffness in the loop, leading to impedance control. This will allow the robot to offer a range of resistive/assistive combinations depending on the level of severity of the patient's impaired leg. This will aim to benefit from the state-of-the-art development in robotic rehabilitation research and the successful development of a failsafe mechanism is paramount. Therefore, a novel bespoke safety-critical solution can be developed to prevent out of range motions and velocities, and provide singularity free/protected hardware/software situations.

A major part of the work is the direct involvement of stroke survivors from the very beginning. Volunteer patients will be engaged in all aspects of development including robot safety system and resistive/assistive control strategy. Furthermore, the work can involve an extensive exploitation and integration of interactive hardware and software system, and its success will depend upon such factors as iterative design, close participatory involvement of patients and a strong bias towards the development of meaningful and credible measures of engagement, usability and impact.

The overall system could be integrated through three levels of control. At the lowest level, the systems actuators are electrically powered and controlled by servo drive motors in active mode. The intermediate level involves the control of parallel mechanisms and assistive manipulators as independent devices in active-assistive mode. The highest level of control comprises controlling the active mechanism and its associated assistive manipulator through the motion signature information and its mapping from the passive mechanism and its associated assistive manipulator.

The research will be aimed to deliver a safe and tested robotic system, which has been subjected to rigorous standard risk and quality analysis as defined by medical device industry. The limited clinical trials will involve several groups of patients who will perform various pre-defined and measurable exercises using the robotic device. The result of the trials will provide extremely valuable knowledge about the functionality and effectiveness of the device in a real medical setting. Use of virtual reality environment, through a VR system, will be made to stimulate patients' mobility by providing goal-driven exercises in simulated real-life settings.

References

1. Zhou, Z., Meng, W., Ai, Q., Liu, Q., & Wu, X. (2013). Practical velocity tracking control of a parallel robot based on fuzzy adaptive algorithm. Advances in Mechanical Engineering, 5, 574896.
2. Xu, G. Z., Song, A. G., & Li, H. J. (2009). System design and control technique of robot-aided rehabilitation. Journal of Clinical Rehabilitative Tissue Engineering Research, 13(4), 717-720.
3. Ling, C., Qingsong, A., Yan, H., Quan, L., & Wei, M. (2012, July). A real-time leg motion recognition system by using Mahalanobis distance and LS_SVM. In Audio, Language and Image Processing (ICALIP), 2012 International Conference on (pp. 668-673). IEEE.
4. Tejima, N. (2001). Rehabilitation robotics: a review. Advanced Robotics, 14(7), 551-564.
5. Zhang, M., Davies, T. C., & Xie, S. (2013). Effectiveness of robot-assisted therapy on ankle rehabilitation–a systematic review. Journal of neuroengineering and rehabilitation, 10(1), 1.
6. Feigin, V. L., Forouzanfar, M. H., Krishnamurthi, R., Mensah, G. A., Connor, M., Bennett, D. A., & O'Donnell, M. (2014). Global and regional burden of stroke during 1990–2010: findings from the Global Burden of Disease Study 2010. The Lancet, 383(9913), 245-255.
7. Rothwell, P. M., Coull, A. J., Giles, M. F., Howard, S. C., Silver, L. E., Bull, L. M., ... & Farmer, A. (2004). Change in stroke incidence, mortality, case-fatality, severity, and risk factors in Oxfordshire, UK from 1981 to 2004 (Oxford Vascular Study). The Lancet, 363(9425), 1925-1933.
8. Sackley, C., Brittle, N., Patel, S., Ellins, J., Scott, M., Wright, C., & Dewey, M. E. (2008). The prevalence of joint contractures, pressure sores, painful shoulder, other pain, falls, and depression in the year after a severely disabling stroke. Stroke, 39(12), 3329-3334.

9. Hackett, M. L., Yapa, C., Parag, V., & Anderson, C. S. (2005). Frequency of depression after stroke a systematic review of observational studies. Stroke,36(6), 1330-1340.
10. Veerbeek, J. M., van Wegen, E., van Peppen, R., van der Wees, P. J., Hendriks, E., Rietberg, M., & Kwakkel, G. (2014). What is the evidence for physical therapy poststroke? A systematic review and meta-analysis. PloS one, 9(2), e87987.
11. Bhakta, B. B., Hartley, S., Holloway, I., Couzens, J. A., Ford, G. A., Meads, D., ... & Farrin, A. J. (2014). The DARS (Dopamine Augmented Rehabilitation in Stroke) trial: protocol for a randomised controlled trial of Co-careldopa treatment in addition to routine NHS occupational and physical therapy after stroke. Trials, 15(1), 316.
12. Simeone, S., Savini, S., Cohen, M. Z., Alvaro, R., & Vellone, E. (2014). The experience of stroke survivors three months after being discharged home: A phenomenological investigation. European Journal of Cardiovascular Nursing, 1474515114522886.
13. Dettori, J. R., & Basmania, C. J. (1994). Early ankle mobilization, Part II: A one-year follow-up of acute, lateral ankle sprains (a randomized clinical trial). Military medicine, 159(1), 20-24.
14. Schmidt, H., Werner, C., Bernhardt, R., Hesse, S., & Krüger, J. (2007). Gait rehabilitation machines based on programmable footplates. Journal of neuroengineering and rehabilitation, 4(1), 1.
15. Carr, J. H. S., & Roberta, B. (1982). A motor relearning programme for stroke.
16. Krebs, H. I., Palazzolo, J. J., Dipietro, L., Ferraro, M., Krol, J., Rannekleiv, K., ... & Hogan, N. (2003). Rehabilitation robotics: Performance-based progressive robot-assisted therapy. Autonomous robots, 15(1), 7-20.
17. Pistarini, C., & Molteni, F. (2009). New technologies and high specialization rehabilitation. Funct Neurol, 24, 169-171.

18. Mohammed, S., Amirat, Y., & Rifai, H. (2012). Lower-limb movement assistance through wearable robots: State of the art and challenges.Advanced Robotics, 26(1-2), 1-22.
19. Saglia, J. A., et al. (2009). "A high performance redundantly actuated parallel mechanism for ankle rehabilitation." The International Journal of Robotics Research
20. Ganguly, K., Byl, N. N., & Abrams, G. M. (2013). Neurorehabilitation: Motor recovery after stroke as an example. Annals of neurology, 74(3), 373-381.
21. Mohammed, S., Amirat, Y., & Rifai, H. (2012). Lower-limb movement assistance through wearable robots: State of the art and challenges. Advanced Robotics, 26(1-2), 1-22.
22. Hesse, S., Schmidt, H., Werner, C., & Bardeleben, A. (2003). Upper and lower extremity robotic devices for rehabilitation and for studying motor control. Current opinion in neurology, 16(6), 705-710.
23. Senanayake, C., Senanayake, S. M. N. A., & Arosha, M. N. (2009, July). Emerging robotics devices for therapeutic rehabilitation of the lower extremity. In Advanced Intelligent Mechatronics, 2009. AIM 2009. IEEE/ASME International Conference on (pp. 1142-1147). IEEE.
24. Díaz, I., Gil, J. J., & Sánchez, E. (2011). Lower-limb robotic rehabilitation: literature review and challenges. Journal of Robotics, 2011.
25. Veerbeek, J. M., van Wegen, E., van Peppen, R., van der Wees, P. J., Hendriks, E., Rietberg, M., & Kwakkel, G. (2014). What is the evidence for physical therapy poststroke? A systematic review and meta-analysis. PloS one, 9(2), e87987.
26. Deutsch, J. E., Paserchia, C., Vecchione, C., Mirelman, A., Lewis, J. A., Boian, R., & Burdea, G. (2004). Improved gait and elevation speed of individuals post-stroke after lower extremity training in virtual environments. Journal of Neurologic Physical Therapy, 28(4), 185-186.

27. Cioi, D., Kale, A., Burdea, G., Engsberg, J., Janes, W., & Ross, S. (2011, June). Ankle control and strength training for children with cerebral palsy using the Rutgers Ankle CP. In Rehabilitation Robotics (ICORR), 2011 IEEE International Conference on (pp. 1-6). IEEE.
28. Blaya, J. A., & Herr, H. (2004). Adaptive control of a variable-impedance ankle-foot orthosis to assist drop-foot gait. Neural Systems and Rehabilitation Engineering, IEEE Transactions on, 12(1), 24-31.
29. Boian, R. F., Deutsch, J. E., Lee, C. S., Burdea, G. C., & Lewis, J. (2003, March). Haptic effects for virtual reality-based post-stroke rehabilitation. In Haptic Interfaces for Virtual Environment and Teleoperator Systems, 2003. HAPTICS 2003. Proceedings. 11th Symposium on (pp. 247-253). IEEE.
30. Girone, M., Burdea, G., Bouzit, M., Popescu, V., & Deutsch, J. E. (2000). Orthopedic rehabilitation using the" Rutgers ankle" interface. Studies in health technology and informatics, 89-95.
31. Latonio, J., Burdea, G. C., & Boian, R. (2001). Post-Stroke Rehabilitation with the Rutgers Ankle System: A Case Study.
32. Deutsch, J. E., Latonio, J., Burdea, G., & Boian, R. (2001, July). Rehabilitation of musculoskeletal injuries using the Rutgers ankle haptic interface: three case reports. In Proceedings of Eurohaptics (pp. 11-16).
33. Deutsch, J. E., Lewis, J. A., & Burdea, G. (2007). Technical and patient performance using a virtual reality-integrated telerehabilitation system: preliminary finding. Neural Systems and Rehabilitation Engineering, IEEE Transactions on, 15(1), 30-35.
34. Boian, R. F., Lee, C. S., Deutsch, J. E., Burdea, G., & Lewis, J. A. (2002). Virtual reality-based system for ankle rehabilitation post stroke. In Proc. 1st Int. Workshop Virtual Reality Rehabilitation (pp. 77-86).

35. Mirelman, A., Bonato, P., & Deutsch, J. E. (2009). Effects of training with a robot-virtual reality system compared with a robot alone on the gait of individuals after stroke. Stroke, 40(1), 169-174.
36. Burdea, G. C., Cioi, D., Kale, A., Janes, W. E., Ross, S. A., & Engsberg, J. R. (2013). Robotics and gaming to improve ankle strength, motor control, and function in children with cerebral palsy—A case study series. Neural Systems and Rehabilitation Engineering, IEEE Transactions on, 21(2), 165-173.
37. Aubin, P. M., et al. (2008). "Gait simulation via a 6-DOF parallel robot with iterative learning control." Biomedical Engineering, IEEE Transactions on 55(3): 1237-1240.
38. Vallery, H., van Asseldonk, E. H., Buss, M., & van der Kooij, H. (2009). Reference trajectory generation for rehabilitation robots: complementary limb motion estimation. Neural Systems and Rehabilitation Engineering, IEEE Transactions on, 17(1), 23-30.
39. Saglia, J. A., Tsagarakis, N. G., Dai, J. S., & Caldwell, D. G. (2009, May). A high performance 2-DoF over-actuated parallel mechanism for ankle rehabilitation. In Robotics and Automation, 2009. ICRA'09. IEEE International Conference on (pp. 2180-2186). IEEE.
40. Saglia, J. A., Tsagarakis, N. G., Dai, J. S., & Caldwell, D. G. (2010, May). Control strategies for ankle rehabilitation using a high performance ankle exerciser. In Robotics and Automation (ICRA), 2010 IEEE International Conference on (pp. 2221-2227). IEEE.
41. Saglia, J. A., Tsagarakis, N. G., Dai, J. S., & Caldwell, D. G. (2009). Inverse-kinematics-based control of a redundantly actuated platform for rehabilitation. Proceedings of the Institution of Mechanical Engineers, Part I: Journal of Systems and Control Engineering, 223(1), 53-70.
42. Liu, G., Gao, J., Yue, H., Zhang, X., & Lu, G. (2006, June). Design and kinematics simulation of parallel robots for ankle rehabilitation. In Mechatronics and Automation, Proceedings of the 2006 IEEE International Conference on (pp. 1109-1113). IEEE.

43. Liu, G., Gao, J., Yue, H., Zhang, X., & Lu, G. (2006, October). Design and kinematics analysis of parallel robots for ankle rehabilitation. In Intelligent Robots and Systems, 2006 IEEE/RSJ International Conference on (pp. 253-258). IEEE.
44. Meng, W., Liu, Q., Zhou, Z., Ai, Q., Sheng, B., & Xie, S. S. (2015). Recent development of mechanisms and control strategies for robot-assisted lower limb rehabilitation. Mechatronics.
45. Jeevamalar, J., & Ramabalan, S. (2012, March). Optimal trajectory planning for autonomous robots-a review. In Advances in Engineering, Science and Management (ICAESM), 2012 International Conference on (pp. 269-275). IEEE.
46. Rakhodaei, H., Saadat, M., Rastegarpanah, A., & Abdullah, C. Z. (2016). Path planning of the hybrid parallel robot for ankle rehabilitation. Robotica, 34(01), 173-184.
47. Rakhodaei, H., Saadat, M., & Rastegarpanah, A. (2014, July). Motion Simulation of a Hybrid Parallel Robot for Ankle Rehabilitation. In ASME 2014 12th Biennial Conference on Engineering Systems Design and Analysis (pp. V003T17A008-V003T17A008). American Society of Mechanical Engineers.
48. Jeevamalar, J., & Ramabalan, S. (2012, March). Optimal trajectory planning for autonomous robots-a review. In Advances in Engineering, Science and Management (ICAESM), 2012 International Conference on (pp. 269-275). IEEE.
49. Marchal-Crespo, L. and D. J. Reinkensmeyer (2009). "Review of control strategies for robotic movement training after neurologic injury." Journal of neuroengineering and rehabilitation 6(1): 20.
50. Montagner, A., Frisoli, A., Borelli, L., Procopio, C., Bergamasco, M., Carboncini, M. C., & Rossi, B. (2007, September). A pilot clinical study on robotic assisted rehabilitation in VR with an arm exoskeleton device. In Virtual Rehabilitation, 2007 (pp. 57-64). IEEE.

51. Wisneski, K. J., & Johnson, M. J. (2007). Quantifying kinematics of purposeful movements to real, imagined, or absent functional objects: Implications for modelling trajectories for robot-assisted ADL tasks**. Journal of NeuroEngineering and Rehabilitation, 4(1), 1.
52. Nef, T., Mihelj, M., & Riener, R. (2007). ARMin: a robot for patient-cooperative arm therapy. Medical & biological engineering & computing, 45(9), 887-900.
53. Kousidou, S., Tsagarakis, N. G., Smith, C., & Caldwell, D. G. (2007, June). Task-orientated biofeedback system for the rehabilitation of the upper limb. In Rehabilitation Robotics, 2007. ICORR 2007. IEEE 10th International Conference on (pp. 376-384). IEEE.
54. Bradley, D., Acosta-Marquez, C., Hawley, M., Brownsell, S., Enderby, P., & Mawson, S. (2009). NeXOS–The design, development and evaluation of a rehabilitation system for the lower limbs. Mechatronics, 19(2), 247-257.
55. Nikitczuk, J., Weinberg, B., Canavan, P. K., & Mavroidis, C. (2010). Active knee rehabilitation orthotic device with variable damping characteristics implemented via an electrorheological fluid. Mechatronics, IEEE/ASME Transactions on, 15(6), 952-960.
56. Girone, M., Burdea, G., Bouzit, M., Popescu, V., & Deutsch, J. E. (2001). A Stewart platform-based system for ankle telerehabilitation. Autonomous robots, 10(2), 203-212.
57. Hogan, N., & Krebs, H. I. (2004). Interactive robots for neuro-rehabilitation. Restorative neurology and neuroscience, 22(3-5), 349-358.
58. Reinkensmeyer, D. J., Emken, J. L., & Cramer, S. C. (2004). Robotics, motor learning, and neurologic recovery. Annu. Rev. Biomed. Eng., 6, 497-525.
59. Emken, J. L., Wynne, J. H., Harkema, S. J., & Reinkensmeyer, D. J. (2006). Robotic device for manipulating human stepping. IEEE Transactions on robotics, 22(1).

60. Lum, P. S., Burgar, C. G., Van der Loos, M., Shor, P. C., Majmundar, M., & Yap, R. (2006). MIME robotic device for upper-limb neurorehabilitation in subacute stroke subjects: A follow-up study. Journal of rehabilitation research and development, 43(5), 631.

61. Patton, J. L., & Mussa-Ivaldi, F. A. (2004). Robot-assisted adaptive training: custom force fields for teaching movement patterns. Biomedical Engineering, IEEE Transactions on, 51(4), 636-646.

62. Burgar, C. G., Lum, P. S., Shor, P. C., & Van der Loos, H. M. (2000). Development of robots for rehabilitation therapy: the Palo Alto VA/Stanford experience. Journal of rehabilitation research and development, 37(6), 663-674.

63. Lum, P. S., Lehman, S. L., & Reinkensmeyer, D. J. (1995). The bimanual lifting rehabilitator: an adaptive machine for therapy of stroke patients. Rehabilitation Engineering, IEEE Transactions on, 3(2), 166-174.

64. Lum, P. S., Reinkensmeyer, D. J., & Lehman, S. L. (1993). Robotic assist devices for bimanual physical therapy: preliminary experiments. Rehabilitation Engineering, IEEE Transactions on, 1(3), 185-191.

65. Luft, A. R., McCombe-Waller, S., Whitall, J., Forrester, L. W., Macko, R., Sorkin, J. D., ... & Hanley, D. F. (2004). Repetitive bilateral arm training and motor cortex activation in chronic stroke: a randomized controlled trial. Jama,292(15), 1853-1861.

66. Hesse, S., Schulte-Tigges, G., Konrad, M., Bardeleben, A., & Werner, C. (2003). Robot-assisted arm trainer for the passive and active practice of bilateral forearm and wrist movements in hemiparetic subjects. Archives of physical medicine and rehabilitation, 84(6), 915-920.

67. Kautz, S. A., & Patten, C. (2005). Interlimb influences on paretic leg function in poststroke hemiparesis. Journal of neurophysiology, 93(5), 2460-2473.

68. Boian, R. F., Bouzit, M., Burdea, G. C., & Deutsch, J. E. (2004, September). Dual Stewart platform mobility simulator. In Engineering in Medicine and Biology Society, 2004. IEMBS'04. 26th Annual International Conference of the IEEE (Vol. 2, pp. 4848-4851). IEEE.
69. Boian, R. F., Kourtev, H., Erickson, K., Deutsch, J. E., Lewis, J. A., & Burdea, G. C. (2003, September). Dual Stewart-platform gait rehabilitation system for individuals post-stroke. In Proceedings of the Second International Workshop on Virtual Rehab (Vol. 93).
70. Nanua, P., Waldron, K. J., & Murthy, V. (1990). Direct kinematic solution of a Stewart platform. Robotics and Automation, IEEE Transactions on, 6(4), 438-444.
71. Wampler, C. W. (1996). Forward displacement analysis of general six-in-parallel SPS (Stewart) platform manipulators using soma coordinates. Mechanism and Machine Theory, 31(3), 331-337.
72. Geng, Z., Haynes, L. S., Lee, J. D., & Carroll, R. L. (1992). On the dynamic model and kinematic analysis of a class of Stewart platforms. Robotics and Autonomous Systems, 9(4), 237-254.
73. Dasgupta, B., & Mruthyunjaya, T. S. (2000). The Stewart platform manipulator: a review. Mechanism and machine theory, 35(1), 15-40.
74. Lebret, G., Liu, K., & Lewis, F. L. (1993). Dynamic analysis and control of a Stewart platform manipulator. Journal of Robotic systems, 10(5), 629-655.
75. Tsai, L. W. (2000). Solving the inverse dynamics of a Stewart-Gough manipulator by the principle of virtual work. Journal of Mechanical design,122(1), 3-9.
76. Zhang, C. D., & Song, S. M. (1992). Forward kinematics of a class of parallel (Stewart) platforms with closed-form solutions. Journal of Robotic Systems,9(1), 93-112.
77. Harib, K., & Srinivasan, K. (2003). Kinematic and dynamic analysis of Stewart platform-based machine tool structures. Robotica, 21(05), 541-554.

78. seng Yee, C., & Lim, K. B. (1997). Forward kinematics solution of Stewart platform using neural networks. Neurocomputing, 16(4), 333-349.

79. Masory, O., Wang, J., & Zhuang, H. (1993, May). On the accuracy of a Stewart platform. II. Kinematic calibration and compensation. In Robotics and Automation, 1993. Proceedings., 1993 IEEE International Conference on (pp. 725-731). IEEE.

80. Gallardo, J., Rico, J. M., Frisoli, A., Checcacci, D., & Bergamasco, M. (2003). Dynamics of parallel manipulators by means of screw theory. Mechanism and machine theory, 38(11), 1113-1131.

81. Dasgupta, B., & Mruthyunjaya, T. S. (1998). A Newton-Euler formulation for the inverse dynamics of the Stewart platform manipulator. Mechanism and Machine Theory, 33(8), 1135-1152.

82. Liu, M. J., Li, C. X., & Li, C. N. (2000). Dynamics analysis of the Gough-Stewart platform manipulator. Robotics and Automation, IEEE Transactions on,16(1), 94-98.

83. Nguyen, C. C., Antrazi, S. S., Zhou, Z. L., & Campbell, C. E. (1993). Adaptive control of a stewart platform-based manipulator. Journal of Robotic systems,10(5), 657-687.

84. Dasgupta, B., & Mruthyunjaya, T. S. (1998). Closed-form dynamic equations of the general Stewart platform through the Newton–Euler approach. Mechanism and machine theory, 33(7), 993-1012.

85. Zhuang, H., & Roth, Z. S. (1993). Method for kinematic calibration of Stewart platforms. Journal of Robotic Systems, 10(3), 391-405.

86. Khalil, W., & Guegan, S. (2004). Inverse and direct dynamic modeling of Gough-Stewart robots. Robotics, IEEE Transactions on, 20(4), 754-761.

87. Liu, K., Fitzgerald, J. M., & Lewis, F. L. (1993). Kinematic analysis of a Stewart platform manipulator. Industrial Electronics, IEEE Transactions on,40(2), 282-293.

88. Verhoeven, R., Hiller, M., & Tadokoro, S. (1998). Workspace, stiffness, singularities and classification of tendon-driven stewart platforms. In Advances in robot kinematics: Analysis and Control (pp. 105-114). Springer Netherlands.
89. Stoughton, R. S., & Arai, T. (1993). A modified Stewart platform manipulator with improved dexterity. Robotics and Automation, IEEE Transactions on, 9(2), 166-173.
90. St-Onge, B. M., & Gosselin, C. M. (2000). Singularity analysis and representation of the general Gough-Stewart platform. The International Journal of Robotics Research, 19(3), 271-288.
91. Dasgupta, B., & Mruthyunjaya, T. S. (1998). Singularity-free path planning for the Stewart platform manipulator. Mechanism and Machine Theory, 33(6), 711-725.
92. Li, H., Gosselin, C. M., & Richard, M. J. (2007). Determination of the maximal singularity-free zones in the six-dimensional workspace of the general Gough–Stewart platform. Mechanism and machine theory, 42(4), 497-511.
93. Jiang, Q., & Gosselin, C. M. (2009). Determination of the maximal singularity-free orientation workspace for the Gough–Stewart platform. Mechanism and Machine Theory, 44(6), 1281-1293.
94. Li, H., Gosselin, C. M., Richard, M. J., & St-Onge, B. M. (2006). Analytic form of the six-dimensional singularity locus of the general Gough-Stewart platform.Journal of Mechanical Design, 128(1), 279-287.
95. Jiang, Q., Gosselin, C. M., Wang, Y., & Fang, C. (2015). Maximal singularity-free orientation workspace over a position region of Gough–Stewart platform.Advanced Robotics, 1-10.
96. Kim, N. I., & Lee, C. W. (1998, May). High speed tracking control of Stewart platform manipulator via enhanced sliding mode control. In Robotics and Automation, 1998. Proceedings. 1998 IEEE International Conference on (Vol. 3, pp. 2716-2721). IEEE.

97. Fasse, E. D., & Gosselin, C. M. (1999). Spatio-geometric impedance control of Gough-Stewart platforms. Robotics and Automation, IEEE Transactions on,15(2), 281-288.

98. Su, Y. X., Duan, B. Y., Zheng, C. H., Zhang, Y. F., Chen, G. D., & Mi, J. W. (2004). Disturbance-rejection high-precision motion control of a Stewart platform. Control Systems Technology, IEEE Transactions on, 12(3), 364-374.

99. Lee, S. H., Song, J. B., Choi, W. C., & Hong, D. (2003). Position control of a Stewart platform using inverse dynamics control with approximate dynamics.Mechatronics, 13(6), 605-619.

100. Kang, J. Y., Kim, D. H., & Lee, K. I. (1996, December). Robust tracking control of Stewart platform. In Decision and Control, 1996., Proceedings of the 35th IEEE Conference on (Vol. 3, pp. 3014-3019). IEEE.

101. Boian, R. F., Bouzit, M., Burdea, G. C., & Deutsch, J. E. (2004, September). Dual Stewart platform mobility simulator. In Engineering in Medicine and Biology Society, 2004. IEMBS'04. 26th Annual International Conference of the IEEE (Vol. 2, pp. 4848-4851). IEEE.

102. Tsoi, Y. H., & Xie, S. Q. (2008, December). Design and control of a parallel robot for ankle rehabiltation. In Mechatronics and Machine Vision in Practice, 2008. M2VIP 2008. 15th International Conference on (pp. 515-520). IEEE.

103. Pastor, I., Hayes, H. A., & Bamberg, S. J. (2012, August). A feasibility study of an upper limb rehabilitation system using Kinect and computer games. InEngineering in Medicine and Biology Society (EMBC), 2012 Annual International Conference of the IEEE (pp. 1286-1289). IEEE.

104. Chang, Y. J., Chen, S. F., & Huang, J. D. (2011). A Kinect-based system for physical rehabilitation: A pilot study for young adults with motor disabilities.Research in developmental disabilities, 32(6), 2566-2570.

105. Gama, A. D., Chaves, T., Figueiredo, L., & Teichrieb, V. (2012, May). Guidance and movement correction based on therapeutics movements for motor rehabilitation support systems. In Virtual and Augmented Reality (SVR), 2012 14th Symposium on (pp. 191-200). IEEE.

106. Wiederhold, B., & Riva, G. (2012). Balance recovery through virtual stepping exercises using Kinect skeleton tracking: a follow-up study with chronic stroke patients. Annual Review of Cybertherapy and Telemedicine 2012: Advanced Technologies in the Behavioral, Social and Neurosciences, 181, 108.

107. Dutta, T. (2012). Evaluation of the Kinect™ sensor for 3-D kinematic measurement in the workplace. Applied ergonomics, 43(4), 645-649.

108. Galna, B., Barry, G., Jackson, D., Mhiripiri, D., Olivier, P., & Rochester, L. (2014). Accuracy of the Microsoft Kinect sensor for measuring movement in people with Parkinson's disease. Gait & posture, 39(4), 1062-1068.

109. Stone, E. E., & Skubic, M. (2011, August). Passive in-home measurement of stride-to-stride gait variability comparing vision and Kinect sensing. In Engineering in Medicine and Biology Society, EMBC, 2011 Annual International Conference of the IEEE (pp. 6491-6494). IEEE.

110. Omer, I. (2003). Image Specific Colour Representation: Line Segments in the RGB Histogram (Doctoral dissertation, Hebrew University of Jerusalem).

111. Alnowami, M., Khan, A., Morfeq, A. H., Alothmany, N., & Hafez, E. A. (2014). Feasibility Study of Markerless Gait Tracking Using Kinect. Life Science Journal, 11(7).

112. Camplani, M., & Salgado, L. (2014). Background foreground segmentation with RGB-D Kinect data: An efficient combination of classifiers. Journal of Visual Communication and Image Representation, 25(1), 122-136.

113. Sadeghi, H., Allard, P., Prince, F., & Labelle, H. (2000). Symmetry and limb dominance in able-bodied gait: a review. Gait & posture, 12(1), 34-45.

114. Hart, S., & Gabbard, C. (1998). Examining the mobilizing feature of footedness. Perceptual and motor skills, 86(3c), 1339-1342.

115. Cappozzo, A., Leo, T., & Pedotti, A. (1975). A general computing method for the analysis of human locomotion. Journal of Biomechanics, 8(5), 307-320.

116. Apkarian, J., Naumann, S., & Cairns, B. (1989). A three-dimensional kinematic and dynamic model of the lower limb. Journal of biomechanics, 22(2), 143-155.

117. Jamshidi, N., Hanife, H., Rostami, M., Najarian, S., Menhaj, M. B., Saadatnia, M., & Salami, F. (2010). Modelling the interaction of ankle-foot orthosis and foot by finite element methods to design an optimized sole in steppage gait. Journal of medical engineering & technology, 34(2), 116-123.

118. Stebbins, J., Harrington, M., Thompson, N., Zavatsky, A., & Theologis, T. (2006). Repeatability of a model for measuring multi-segment foot kinematics in children. Gait & posture, 23(4), 401-410.

119. Reza N.jazar ,(2007) Theory of applied robotics , springer ,ISBN 978-1-4419-1750-8

120. Jamshidi N., Esfahani M. H., Farzad, A., & Jamshidi, M. (2012). Design and testing of statistical methods to classify the severity of steppage gait based on center of pressure data. Medical Hypotheses.

121. Rastegarpanah, A., Saadat, M., Sadeghein N. (2016). Biomechanical relationships of the lower limbs. (Internal communication, School of Mechanical Engineering, University of Birmingham).

122. Patla, A. E., Robinson, C., Samways, M., & Armstrong, C. J. (1989). Visual control of step length during overground locomotion: task-specific modulation of the locomotor synergy. Journal of Experimental Psychology: Human Perception and Performance, 15(3), 603.

123. Wearing, S. C., Urry, S. R., & Smeathers, J. E. (2000). The effect of visual Targeting on ground reaction force and temporospatial parameters of gait. Clinical biomechanics, 15(8), 583-591.

124. Gundersen, L. A., Valle, D. R., Barr, A. E., Danoff, J. V., Stanhope, S. J., & Snyder-Mackler, L. (1989). Bilateral analysis of the knee and ankle during gait: an examination of the relationship between lateral dominance and symmetry. Physical Therapy, 69(8), 640-650.

125. Barr, A., Andersen, J. C., & Danoff, J. V. (1987). Symmetry of temporal, Spatial and kinematic events during gait. In Read at the Third Annual East Coast Gait Laboratory Conference, Bethesda, MD.

126. Stefanyshyn, D. J., & Engsberg, J. R. (1994). Right to left differences in the ankle joint complex range of motion. Medicine and science in sports and exercise, 26(5), 551-555.

127. Singh, I. (1970). Functional asymmetry in the lower limbs. Cells Tissues Organs, 77(1), 131-138.

128. Abendroth-Smith, J. (1996). Stride adjustments during a running approach toward a force plate. Research quarterly for exercise and sport, 67(1), 97-101.

129. Grabiner, M. D., Feuerbach, J. W., Lundin, T. M., & Davis, B. L. (1995). Visual guidance to force plates does not influence ground reaction force variability. Journal of biomechanics, 28(9), 1115-1117.

130. Menegolo, A. Simtk. org: Upper and Lower Body Model: Overview. Simtk, https://simtk. org/home/ulb_project (参照日 2013 年 6 月 8 日).

131. Rastegarpanah, A., Saadat, M. (2016). Lower Limb Rehabilitation Exercises Using a Parallel Robot. (Internal communication, School of Mechanical Engineering, University of Birmingham)

132. Alhwarin, F., Ferrein, A., & Scholl, I. (2014). IR stereo Kinect: improving depth images by combining structured light with IR stereo. In PRICAI 2014: Trends in Artificial Intelligence (pp. 409-421). Springer International Publishing.

133. Rastegarpanah A, Saadat M (2016) Lower limb robotic rehabilitation using patient data. (Internal communication, School of Mechanical Engineering, University of Birmingham)

134. Syrseloudis, C. E., & Emiris, I. Z. (2008, October). A parallel robot for ankle rehabilitation-evaluation and its design specifications. In BioInformatics and BioEngineering, 2008. BIBE 2008. 8th IEEE International Conference on (pp. 1-6). IEEE.

135. Rakhodaei, H., Ding, C., Saadat, M., & Rastegarpanah, A. (2013). Free Singularity Path Planning of Hybrid Parallel Robot. In Proceeding of the 11th International Conference on Manufacturing Research, ICMR (pp. 313-318).

136. Rastegarpanah, A., Saadat, M., & Rakhodaei, H. (2012). Analysis and simulation of various Stewart Platform configurations for lower limb rehabilitation. BEAR conference, University of Birmingham.

137. Rastegarpanah A, Saadat M (2016) Unilateral and Bilateral Lower Limb Robotic Rehabilitation System, Journal of Advances in materials Science and Engineering. (Internal communication, School of Mechanical Engineering, University of Birmingham)

Appendices

Appendix A: Kinect analysis

The Kinect camera was fixed on the wall. In order to calculate the accuracy of the robot, the position of color markers changed over 10 times with 30mm displacement along x, y and z axes. The measured position by Kinect was compared with actual displacements in order to calculate the position error.

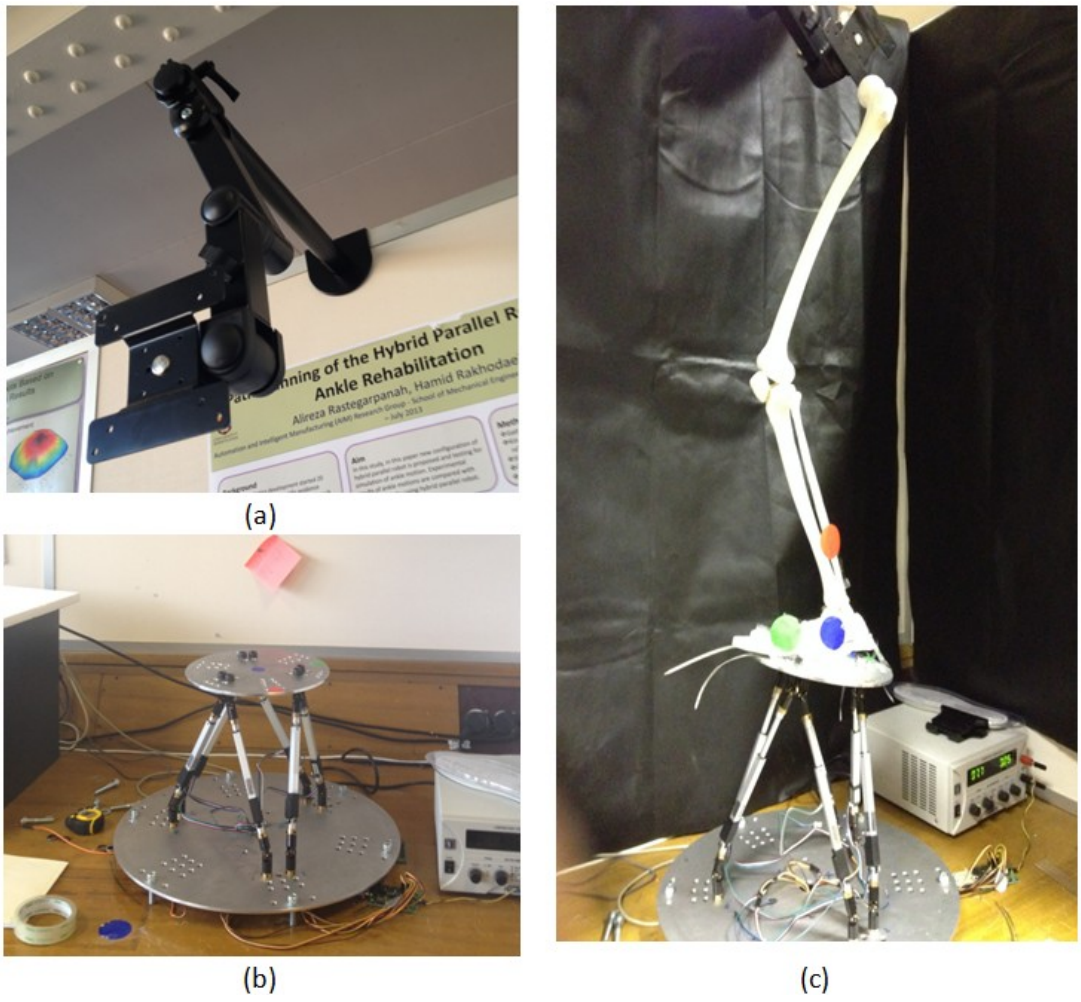

Figure A-1: Test rig (a) Kinect holder, (b) Parallel robot, (c) Skeleton model placed on the robot

In order to reduce the noise created by the light reflection, an environment was built and all experiments performed inside this environment (Figure A.2).

Figure A-2: Environment created to reduce lighting conditions for the KCB application.

In Figure A.3, the white circle is the target colour marker and the small dot illustrates the available noises in the environment. Better results obtained with non-colour background than colourful background. For example, the combination of red image with yellow background was very noisy (Figure A.4(c)). Results show that the best background for the system would be non-reflection and black one (Figure A.4 (j) (k) (l)).

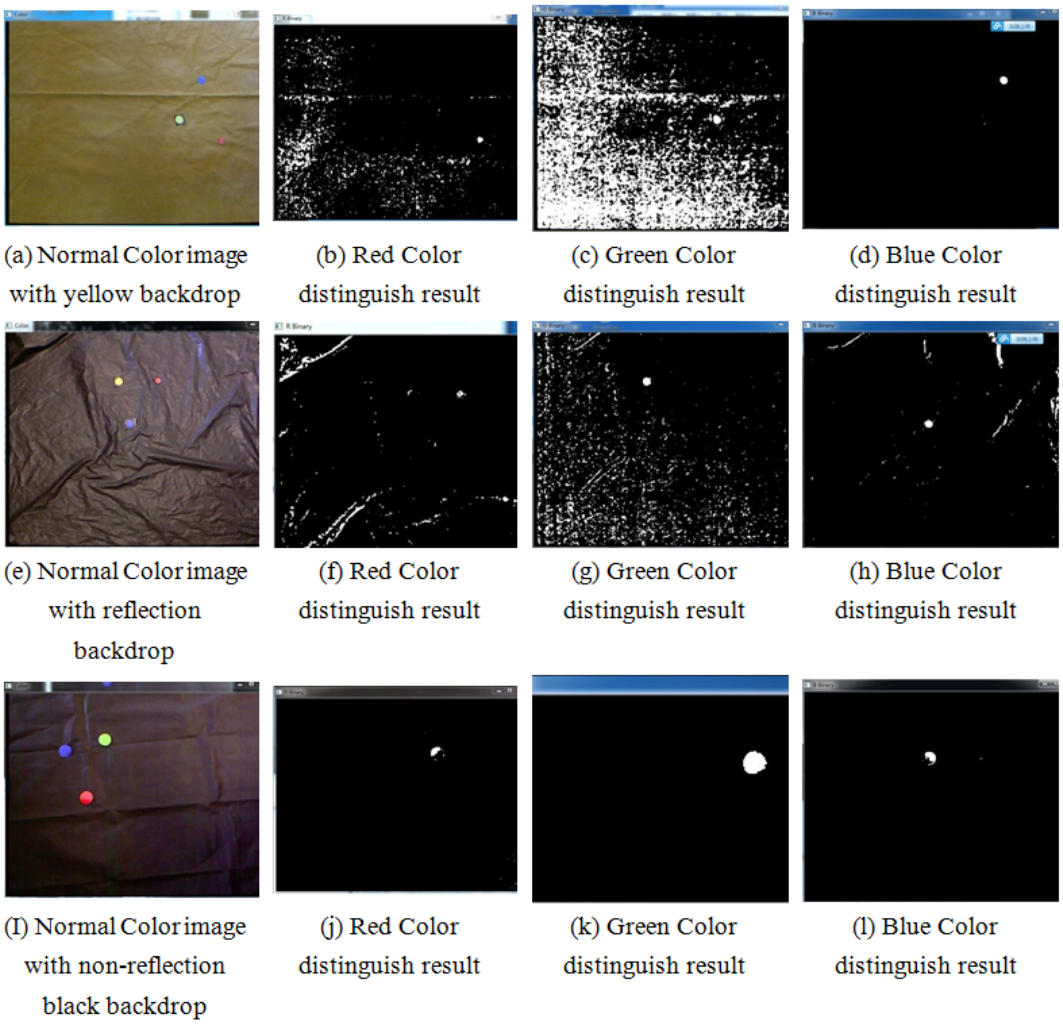

Figure A-3: Environment test result

Ten different color markers were used to test the ability of the camera to detect the color markers. The result shows that Kinect was able to distinguish red-orange, blue-purple and green-yellow colors. Another test was performed to find the smallest color marker diameter which was detectable by Kinect camera in typical indoor environment with the non-reflection black background. The result presented in Table A.1.

Table A -1: Block diameter experiment result

Block Diameter	Maker position	30mm	25mm	20mm	15mm	13mm	12mm	11mm	10mm	9mm	8mm
Detect result (Symbol Find: √ Miss: X)	1	√	√	√	√	√	√	√	√	√	X
	2	√	√	√	√	√	√	√	√	X	X
	3	√	√	√	√	√	√	√	√	√	√
	4	√	√	√	√	√	√	√	X	√	√
	5	√	√	√	√	√	√	√	√	√	√
	6	√	√	√	√	√	√	√	√	X	√
	7	√	√	√	√	√	√	√	X	X	X
	8	√	√	√	√	√	√	√	X	X	√
	9	√	√	√	√	√	√	X	√	√	√
	10	√	√	√	√	√	√	√	√	√	X
Total lose times		0	0	0	0	0	0	1	1	3	4

Blue markers with different diameter (8mm to 30mm) were used. The position of marker was changed every 100mm in order to observe if the marker can be detected by Kinect. The marker with diameter of 12mm was detected in all 10 different positions and it was selected as standard diameter during different tests.

Basic robot test was performed in order to investigate the accuracy of the Kinect camera. The test rig for this test has been shown in the Figure A.4.

Figure A-4: System controller parameter setting and Test environment

Seventy five trials were performed with different positions (x, y, z) and 30 trials were performed with different (α, β, θ) degrees. In summary, the maximum position error was 6mm during 225 trials, and the mean error was 1.6mm. The maximum orientation error was 6.5° while the mean error was 2.2°.

An skeleton model of lower limb was placed on the moving platform and color markers attached to the foot segment. As it is shown in the following Figure, Kinect camera tracked the position of the foot segment during different motions.

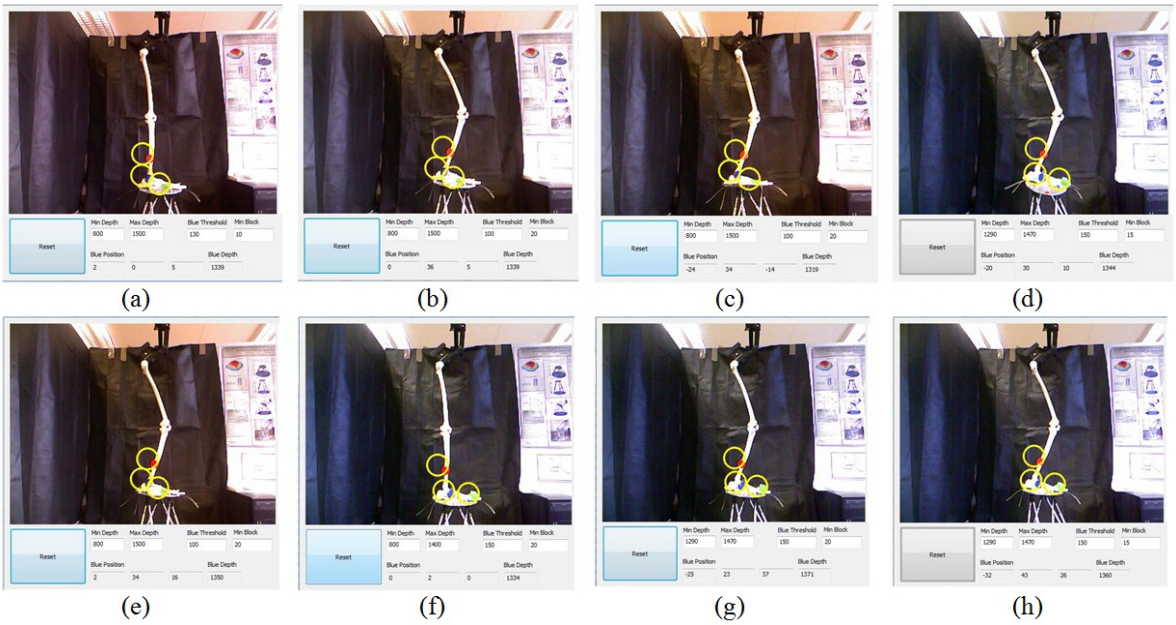

Figure A -5: Foot tracking during 8 different positions

Rehabilitation exercises using Stewart platform and Skeleton model of lower limb

Figure A-6: Performing rehabilitation exercises using parallel robot

Appendix B: FEA analysis

FEA analysis of the prototype of parallel robot

Different load in different heights applied on the moving platform in order to measure the displacement of the robot in different conditions. All the measurements have been performed in Solidworks and results have been displayed in the following Figures:

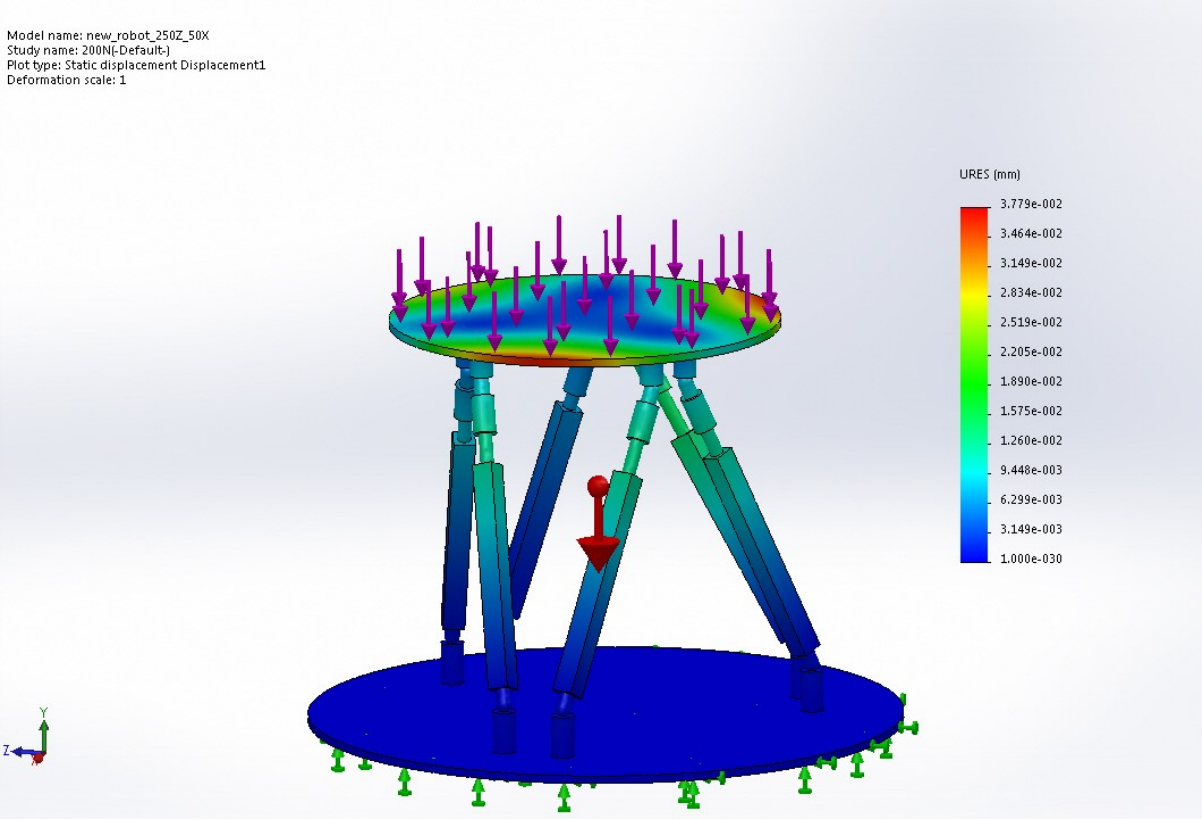

Figure B-1: Displacement of the robot by applying 200N when the location of robot is (X=50mm, Y=0mm, Z=250mm)

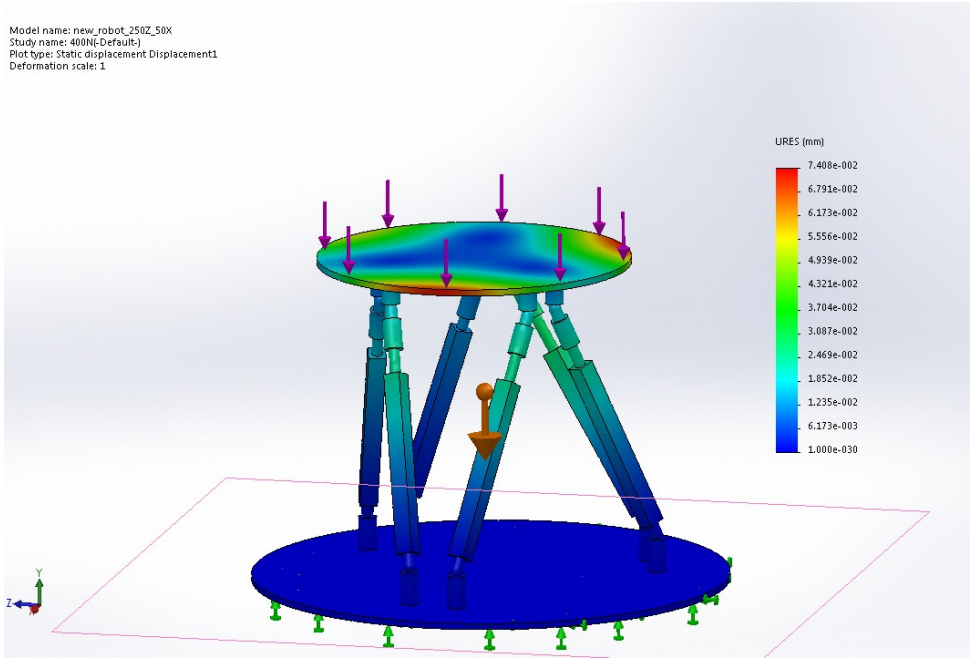

Figure B-2: Displacement of the robot by applying 400N when the location of robot is (X=50mm, Y=0mm, Z=250mm)

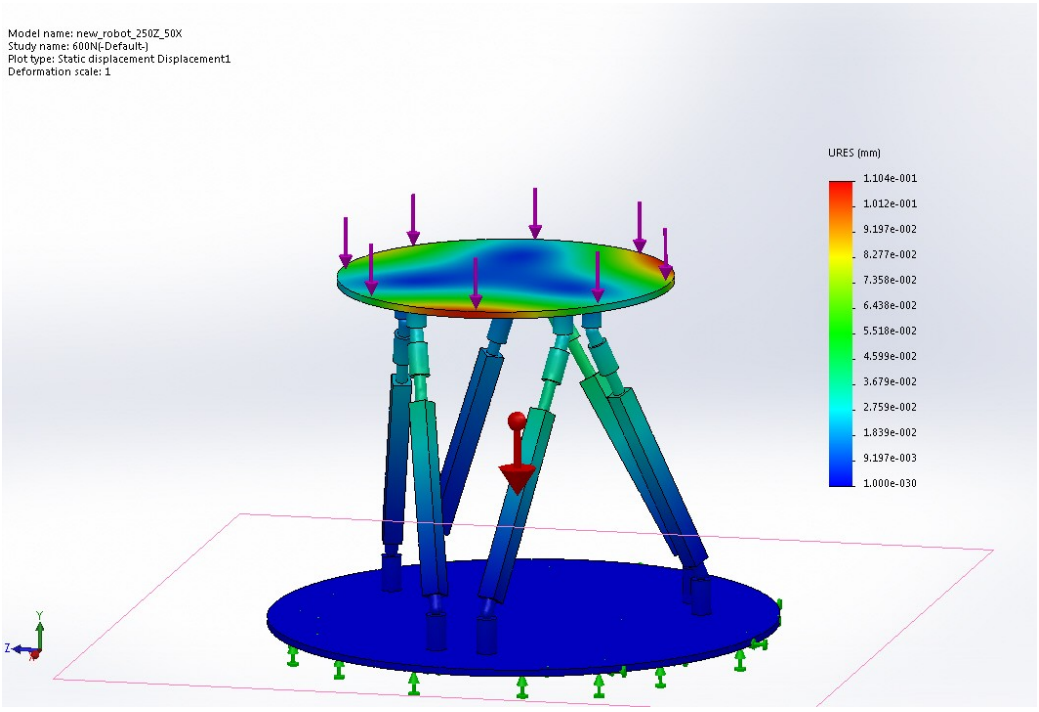

Figure B-3: Displacement of the robot by applying 600N when the location of robot is (X=50mm, Y=0mm, Z=250mm)

FEA analysis of parallel robot with 30cm actuator stroke size

Replicating the hexapod platform in CAD using SolidWorks, the deformation of the structure in its static state under varying loads is simulated. The model is applied with loads of 200 N, 400 N and 600 N in the following configurations as pictured below:

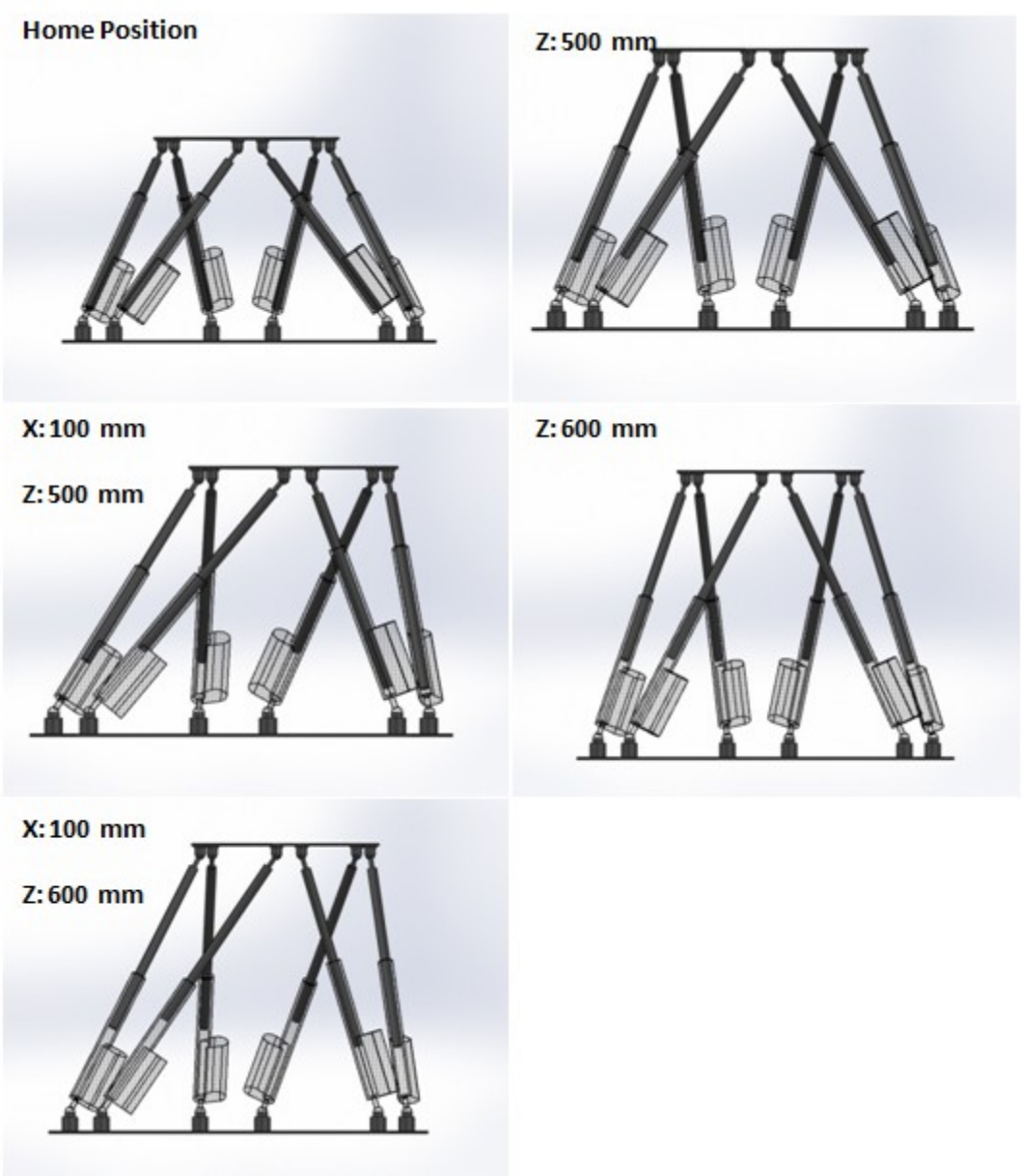

Figure B-4: Configurations of parallel platform for simulation (all co-ordinates are relative to the centroid of the static platform)

Finally a test for failure is conducted under a massive load of 10000 N to check for points on the model where failure is likely to occur under the given static load.

In the following simulation, the model is loaded with a given average force spread along the top face of the entire area of the mobile platform to replicate the load on the platform from the subject. A torque of 1 N.m was also applied to the upper part of the actuators as a test to simulate the torsion that acts along the axis of the actuators due to the nature of the universal joints on either side of the actuators.

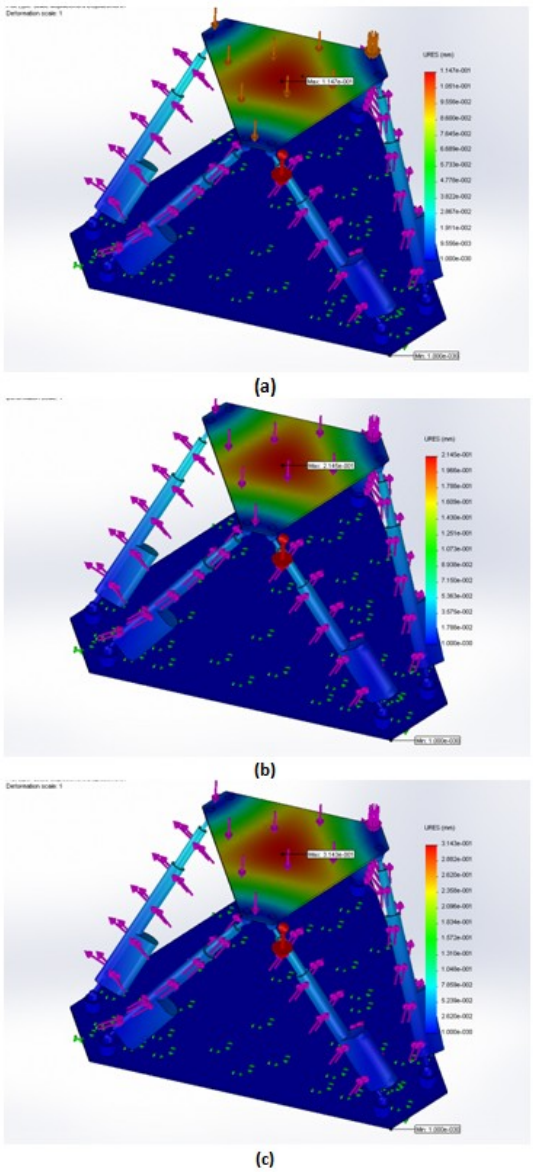

Figure B-5: Displacement Plot at (a) 200N, (b) 400N and (c) 600N (loading at home position)

With respect to the plots above, most of the deformations occur on the centre of the base, as the stresses seem to act entirely on the base only with little deformation occurring in the actuators. The flat profile of the base is designed such that the force does not run through the length of the actuators to prevent damage to the essential parts of the platform.

Taking the maximum displacement that occurs in the centre of the platform, there is a linear relationship between the applied load and the displacement of the structure in this configuration. This case lies true for all configurations including those of translations in more than one axis.

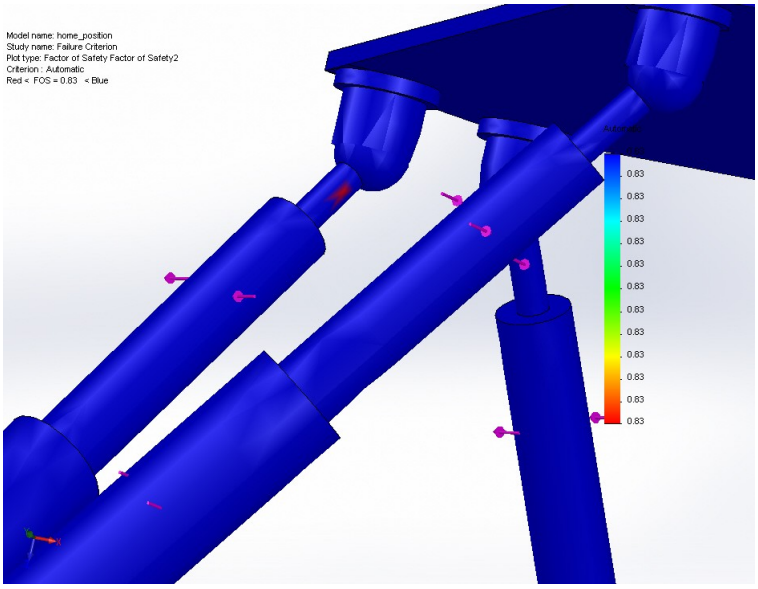

Figure B-6: Failure Point at FoS 0.83

The distribution plot is used to determine the minimum required Factor of Safety with respect to the loads and material yield stress. The distribution plot itself is not essential to the analysis, however the minimum Factor of Safety determined from will be substituted back into finding the failure point.

The failure point in this configuration appears to occur just above the clevis, where the diameter of the ‘leg’ thins down to the ball-socket bearing. The structure in that area can be improved by increasing the diameter above the clevis or filleting the vertices, however it must be noted that any changes to the geometry around the bearing will limit the platform’s degree of freedom.

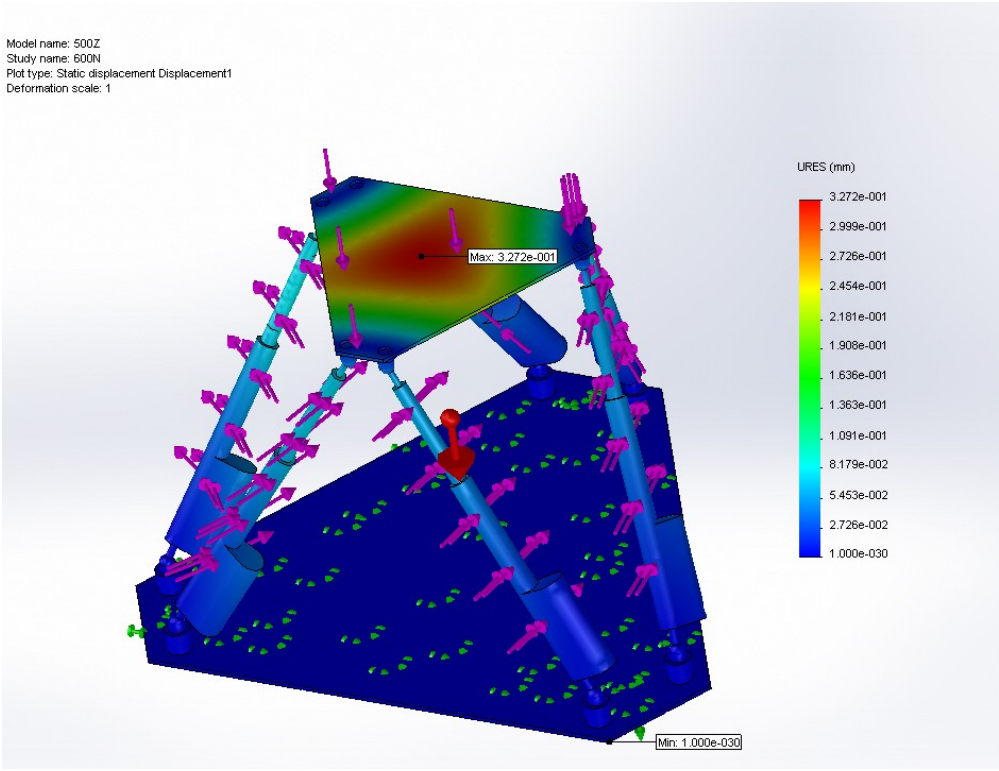

Figure B-7: Displacement plot at 600 N loading ; Loading at (Z: 500 mm)

Comparing the displacements at 500 mm and 600 mm respectively, the displacements of the actuators at 600 mm is marginally higher, a pattern also observed when comparing between the home position and 500 mm height models. Otherwise, the distributions of the displacements are similar to that of all other simulations with translations solely in the Z-axis.

Results suggests that the extra 100 mm displacement vertically gives rise to a less reliable configuration and must be incorporated when designing.

Table B-1: Summary of obtained data

Configuration	Minimum Factor of Safety	Maximum Displacement (mm)
Home Position	0.83	0.3143
Z: 500 mm	0.67	0.3272
X: 100 mm, Z: 500 mm	0.65	0.3227
Z: 600 mm	0.63	0.3215
X: 100 mm, Z: 600 mm	0.72	0.3315

Taking the collective values of FoS, it can be recommended that the Factor of Safety when designing the platform should be at least 0.63 to avoid yielding. A majority of the yielding under large loads occur above the clevises and on the ball-socket joints, therefore that specified section of the structure could be redesigned to make the platform much more reliable, however the yielding occurs at forces of 10000 N. This is a much more aggressive test than the loads that the actual robot will be under, as a harness will support most of the patient's weight in practice.

The limitations of the simulation must be considered to analyse its accuracy. The model had to be simplified from the real structure to reduce the amount of complex contact points and meshing errors in the FEA simulation. This mainly involves simplification of the joints such as the bottom joints that were changed from the original universal joints to a simple ball-socket element.

As a test, a torque was applied along the length of the actuators to simulate the torsion applied to the upper part of the actuators. This was manually added into the simulation instead of creating the correct contact sets for the inner and outside walls of the actuators. To further improve this simulation, at least some rough calculation of the moment should be calculated based on the product of the loadings and stroke lengths for each actuator in each configuration.

To enhance the analysis, loads acting on configurations that have rotations in the top platform should also be simulated. However, a solution to positioning the platform in SolidWorks to the desired angles must first be found as using mates and suppressing those causes some over-defining errors and faces being unable to mate due to geometrical constraints.

Appendix C: Drawing

Drawing of Active platform

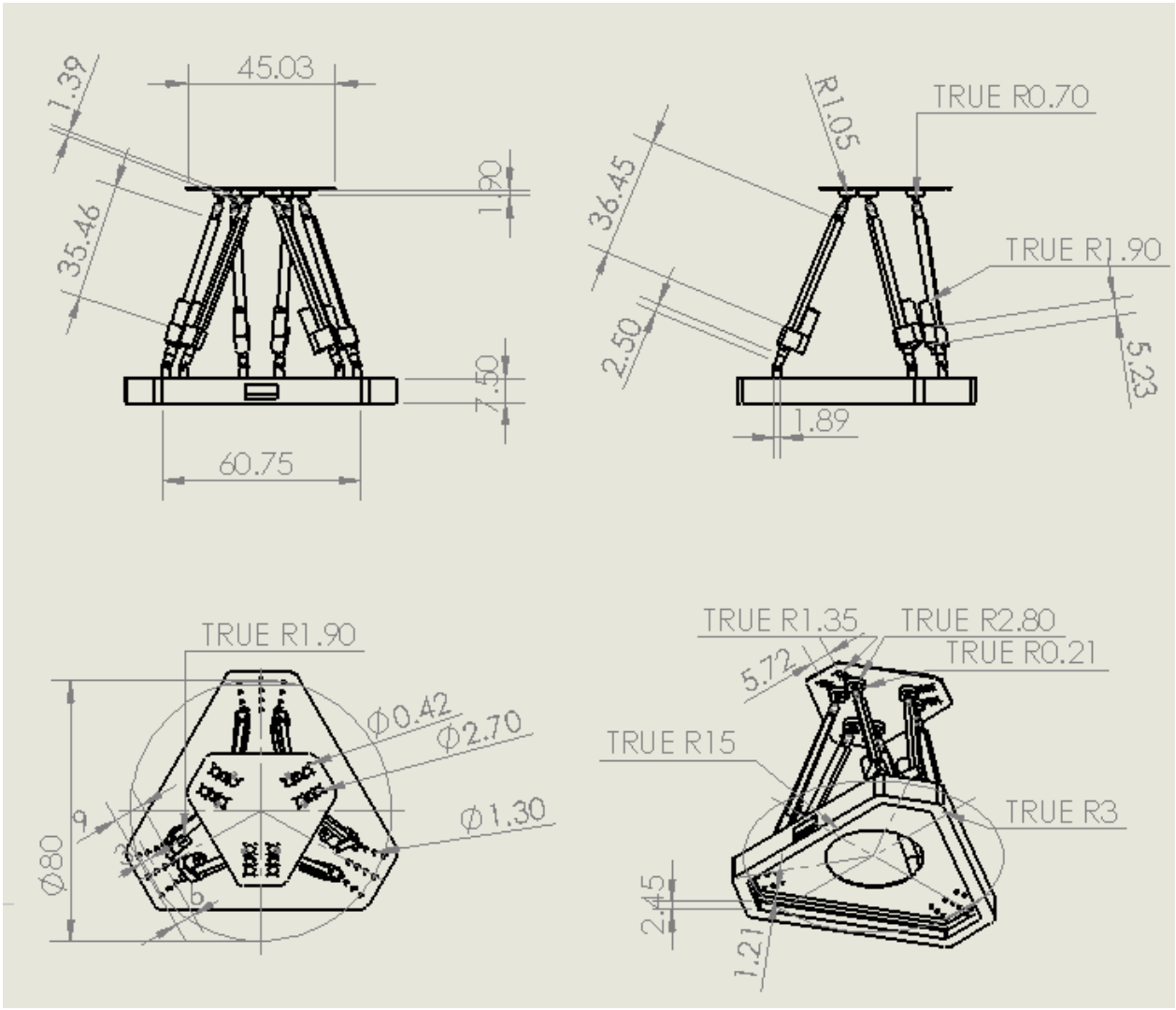

Figure C-1: Dimensions of the active platform (in mm)

Drawing of Passive platform

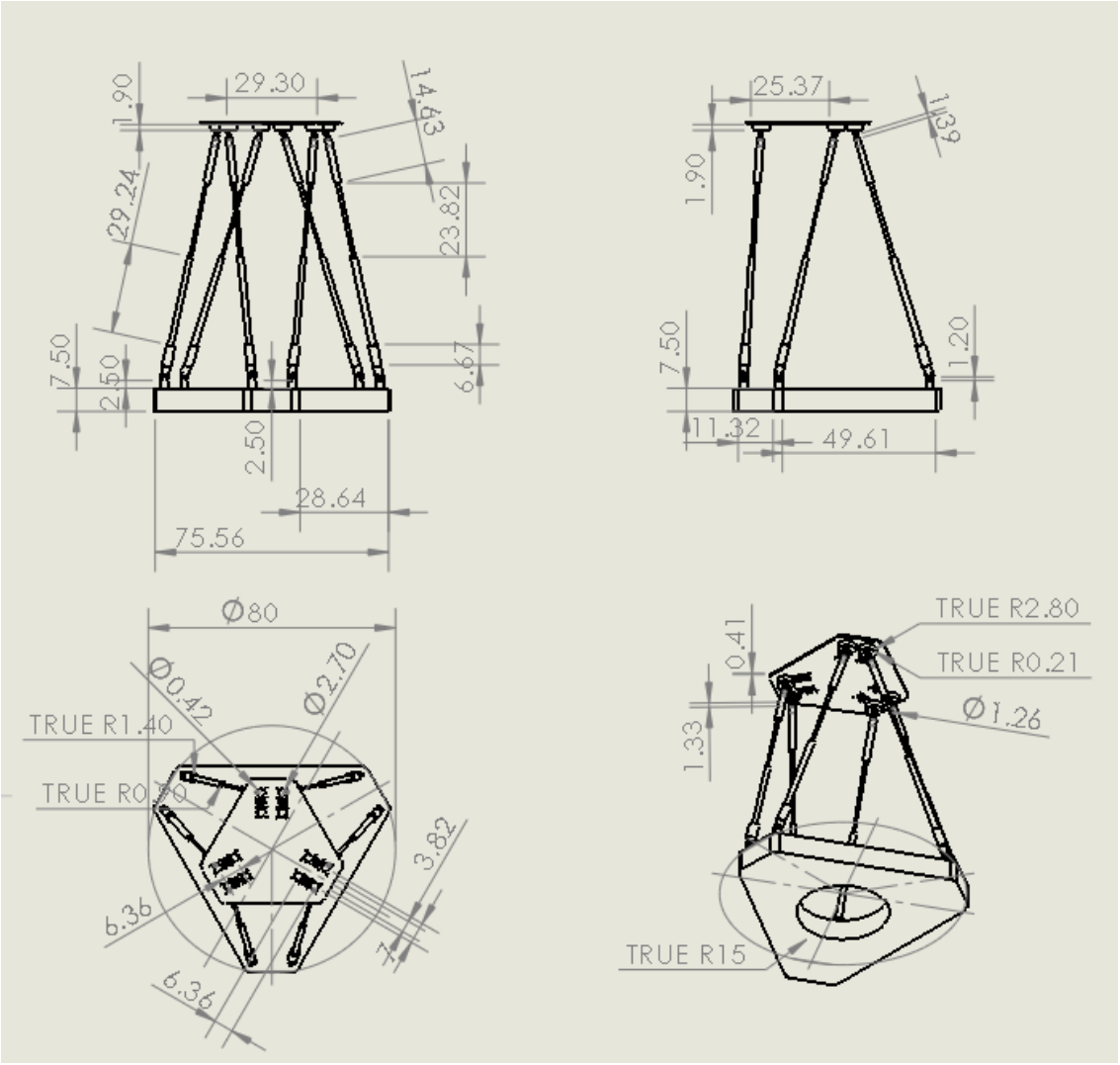

Figure C-2: Dimensions of the passive platform (in mm)

Drawing of the external 3D printed component used to increased the pivot angle of the spherical joints

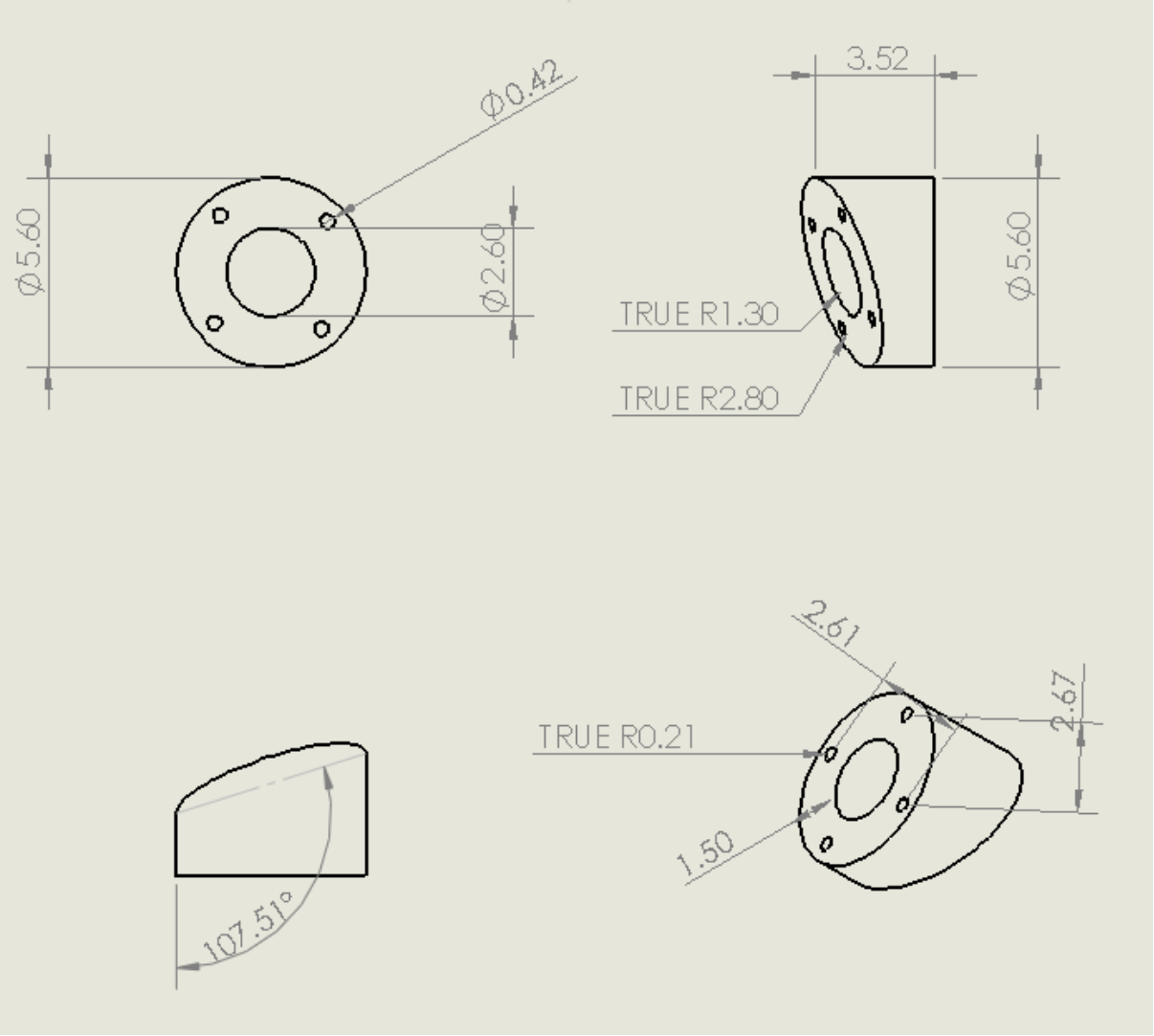

Figure C-3: Dimensions of the external component used to increase the pivot angle of the spherical joints (in mm)